ÇUKUROVA UNIVERSITY
INSTITUTE OF NATURAL AND APPLIED SCIENCES

MSc. THESIS

Özgür ÇAKIR

FLOW STRUCTURE BEHIND TANDEM CYLINDERS IN SHALLOW WATER FLOW

DEPARTMENT OF MECHANICAL ENGINEERING

ADANA, 2008

ÇUKUROVA ÜNİVERSİTESİ
FEN BİLİMLERİ ENSTİTÜSÜ

FLOW STRUCTURE BEHIND TANDEM CYLINDERS IN SHALLOW WATER FLOW

Özgür ÇAKIR

MASTER TEZİ

MAKİNA MÜHENDİSLİĞİ ANABİLİM DALI

Bu Tez ..../..../2008 Tarihinde Aşağıdaki Jüri Üyeleri Tarafından Oybirliği/Oyçokluğu İle Kabul Edilmiştir.

İmza:	İmza:	İmza:
Doç. Dr. Hüseyin AKILLI DANIŞMAN	Doç. Dr. Ahmet PINARBAŞI ÜYE	Doç. Dr. Galip SEÇKİN ÜYE

Bu Tez Enstitümüz Makina Mühendisliği Anabilim Dalında Hazırlanmıştır.

Kod No:

Prof. Dr. Aziz ERTUNÇ
Enstitü Müdürü

ABSTRACT

M.Sc. THESIS

FLOW STRUCTURE BEHIND TANDEM CYLINDERS IN SHALLOW WATER FLOW

Özgür ÇAKIR

DEPARTMENT OF MECHANICAL ENGINEERING
INSTITUTE OF NATURAL AND APPLIED SCIENCES
UNIVERSITY OF ÇUKUROVA

Advisor : Assoc. Prof. Dr. Hüseyin AKILLI
Year : 2008, Pages: 96
Jury : Assoc. Prof. Dr. Hüseyin AKILLI
Assoc. Prof. Dr. Ahmet PINARBAŞI
Assoc. Prof. Dr. Galip SEÇKİN

In this study, the flow characteristics of two tandem cylinders having different spacing was investigated experimentally by Particle Image Velocimetry (PIV) technique. In all experiments, two Plexiglas cylinders having the diameter of D=50 mm were used and the distance between cylinders was changed between G=0mm and 225mm. All experiments were carried out in 25 mm water height. The value of Reynolds number based on the cylinder diameter was Re=5000. Time-averaged flow characteristics such as velocity vector field, corresponding vorticity contours, streamline topology and Reynolds stress concentrations were obtained from averaging 300 images which were acquired at 15 Hz frequency.

Flow characteristics downstream of the cylinders do not affect from each other after the gap ratio of G/D=3.0

Keywords: PIV, tandem arrangement cylinders, shallow water

ÖZ

YÜKSEK LİSANS TEZİ

SIĞ SU AKIŞINDA ARDI ARDINA DİZİLİ SİLİNDİRLER ARKASINDAKİ AKIŞ YAPISININ İNCELENMESİ

Özgür ÇAKIR

ÇUKUROVA ÜNİVERSİTESİ
FEN BİLİMLERİ ENSTİTÜSÜ
MAKİNA MÜHENDİSLİĞİ ANABİLİM DALI

Danışman : Doç. Dr. Hüseyin AKILLI
Yıl : 2008, Sayfa: 96
Jüri : Doç. Dr. Hüseyin AKILLI
Doç. Dr. Ahmet PINARBAŞI
Doç. Dr. Galip SEÇKİN

Bu çalışmada, farklı silindir arası boşluğa sahip ardı ardına dizili iki silindir arasındaki akış özellikleri parçacık görüntülemeli hız ölçüm tekniği (PIV) kullanılarak deneysel olarak araştırılmıştır. Bütün deneylerde çapı D=50 mm olan iki adet pleksiglas silindir kullanılmış olup silindirler arası boşluk G=0 mm ve 225 mm arası mesafelerde değişmiştir. Bütün deneyler 25 mm su yüksekliğinde gerçekleştirilmiştir. Silindir çapına bağlı Reynolds sayısı değeri Re=5000 olarak alınmıştır. Ortalama hız vektörleri, akım çizgisi, girdap değerleri ve reynolds gerilim yoğunlaşması gibi akış özellikleri 15 Hz frekansta 350 anlık görüntü ile elde edilmiştir.

Aralık oranı G/D=3.0’dan sonra silindirler aşağı akış bölgesinde akış özellikleri olarak birbirlerini etkilememektedir.

Anahtar kelimeler: PIV, ardı ardına dizili silindirler, sığ su

ACKNOWLEDGEMENTS

I would like to express my gratitude to everyone who assisted in this study.

First and Foremost, I would lie to thank my advisor, Assoc. Prof. Hüseyin AKILLI for his support, guidance and encouragement. He has been a great source of motivation, both personal and professional. I shall always be grateful to him for what I have learned from him.

I would like to thank Prof. Dr. Beşir ŞAHİN for his continues support, help and encouragements.

I would like to thank Research Assistant Arif ÖZBEK for sharing his knowledge, for his friendship and his support.

I would like to thank Research Assistant Atakan AKAR and Kamil PAYDAŞ for their support during the experiments.

In addition, I would like to thank all the staff of Department of Mechanical Engineering at Çukurova University.

NOMENCLATURE

C_f : Bed (skin) friction coefficient

C_p : Base pressure coefficient ($Cp=(P-P_\infty) / (1/2\rho U^2{}_\infty)$)

D : Diameter of cylinder (mm)

f : Frequency of Kármán vortex formation (Hz)

G : Distance between cylinders walls

H : Height of water channel (mm)

h_w : height of water level (mm)

h : Flow depth (mm)

L : Distance between centers of cylinders (mm)

Re_d : Reynolds number based on the diameter of cylinder $(Re_d = UD/\nu)$

Re_h : Reynolds number based on the height of water level $(Re_d = Uh_w/\nu)$

Sc : Wake stability parameter $(S = C_f D/h_w)$

St : Strouhal number $(St = fD/\overline{U})$

t : Time (sec)

U : Free stream velocity (maximum velocity) (mm/sec)

$\overline{U}$: Depth-averaged velocity (mm/sec)

$\langle V \rangle$: Time-averaged total velocity vector (mm/sec)

V : Instantaneous velocity

W : Width of water channel (mm)

X : Horizontal length (mm)

$\langle \psi \rangle$: Time averaged streamline

$\langle \omega \rangle$: Time averaged vorticity

ω : Instantaneous vorticity

ν : Kinematic viscosity (mm/sec2)

TABLE OF CONTENTS **PAGE**

LIST OF FIGURES **PAGE**

1. INTRODUCTION

External flows past objects have been studied extensively because of their many practical applications that include marine structures, offshore structures, process industries (turbine blades, heat exchanger tubes, cooling systems for nuclear power plants, power transmission lines), underwater acoustics, civil, wind and aerospace engineering. In this study, it is going to be investigated the flow past two circular cylinders and study the turbulent wake flow field using the Particle Image Velocimetry (PIV) technique. Based on the PIV velocity field measurements and other reference information, a comprehensive discussion about many important flow concepts such as: boundary layer flow separation, wake flow, vortex shedding on an immerse body and shallow water will be given in the following sections.

1.1 Flow Over a Circular Cylinder

Flow past a blunt body, such as a circular cylinder, usually experiences boundary layer separation and very strong flow oscillations in the wake region behind the body. In certain Reynolds number range, a periodic flow motion will develop in the wake as a result of boundary layer vortice being shed alternatively from either side of the cylinder. This regular pattern of vortices in the wake is called a Karman vortex street. It creates an oscillating flow at a discrete frequency that is correlated to the Reynolds number of the flow. The periodic nature of the vortex shedding phenomenon can sometimes lead to unwanted structural vibrations. When the vortex shedding occurs behind a cylinder, drag on the cylinder increases and the body suffers from the periodic force in the normal direction to the main stream. This force makes the life of the structure shorten. On the other hand, the vortex shedding enhances mixing behind the cylinder. Figure 1.1 show the schematic flow over a circular cylinder.

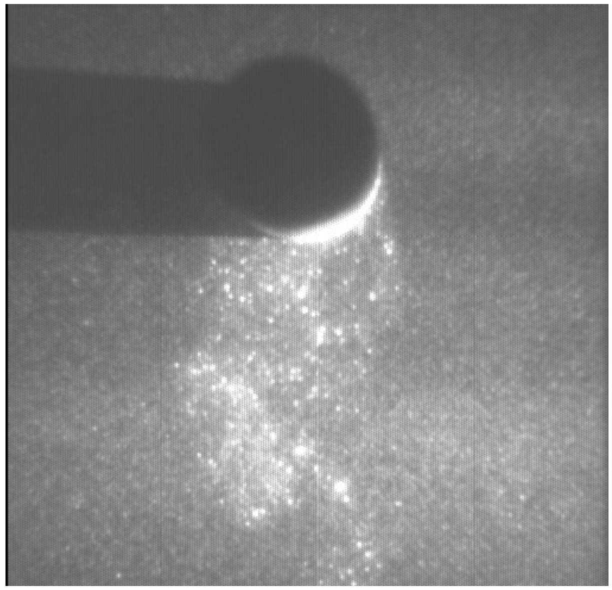

Figure 1.1. Flow over a circular cylinder.

1.1.1. Flow Separation

All solid objects travelling through a fluid (or alternatively a stationary object exposed to a moving fluid) acquire a boundary layer of fluid around them where viscous forces occur in the layer of fluid close to the solid surface. Boundary layers can be either laminar or turbulent. A reasonable assessment of whether the boundary layer will be laminar or turbulent can be made by calculating the Reynolds number of the local flow conditions. Flow separation occurs when the boundary layer travels far enough against an adverse pressure gradient that the speed of the boundary layer falls almost to zero. The fluid flow becomes detached from the surface of the object, and instead takes the forms of eddies and vortices. In aerodynamics, flow separation can often result in increased drag, particularly pressure drag which is caused by the pressure differential between the front and rear surfaces of the object as it travels through the fluid. For this reason much effort and research has gone into the design of aerodynamic and hydrodynamic surfaces which delay flow separation and keep the local flow attached for as long as possible.

1.1.2. Wake

When a fluid particle flows within the boundary layer around the circular cylinder is considered from the pressure distribution, the pressure is a maximum at the stagnation point and gradually decreases along the front half of the cylinder. The flow stays attached in this favorable pressure region as expected. However, the pressure starts to increase in the rear half of the cylinder and the particle now experiences an adverse pressure gradient. Consequently, the flow separates from the surface and creating a highly turbulent region behind the cylinder called the wake. The pressure inside the wake region remains low as the flow separates and a net pressure force (pressure drag) is produced. Figure 1.2 shows the turbulent wake, separation and laminar boundary layer regions.

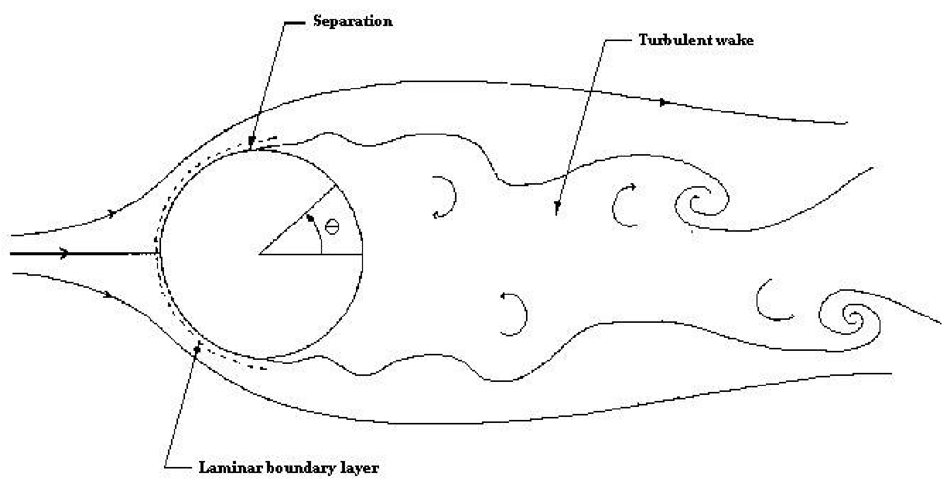

Figure 1.2. Turbulent wake flow behind cylinder.

1.1.3. Vortex Shedding

The boundary layer separates from the surface as a free shear layer and this shear layer will finally roll into a different vortex and detach from the surface. This is called “vortex shedding”. Vortex shedding is an unsteady flow that takes place in special flow velocities (according to the size and shape of the cylindrical body). In this flow, vortices are created at the back of the body and detach periodically from either side of the body. The flow past the object creates alternating low-pressure vortices on the downstream side of the object. The object will tend to move toward the low-pressure zone.

Eventually, if the frequency of vortex shedding matches the resonance frequency of the structure, the structure will begin to resonate and the structure's movement can become self-sustaining. Tall chimneys constructed of thin-walled steel tube can be sufficiently flexible that, in air flow with a speed in the critical range, vortex shedding can drive the chimney into violent oscillations that can damage or destroy the chimney.

1.2. Shallow water

Shallow flow is defined as a predominantly horizontal flow where the horizontal dimensions greatly exceed the vertical dimension. The presence of a bottom wall, parallel to a free surface, and with a relatively short distance between them, has important effects in several respects. An important characteristic of shallow flows is the vertical confinement restriction that prevents the three-dimensional stretching and breakdown (via secondary or spanwise instabilities) of the main two-dimensional structures. Another dramatic influence of the shallow flow comes from the bottom friction effect. The bottom resistance is associated with small-scale three- dimensional turbulence, which can “stabilize” the transverse shear flow. This effect will eventually attenuate and suppress the instability of the horizontal, large-scale, quasi twodimensional flow structure.

Flows in wide rivers, in estuaries and coastal waters, in shallow lakes or in the upper mixed layer of deep stratified lakes or reservoirs are important examples of hydraulic or environmental engineering concern. Yet larger scale geophysical flows in the shallow atmosphere surrounding the earth or in ocean basins in both cases with or without the influence of stratification that further enhances layer formation are also in that category.

The principles discussed about shallow water flow are equally valid for island wakes in shallow water. Wake formation and behaviour are again controlled by the ratio of inertial to frictional forces. The differences become apparent when the details of the frictional processes are addressed. The discussion of the deep ocean situation was based on the assumption that the friction experienced by the flow field originates from the island's coastal boundary. We know that frictional effects are also important in the surface and bottom boundary layers of the ocean. The assumption that the only frictional effects produced by a deep ocean island originate from its (quasi-vertical) coast implies that frictional effects from the surface and bottom boundary layers are negligible in comparison. Quantitatively this is true if these boundary layers make up a negligible fraction of the total water depth. This condition is no longer satisfied in the coastal ocean under all circumstances.

A particularly clear observation of vortex development behind an island was observed in Lake Eyre, a salt lake of southern Australia. Lake Eyre is usually a dry lake indicated by a vast expanse of encrusted salt. When it occasionally floods it reaches a depth of 1 - 2 m. Strong contrast between silt laden water and water formed over the dissolving salt crust provides for excellent flow visualisation. Lake Eyre is maintained by a large inland drainage system but is mostly a dry salt lake. The flow pattern after flooding is made visible by the contrast between water stemming from the dissolved salt crust and water containing fine silt. Figure 1.3. shows a variety of flow phenomena in 1.5 m water depth, including vortex formation behind a small sand island.

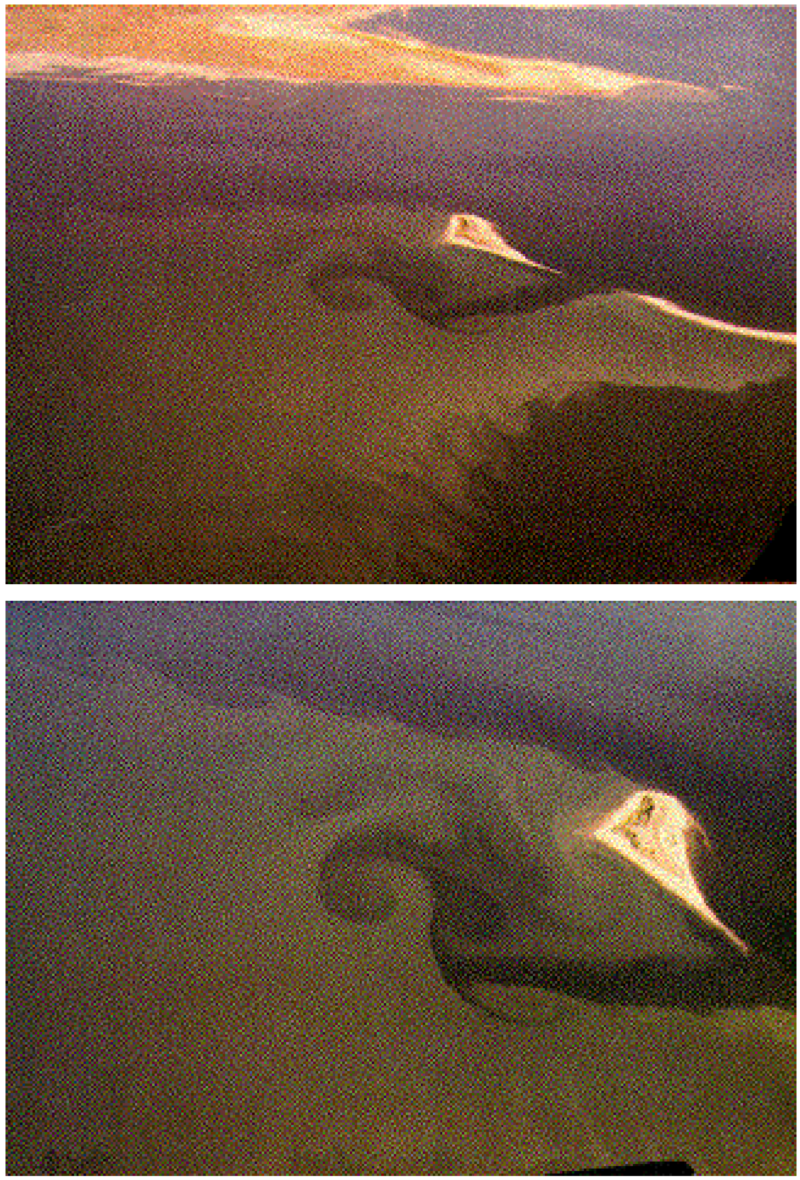

Figure 1.3. Lake Eyre, South Australia, shortly after flooding in January 1984.

1.3. Turbulent wakes generated by tandem cylinders

Flow interference is responsible for several changes in the characteristics of fluid loads when more than one body is placed in a uniform fluid stream. When more than one bluff body is placed in a uniform flow, the aerodynamic parameters and vortex-shedding patterns are completely different from the case of a single body. Because their wakes or vortex streets interference in a complex manner depending on the arrangement or spacing of the plates. The flow structure downstream of the cylinders related with the spacing between adjacent cylinders and the diameter of the cylinders, D, and the Reynolds number, Re.

The turbulent wakes generated by two and more cylinders has drawn attention in the past because of its inherent importance and practical significance in many branches of engineering. For example turbulent wakes are found; the blades of multistage turbo–machines, in the design for heat exchangers, tube bundle in heat exchangers, flow – induced vibration of tubes in heat exchangers, oil and gas pipelines, fuel and control guide rods in nuclear reactors, cooling systems for nuclear power plants, cooling tower arrays, offshore structures, marine structures, the local strong wind around a group of skyscrapers (a group of tall buildings), bridges, suspension bridges , piers and bridges pilings, chimneys, power lines, struts.

The flow pattern about a cylinder is characterized part, by the magnitude of the base pressure coefficient ($C_p=(P-P_\infty) / (1/2\rho U^2_\infty)$, which always negative (hereafter, for simplicity, only the magnitude of C_p is used when geometries). Hence, the phrase “higher C_p” refers to a more negative C_p magnitude while the phrase “lower C_p” refers to a less negative C_p magnitude.

Research into this kind of flows has been largely focused on the Strouhal map, the pressure, the mean and fluctuating lift and drag coefficient, measured in immediate vicinity of the cylinders (Bearman and Wadcock, 1973; Zdravkovich, 1977), while data in the downstream region in mostly limited to qualitative descriptions.

It is therefore important to understand the flow patterns and aerodynamic characteristics behind multiple bluff bodies in order to estimate gust – wind effects and aerodynamics forces on downstream structures or to determine the heat transfer of cross – flow heat exchangers. It is well known that the cross flow is depend on, for example Reynolds number, surface roughness, blockage and free–stream turbulence.

Among the many possible arrangements in which two circular cylinders can be positioned relatively to a cross-flow, one that has been extensively studied is the tandem arrangement, as sketched in Figure 1.4. In this configuration, the type of interference present is wake interference, where the wake of the upstream cylinder touches the downstream one (Zdravkovich, 1987). The effect of this interference is seen, for example, in the variation of the Strouhal number, St and force coefficients with the Reynolds number, Re and with the centre-to-centre distance, L. The Strouhal number is the nondimensional frequency of vortex shedding and is defined as follows: St $= f\,D/U_\infty$, where f is the dimensional frequency in Hz.

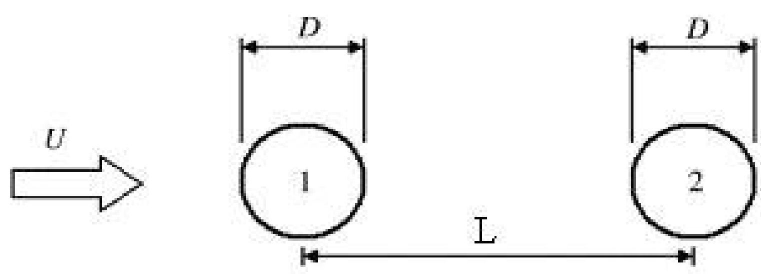

Figure 1.4. Nomenclature two tandem arrangement circular cylinders of equal diameter in steady cross-flow.

The flow around two circular cylinders identified diverse interference regimes and were based primarily on flow visualization in experiments. The classification of Igarashi (1981) deals essentially with tandem arrangements. According to this classification, six different interference regimes can be identified as seen in Figure 1.5.

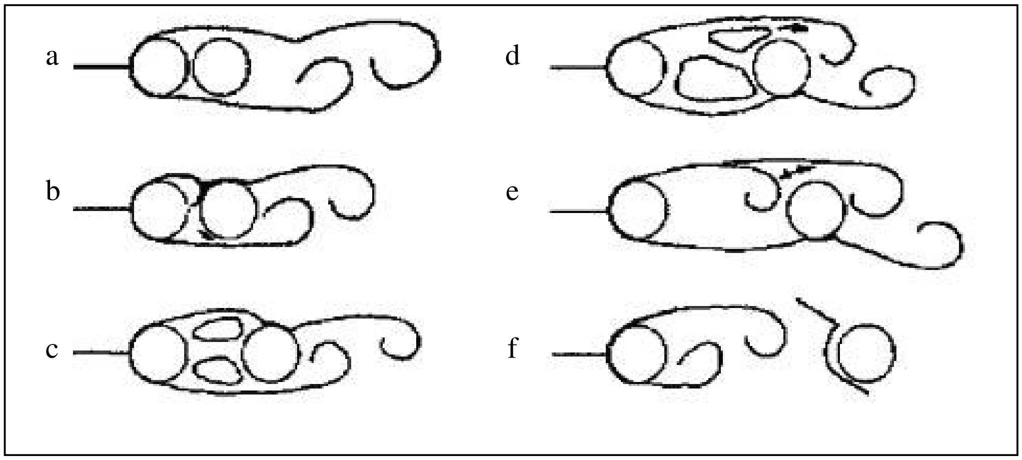

Figure 1.5. Interference regimes in the flow around pairs of circular cylinders in tandem arrangements. [Igarashi (1981)].

These regimes means;

a-) the free shear layers that originate from the separation on the surface of the upstream cylinder do not re-attach to the surface of the downstream cylinder,

b-) the shear layers that come from the upstream cylinder are captured by the downstream one, but there is no vortex formation in the gap between the bodies,

c-) symmetric vortices are formed between the cylinders,

d-) the symmetric vortices become unstable and start to grow in proximity to the downstream cylinder,

e-) the shear layers originating from the upstream cylinder roll up very near the downstream cylinder and

f-) the near wake region (formation region) ends before the downstream body and vortices are shed in the gap region in a regular way.

From regime a to regime d, the drag coefficient in the downstream cylinder is considerably lower than in the upstream cylinder. This can be understood when we note that, from a to d, the downstream cylinder is inside the near wake behind the upstream cylinder and therefore is in a low pressure region. In these cases, the drag in the second cylinder is usually negative. When the flow is in regime f, the drag in the downstream cylinder is positive. The spacing at which the downstream cylinder drag changes sign is called drag inversion spacing or critical spacing, and it depends on the Re.

Flows around two cylinders in tandem with a centre-to-centre distance L of 3D tested. These configuration is denoted respectively as t3d. The Reynolds numbers tested were 240, 270 and 300. The t3d configuration shows a decrease between Re=240 and 270, followed by a jump to a much higher value of St at the next point, Re=300. This behaviour is caused by the drag inversion that occurs for these configurations, evidenced by the vorticity contours in Figure 1.6., where one can clearly observe how the near wake of the first cylinder is influenced by the presence of the second one. For Re=270, where a bistable regime takes place when compared with the results for Re=240 and 300.

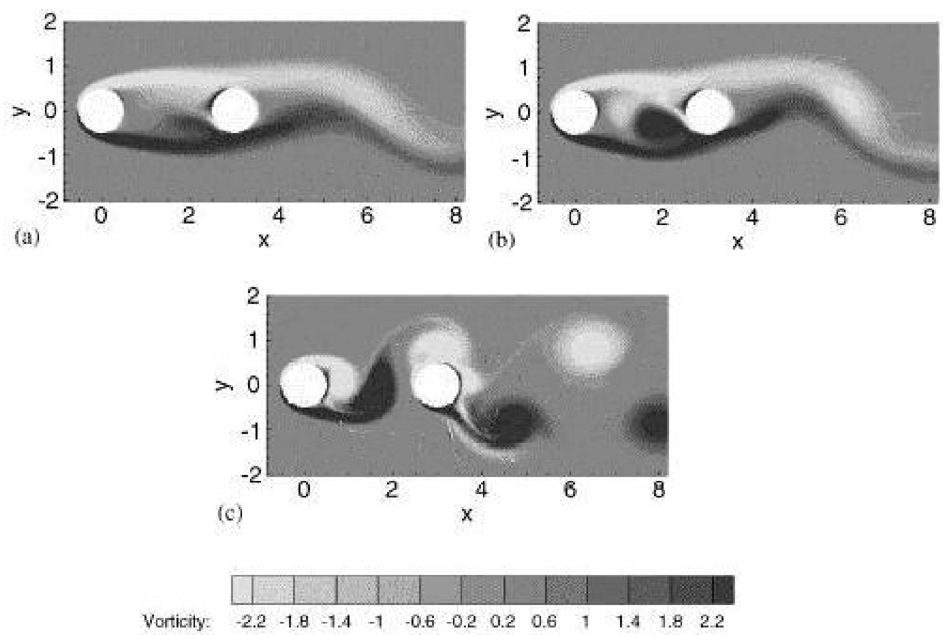

Figure 1.6. Vorticity contours centre-to-centre distance 3D (t3d case), two-dimensional simulations: (a) Re=240; (b) Re=270; and (c) Re=300. Vorticity has been nondimensionalized by the cylinder radius. [Carmo and Meneghini (2005)].

Two different regimes t1.5d and t3d were dealing, as one can observe in Figure 1.7. The simulations with L=1.5D , where symmetric vortices appeared in the region between the cylinders and the simulation L=3.5D. We believe that, for L=3.5D the downstream cylinder is positioned in a way that more circulation remains retained between the bodies, the shear layer that is originated in the second cylinder has less circulation. In this regime, there was no true formation region behind the downstream cylinder, and vortices were shed directly from its surface. It appears, therefore, that it is not the dynamics in the near wake that determines the shedding frequency of the downstream body, but rather the incident oscillatory flow; the alternate vortices that hit the body force the shedding in the downstream cylinder to occur at the same frequency.

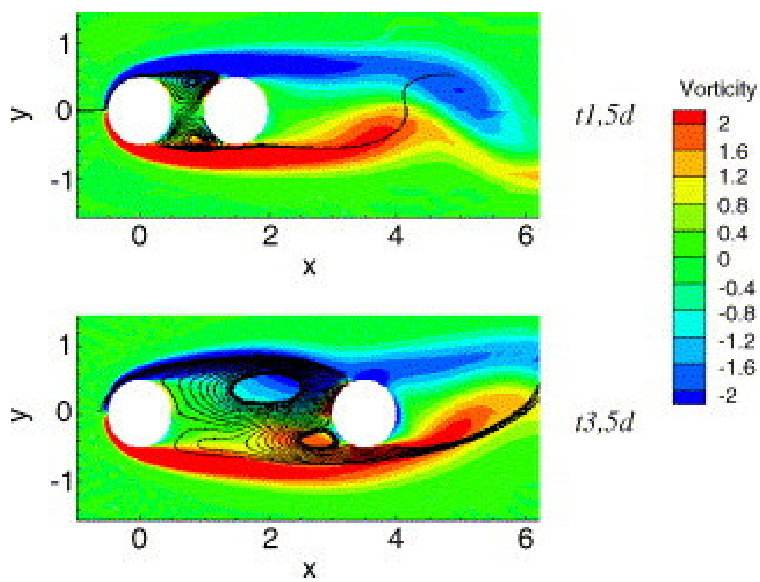

Figure 1.7. Vorticity contours and instantaneous emission lines, Re=200, two-dimensional simulations. [Carmo and Meneghini (2005)].

A critical spacing is found in the range of 3.5<L/D<4. When L/D⩽3.5, vortex shedding does not take place between the two cylinders, and when L/D⩾4, each cylinder produces a vortex wake. Figure 1.8. shows the wake configuration with instantaneous streamlines. All the above results are consistent with the phenomena obtained by Meneghini et al. (2001).

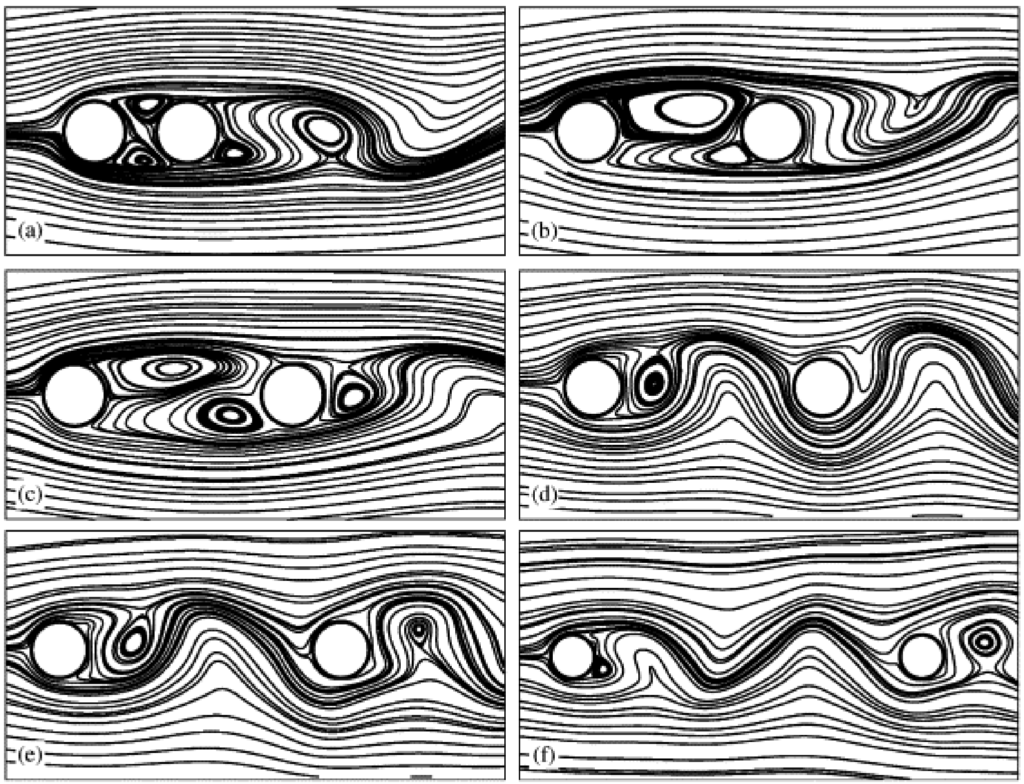

Figure 1.8. Streamlines of flow around two tandem cylinders in 2-D simulations. L/D= (a) 1.5, (b) 3, (c) 3.5, (d) 4, (e) 5, (f) 8.

2. PREVIOUS STUDIES

2.1. Shallow Water

Many of which studies have been conducted in wind tunnels and water channels where the flow is considered deep and the aspect ratio is high. However, many turbulent shear flows exist in shallow environments.

Wolanski et al. (1984) investigated wakes flow behind Rattray Island in shallow coastal waters. The island is located in northeast Australia. Their results showed that the length of the wake in the lee of the island, as documented by aerial photographs and satellite imagine, appeared to equal that of wake behind a flat in two-dimensional flow at Reynolds number of 10.

Ingram and Chu (1987) studied shear flows on the effect of bottom (bed) friction around an island. They observed two basic pattern of wake flow around the island. A vortex street wake was formed when transverse shear was large, as in flow around the small islands. On the other hand, for small transverse shear, as in flows around large islands, the shear layers were stabilized by bottom friction and, in that case, a clear water wake of low turbulence and low sediment concentration was observed.

Chu et al. (1991) theoretically studied the stability of shear flows in shallow open channels and defined a dimensionless stability number S also known as shallow wake parameter to account for the stabilizing effect of the bed friction and destabilizing effect of the transverse shear. The S parameter for the bluff body is $S = C_f D/h$ (denoted as ”S_c”). It is based on the ratio of the small-scale kinetic energy loss to the production of large-scale turbulence kinetic energy. Here, D is the diameter of cylinder, and h is the water depth and C_f is the friction coefficient.

Schar and Smith (1993) studied the global normal mode of instability for an inviscid flow as it passes an isolated topography. Their studies consisted of two parts. In the first part of their study, steady numerical solutions for flow past circular topography were obtained by imposing symmetrical conditions that essentially suppressed vortex shedding. In the second part, this symmetrical condition was relaxed in order to study the transition into vortex shedding regime. They used finite difference numerical simulations to derive the most unstable global normal mode leading to the break-up of the study wake into an oscillating Karman vortex street. The frequency of eddy shedding in their numerical simulations agreed well with that from observations of eddies behind mountainous islands.

Grubisic et al. (1995) carried out a local absolute stability analysis for a piecewise-linear velocity profile, which missed the two inflection points. The reserve flow velocity was determined by magnitude of bottom friction, which also defined the velocity profile. A surface number r was defined as the product of the drag coefficient and the ratio of horizontal length scale and the height of fluid layer. (This definition is analogous to the wake stability parameter S given above but differs by a factor of due to the choice of the drag coefficient.) A critical value of r =1 was obtained from their stability analysis.

Chen and Jirka (1995) performed experimental studies on the shallow two-dimensional turbulent wake flows on the large-scale water table. The "shallow wake" was generated by vertical cylindrical bodies extending over the water depth. The ambient flow was characterized by two main features: one was the existence of a free surface and bottom by which the shallow water layer was bounded and the other was a fully developed turbulent layer. Here, the transverse body dimension D greatly exceeds the water depth h_w ($D/h_w > 1$). The wake Reynolds number $Re_D = U_\infty D/\nu$ was greater than 10000, while the ambient flow Reynolds number that governs the shear flow in the transverse dimension $Re_h = U_\infty h_w/\nu$ was always larger than 1500. U_∞ is the depth-averaged ambient velocity and ν is the kinematic viscosity. Re_h is thus well above the transition value of about 500. Different types of bodies were investigated, including cylinders, flat plates and porous plates oriented transversely to the ambient flow. The flow patterns fell into three categories: First type of stability (vortex Street- VS) showed a formation, which resembled a von Karman vortex street, although here the cylinder Reynolds number Re_d was substantially larger than that of in the unbounded case. It was characterized by the alternate separation of large vertical structures directly from the cylinder shoulders, which were then advected downstream and decayed due to the continuous influence of bottom shear. If, compared to the ambient flow conditions in the VS case, the stabilizing effect of bottom friction increases or the destabilizing transverse shear is reduced, the convectively unstable VS wake flow undergoes transition: an absolutely unstable recirculating region (unsteady bubble-UB) develops behind the obstacle, alternately large eddies shed from the downstream edge of the bubble and advect downstream until disintegrate and the flow stabilizes. If the forcing due to transverse shear is even weaker, then generation of large-scale vortices at the end of recirculation zone is completely suppressed ("steady bubble"-SB).

Chen and Jirka (1997) investigated the effect of bottom friction on absolute/convective and local/global stability characteristic of shallow wake flows by means of a linear stability analysis, and interpreted and compared it with the results of their previous experiments (1995). They also proposed critical values of S (denoted as S_c) to signify the onset of particular flow patterns.

Lloyd and Stansby (1997) made extensive experimental and numerical investigations in shallow wakes behind conical model islands with gentle slopes. Four islands were used with side shapes ranging from 8.0 to 33.1 degrees. For small values of the wake stability parameter, for example S< 0.2, the island wakes were characterized well-organized vortex shedding systems. The island side slope had a small effect on the wakes produced. With slope angles varying from 8.0 to 33.1 degrees, the basic mechanism generating the wake was found to be the same.

In shallow flows, bed friction effects became very important and were quantified in terms of a friction length scale, which is usually defined as the ratio of depth of flow (h_w) to the skin friction coefficient (C_f). Balachandar et al. (1997) have defined a bed friction parameter ($S=C_fX/h$) as Chu et al (1991) to describe the influence of bed friction in shallow flows. Here, X is a horizontal length scale. It is clear that, the bed friction effects are expected to be minimized in deep flows.

Balachandar et al. (1999) developed a theoretical model to predict the spread of wake in shallow flows. They investigated the effects of flow depth and plate width on the spread of the wake. Some useful remarks on the wake stability parameter ($S_c=C_fD/h$) were presented therein. The range of velocities and the depths

(10 mm $\leq$ h $\leq$ 80 mm) of flow considered in Balachandar et al. (1999) and Lloyd and Stansby (1997) studies are similar. However, the size of the wake generators used by Lloyd and Stansby (1997) are about 8 to 30 times larger than that used by Balachandar et al (1999). From careful visual observations and concentration measurements, it was found by Balachandar et al. (1999) that for $S_c \leq 0.008$ distinct and continuous Karman vortices were noted. For $S_c \approx$ 0.009-0.018, weak and intermittent Karman vortices were observed, while the Karman vortex street was completely annihilated when $S_c \geq 0.021$. In fact, for a given velocity and cylinder of plate width, no significant difference between the nature of the Karman vortex street and the development (or spread) of the wake was observed for h $\geq$ 30 mm. Based on these observations, shallow wakes were reclassified into shallow-wakes and deep-shallow wakes. Given the significant difference in the reported values of the critical wake stability parameter, an alternate measure using the wake velocity data may be more appropriate. In the study reported by Balachandar et al. (1999), only an intermittent Karman vortex street was observed at a flow depth of 20 mm in the wakes generated by a 20 mm and a 40 mm wide flat plate.

Balachandar et al. (2000) investigated characteristics of shallow turbulence near wakes at low Reynolds numbers. Reynolds number based on the test body width was maintained nearly constant (Re $\approx$ 4.000). Velocity and the concentration in the near region of shallow turbulent wakes were measured using a LDA and video-imaging techniques. A 40 mm wide flat plate placed normal to the flow was used as a wake generator. It was concluded that the wake stability parameter pointed out earlier was not quite approximate to characterize the relative effects of transverse and bed friction. In their study, a new definition as a transverse parameter was proposed to characterize wake stability. It was reported that the wake velocity defect data collapsed fairly onto a single curve and were independent of the measurement location and depth of the flow. The wake half-width data based on the concentration profiles show a higher spread compared with the velocity data.

Tachie and Balachandar (2001) investigated behaviour of the shallow turbulent wakes generated on smooth and rough surfaces. They used a flat plate as the wake generator placed normal to the flow. The wakes were generated on two types of surfaces: i) a hydraulically smooth surface (brass channel bottom) and ii) a rough surface created using wire mesh. The mesh was made of a 0.6 mm diameter wire with 7.0 mm centerline spacing. The wire was 1.8 m long and 0.45 m wide and fixed to the channel bottom by means of a double-sided tape. They measured mean and turbulence intensity to understand shallow wakes generated on smooth and rough surfaces. Using the local minimum and maximum velocity at any axial location to define velocity scale, the velocity profiles across the wake generated on smooth and rough surfaces collapsed onto a single curve. Their study indicates that for $x/d \leq 5.0$ (d is the plate width), the width of the wake increases from the wake generator with increasing axial distance, attains a maximum value at about x/d=2.0 and decreases to a minimum value at x/d=5.0. It was found that at similar Re_d the spread rate of the wake on rough surface was significantly lower than observed for a smooth surface due to a stronger bed friction effect.

Balachandar and Tachie (2001) investigated the interaction between the boundary layer on a horizontal floor of a shallow open channel flow and the wake of a thin flat plate mounted vertically on the floor of a channel. They used LDA technique to measure the velocity of the flow. Measurements were obtained upstream and downstream of a smooth flat plate wake generator. They used plates are two having different aspect ratios. Their results showed that the profiles in the near wake region were quite distorted and the recovery of the boundary layer to the upstream condition was slow. They stated that the inner region appeared to develop more quickly than the outer region of the boundary layer. When compared with the approaching flow, the stream wise turbulence intensity values increased in the near wake region followed by a gradual but slow decrease with increasing axial distance.

Akıllı and Rockwell (2002) investigated the near wake of a vertical, circular cylinder in shallow water using a combination of a visualization marker and particle image velocimetry technique. They located laser sheets parallel to the bed of the water channel at different heights to investigate the flow characteristics at the bed and at the various locations above it. At the bed, the time averaged streamline topology downstream of the base of the cylinder took on a form known as an owl face of the first kind, which was originally defined for a completely different exterior flow. Immediately adjacent to the base of the cylinder, an additional system of saddle points was located at either end of a nodal line. At locations above the bed, one of the two principle saddle points of the owl face of the first kind disappeared and the principle foci were transformed from a stable to an unstable state.

Kahraman et al. (2002) investigated vortex formation of a vertical cylinder in shallow water and the control technique of these vortices. In order to control vortex formation behind a cylinder, a narrow transverse strip of roughness elements having different heights was placed behind the cylinder on the bottom surface channel. They employed a technique of high-image-density particle image velocimetry (PIV) to obtain global, instantaneous representations of the flow patterns, which lead to phase- and time-averaged patterns of streamline topology, velocity, vorticity and Reynolds stress on planes above the bed.

Fu and Rockwell (2005) studied on flow control of near wake past a cylinder at shallow flow. Their experiments were performed in a large-scale free-surface water channel. A long plate (width of 610 mm, length of 3660 mm) with an elliptical leading edge was employed to generate a shallow free-surface layer of desired thickness and inflow velocity. It was at an elevation of 254 mm above the floor of the main test section. And an adjustable inclined plate allowed fine tuning of the volume flow along the upper and lower surface of the plate, and thereby the location of the stagnation point at the elliptical leading edges. And a transparent Plexiglas cylinder was used. The cylinder of diameter D= 101.6 mm was located a distance of 3048 mm from the leading edge of the plate. Their experiments examined the effect of passive base bleed through a slot of width G. They used the high-image density particle image velocimetry technique to characterize the instantaneous and averaged flow structures in the approach and near-wake regions of the cylinder.

2.2. Turbulent wakes generated by tandem arrangement cylinders

Zdravkovich (1968) conducted a smoke visualization of laminar wake behind the three cylinders in various triangular configurations. He observed that multiple

Karman vortex streets could co-exist. However, the vortices decayed very quickly and an entirely new single vortex street was formed.

Bearman and Wadcock (1973) are the first scientists to study quasi-stable behavior and flopping for a two-cylinder array as a function of cylinder spacing. Their specific goal was to locate the critical spacing where the wakes downstream of the two cylinders stopped behaving as individual cylinder wakes and combined to form a single wake.

Le Gal et al. (1990) performed studies using two cylinder having gaps between $1 \leq L/D \leq 7.5$ and Re=110 and found wake interaction at ratio as high as 5.5. Probably because of their low Reynolds number value, they stated that flopping was really difficult to observe. However, they did observe quasi-stable behavior and perform a flow visualization study, which was in agreement with the large-wake, small-wake model of Williamson (1985).

Mahir and Rockwell (1996) investigated the wakes between and downstream of a tandem arrangement of two cylinders. Experiments were carried out in a free-surface, closed-loop water channel. The freestream velocity in the channel was U =30 mm/s, giving a Reynolds number Re=160, based on the cylinder diameter D= 4.7 mm. The test-section of the water channel was constructed entirely of Plexiglas. The submerged length, L=508 mm, gave a length to diameter ratio of L/D=108.

Mittal et al. (1997) studied on a stabilized finite element formulation is employed to study incompressible flows past a pair of cylinders at Reynolds numbers 100 and 1000 in tandem and staggered arrangements. Computations are carried out for three sets of cylinder arrangements. In the first two cases the cylinders are arranged in tandem and the distance between their centres (L) is 2.5 and 5.5 diameters. It is observed that the qualitative nature of the flow depends strongly on the arrangement of cylinders and the Reynolds number. In all cases, when the flow becomes unsteady, the downstream cylinder, which lies in the wake of the upstream one, experiences very large unsteady forces that may lead to wake-induced flutter.

Sumner et al. (1999) observed the impulsively started flow field for circular cylinders of equal diameter arranged in tandem was investigated using flow visualization and particle image velocimetry (PIV), over a longitudinal pitch ratio range of L/D=1.0-3.0, and for Reynolds numbers from Re=1200-3800. Measurements of vortex strength and vortex position relative to the cylinders were obtained from these data. Three types of fluid behaviour were identifed based on L/D: single bluff-body behaviour when the cylinders are in contact, constrained streamwise growth and lateral expansion of the gap recirculation zones at small and intermediate L/D, and independent formation of recirculation zones similar to a single impulsively started circular cylinder at larger L/D.

Laneville and Brika (1999) observed the effect of the fluid and mechanical coupling between two flexible circular cylinders on their vortex-induced oscillations is examined in a wind tunnel. The cylinders are in a tandem arrangement and a mechanical coupling allows vibrations in phase and out of phase. The separation between the cylinders ranges between 7 and 25 diameters. When the cylinders are coupled only by fluid, the upstream cylinder behaves as an isolated one, while the downstream cylinder response depends on the separation and presents a hysteresis and three discontinuities. The hysteresis and its discontinuities agree with those of the upstream cylinder and the third discontinuity coincides with the end of synchronization of the windward cylinder.

Zhou et al. (2000) measured the velocity and temperature fluctuations at Re=1800 in the two- and three-cylinder case. They observed that the cross-stream distributions of the Reynolds stresses and heat flux varied significantly, which were ascribed to different flow patterns, as L/D reduced from 3.0 to 1.5.

Sumner et al. (2000) measured the flow patterns of two cylinders in a staggered arrangement. They observed nine flow patterns and found that vortex shedding frequencies were more properly associated with individual shear layers rather than with cylinders.

Patnaik et al. (2000) simulated numerically flow past an isolated circular cylinder and two cylinders in tandem arrangement, under the influence of buoyancy aiding and opposing the flow. A modified velocity correction method was employed, which had second order accuracy in both space and time. The influence of buoyancy on the temporal fluid flow patterns was investigated, with respect to streamlines, isotherms and streaklines. Comparisons were made with respect to mean center linevelocities, drag coefficients, Strouhal number and streakline patterns. Some conclusions of the study can be outlined as; for an isolated circular cylinder, buoyancy opposed convection could trigger the twin vortices naturally formed in the wake region into a "Karman vortex street" over an Re range of 20 to 40 and zones of vortex shedding and twin eddies were demarcated for flow past a circular cylinder and two cylinders in tandem. Branches of steady state and periodic solutions met along this boundary, dividing the two zones.

Itoh and Himeno (2001) computed three-dimensional fluid flow around two circular cylinders in tandem arrangement with the finite difference method without a turbulence model. Two kinds of grid systems was employed to catch the flow interference between the two tandem cylinders. This study confirmed that the variation in wake structures, the Strouhal number and the time-averaged drag coefficient can be numerically predicted according to the distance between the centers of the circular cylinders. The possibility of numerical prediction for the flow interference among several objects was shown in this study.

Meneghini et al. (2001) investigated the shedding of vortices and flow interference between two circular cylinders in tandem and side-by-side arrangements are numerically. A Fractional Step Method is used for the simulations and the flow is assumed two-dimensional. The calculations are carried out on a three-noded unstructured mesh. The simulations are performed for a Reynolds number range varying from 100 to 200, and the flow is solved through the finite-element method.

Mittal and Kumar (2001) studied on a stabilized finite element formulation is employed to study flow-induced oscillations of a pair of equal-sized cylinders in tandem and staggered arrangement placed in uniform incompressible flow. Computations, restricted to 2-D, are carried out for Reynolds numbers 100 for various values of the structural frequency of the oscillator. The cylinders are separated by 5.5 times the cylinder diameter in the streamwise direction. For the staggered arrangement, the cross-flow spacing between the two cylinders is 0.7 times the cylinder diameter. In this arrangement, the downstream cylinder lies in the wake of the upstream one and therefore experiences an unsteady in-flow. Since the spacing between the two cylinders is beyond the critical value for proximity interference, it is expected that the upstream cylinder behaves like an isolated single cylinder, while the downstream one experiences wake-induced cutter. The Re 100 flow leads to a very organized wake and large amplitude motion is observed for the downstream cylinder. The trajectory of the upstream cylinder resembles a "gure-of-eight. The downstream cylinder shows a similar behaviour for the tandem arrangement. However, for the staggered arrangement, the trajectory of the rear cylinder resembles a tilted oval. Soft lock-in is observed in almost all the cases.

Alam et al. (2002) examined the suppression of fluid forces acting on two square prisms in a tandem arrangement in which a flow approaching the upstream prism was controlled by a thin flat plate, with variation in spacing between the plate and the upstream prism. The upstream prism was found to be insensitive to the existence of the downstream prism when the latter was located downstream, approximately six or more times the prism width.

Sakamoto et al. (2002) investigated experimentally Aerodynamic characteristics of two circular cylinders in a tandem arrangement in a uniform flow at a Reynolds number of 6.5×10^4. When the spacing between the cylinders was changed, mutual interference between the two cylinders at close proximity caused significant change in parameters of the aerodynamic characteristics, such as fluctuating lift and drag forces, time-averaged and fluctuating pressure distributions, Strouhal number, and vortex-shedding patterns.

Lin et al. (2002) examined a technique of high-image-density particle image velocimetry is employed to characterize the instantaneous and averaged patterns of velocity, vorticity and Reynolds stress due to flowpast two cylinders in tandem. These features of the flow patterns are characterized in the gap region as a function of the distance between the cylinders. In turn, they are related to the patterns in the near-wake of the two-cylinder system. Along the gap between the cylinders, small-scale concentrations of vorticity are formed in the separated shear layers. Within the gap, the instantaneous structure of the recirculation zones can exhibit both symmetrical and asymmetrical patterns.

Wolfe and Ziada (2003) experimentally investigated the effect of feedback control on vortex shedding from two tandem cylinders in cross-flow. The objective is to reduce the downstream cylinder response to vortex sheddingand turbulence excitations. Feedback control is applied to a resonant case, where the frequency of vortex shedding coincides with the resonance frequency of the downstream cylinder, and to a nonresonant case, in which the shedding frequency is about 30% higher than the downstream cylinder resonance frequency.

Lama and Chana (2003) investigated the flow around four cylinders in a square configuration with a spacing ratio of 4 and at a Reynolds number of 200, using laser-induced fluorescence (LIF) visualization and particle image velocimetry (PIV) for angles of incidence ranging from 0^o to 45^o at a 5^o interval. Several distinct flow patterns were observed. Dependent on the flow was classified into three basic flow regimes. Each regime has its own dominant flow pattern and could lead to different problems. Two distinct flow patterns, which could lead to strong flow-induced vibration, were observed in this experiment. One is the impingement of oncoming vortices on the cylinders directly. The other is the formation of a jet flow between the near wake of the upstream cylinder and downstream cylinder.

Fitzpatrick (2003) has investigated the noise generated by two tandem cylinders in a cross-flow. Measurements of turbulence and of fluctuating pressure have been obtained between the two cylinders for different flow velocities and incident levels of turbulence. Although, for a number of cases, up to four peaks related to vortex shedding were evident in the spectrum, most measurements exhibited two peaks, a dominant one at the vortexshedding frequency, with a secondary peak at twice this value. The measurements show that vortex generated noise is strongest at the mid-point between the cylinders and at the rear cylinder with levels of 130 dB.

Surmas et al. (2003) studied on a two-dimensional numerical simulation of fluid flow around a couple of identical circular cylinders aligned, respectively, along and orthogonal to the main-flow direction, at several distances. A lattice Boltzmann (LB) method is used. The forces resulting from fluid–solid interaction are calculated by considering the momentum exchanged between the fluid and the solid surfaces. Bluff body wake interference and its effect on drag and lift forces is studied in detail. The drag and the lift coefficients are obtained and compared with other existing results. A transition regime is obtained when the cylinders are aligned orthogonal to the main-flow direction and separated by distances smaller than about 2D.

Jester and Kallinderis (2003) performed a comprehensive numerical investigation of incompressible flow about fixed cylinder pairs. Cylinder arrangements include tandem, side-by-side, and staggered and Reynolds numbers of 80 and 1000 are considered. Qualitative and quantitative comparisons with published experimental data are made which show the ability of the present numerical method to capture complex, unsteady flow features. Experimentally observed flow physics such as hysteresis effects in tandem arrangements and bistable biased gap flow in tandem arrangements have been reproduced by the present numerical method.

Hall et al. (2003) rigidly mounted a single cylinder and two tandem cylinder configurations with longitudinal pitch ratios L/D=1.75 and 2.5 in an open circuit wind tunnel. They imposed a standing acoustic pressure wave. They investigated the effect of sound on the vortex-shedding for various amplitudes, by means of pressure taps on the cylinders and wake hot-wire probes. These tests showed that applied sound can entrain and shift the natural vortex-shedding frequency to the frequency of excitation and produce nonlinearities in the wake.

Alam et al. (2003) investigated the effects of tripping rods on flow characteristics and fluid forces acting on a single cylinder and on two cylinders in side-by-side and tandem arrangements in a smooth cross stream at a Reynolds number of $5.5x10^4$. In the case of tandem cylinders with tripping rods, fluid forces acting on the upstream cylinder were almost independent on the downstream cylinder at any spacing of the cylinders. The critical spacing at which a bistable flow appears was found at spacing ratios of 3.0 and 2.6 for the plain cylinders and the cylinders with tripping rods, respectively.

Xu and Zhou (2004) measured the dominant vortex frequencies fs in the wake of two tandem circular cylinders of identical diameter D simultaneously using two hot wires placed behind each cylinder. The present measurements reconfirm the previous observation of a bi-stable flow at the transition from the reattachment to co-shedding regime.

Obi and Tokai (2005) experimentally investigated the flow around a pair of bluff bodies set in tandem in uniform flow. The three-level decomposition of the velocity data obtained by PIV had revealed that the strong turbulence intensity found between the bodies was caused by the oscillatory motion due to vortex shedding. The effect of vortex motion was recognized as a strong correlation between velocity and pressure gradient.

Deng et al. (2006) numerically studied the spatial evolutions of vortices and transition to three dimensionality in the wake of two tandem circular cylinders. The virtual body method developed from virtual boundary method was applied to model the no-slip boundary condition of the cylinders. The three-dimensional results were compared with the two-dimensional flow.

Alama et al. (2006) examined the effect of a T-shaped plate on reduction in fluid forces on two tandem circular cylinders in a uniform cross-flow at a Reynolds number of 6.5×10^4. From the result, it was found that, when the T-shaped plate with a trail length of 0.70–1.00 times the cylinder diameter is used, an optimum reduction in fluid forces occurs, and the interference effect of the downstream cylinder on the upstream cylinder is completely suppressed.

3. MATERIAL AND METHOD

3.1. Experimental Arrangement

3.1.1.Water Channel System

Experiments were performed in a large-scale water channel located in the Fluid Mechanics Laboratory at Çukurova University. The water channel as seen in Figure 3.1., test section which has the following dimensions: a length of 8000 mm, width of 1000 mm, and a depth of 750 mm was constructed of transparent Plexiglas with upstream and downstream fiberglass reservoirs. It also has honeycomb screen arrangement, which is located at the entrance of contraction. These reservoirs and honeycomb screen arrangements are used to maintain the turbulence intensity below 0.1 %. During all experiment, the water level was (h_w) maintained at the depths of 25 mm and the water flow speed was controlled by an axial flow pump. Pump rotation speed was controlled by an ABB controller unit.

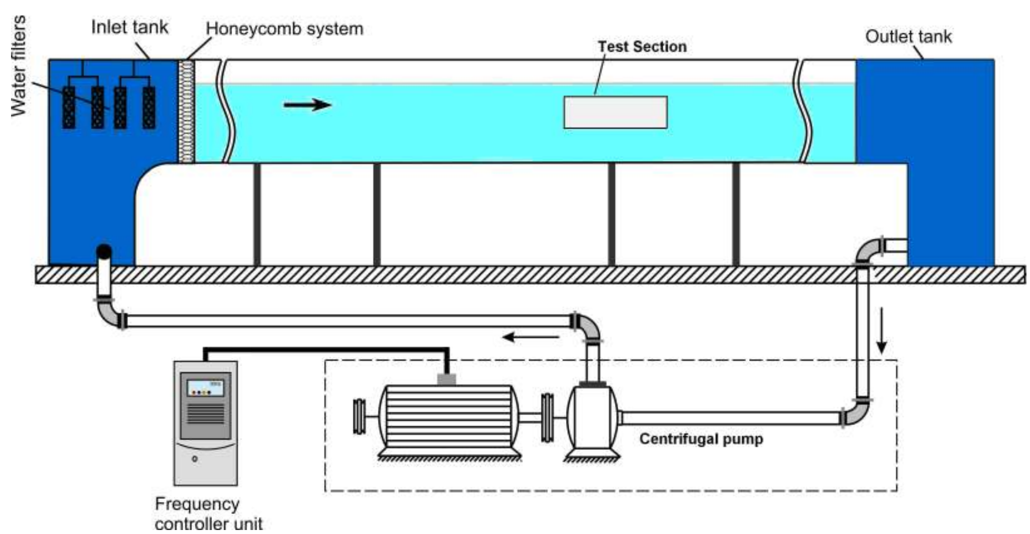

Figure 3.1. Schematic over view of water channel flow.

3.1.2. Experimental Model

The water level was (h_w) maintained at the depth of 25mm. Experiments were carried out at a free-stream velocity yielding Reynolds number based on the cylinder diameter of Re_D = 5000.

The cylinders used during the experiments were made of plexiglas material and their diameter was D=50 mm. During the experimental study, the effect of the distance (G) between cylinders was investigated. In order to understand the effect of the distance between cylinders, four types of experiments were performed. The cylinders were placed onto a platform that gives the water height in the flow. For each experiment the distance (G) between the cylinders were changed in the interval of 0 mm and 225 mm. Totally 114 experiments were carried out variable distances with three sets. Each set includes 350 instantaneous images.

By using the PIV tecnique, instantaneous velocity vectors can be measured in a region illuminated by a two-dimensional laser sheet. Velocity vector measurements have been carried out using dantec PIV system. The flow field illumination was provided by two Nd: Yag pulsed laser sources of a wavelength of 532 nm, each with a maximum energy output of 120 mJ. Dantec Flow Map Processor, that controlled the timing of the data acquisition, was used to synchronize the image taking and laser unit. The thickness of the laser sheet illuminating the flow field was approximately 1 mm. The water was seeded with the neutrally buoyant spherical particles of 12μm in diameter. The movement of the particles was recorded by using a CCD camera with a resolution of 1024x 1024 pixels. The camera was equipped with a 60 mm focal-length lens. Dantec flow grabber digital PIV software employing frame- to- frame

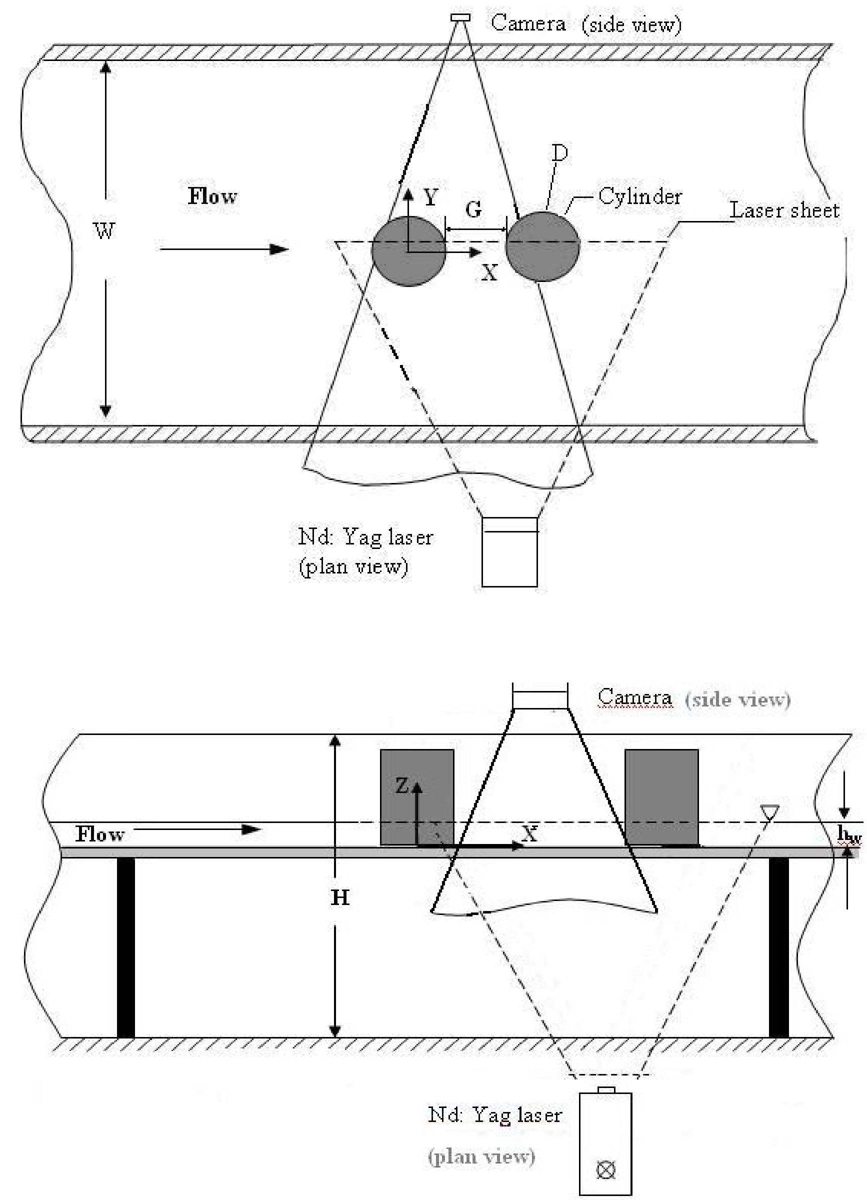

Figure 3.2. Overview of tandem arrengement cylinders in shallow water.

cross-correlation technique was employed to calculate the raw displacement vector field from the particle image velocity data. In the image processing, 32x32 pixels rectangular effective interrogation windows were used. During the interrogation process, an overlap of 50% was employed in order to satisfy Nyquist criterion. In the post-processing step, interpolation between surrounding vectors was used in order to remove erroneous vectors. Displacement of vector field could be measured and by using this, velocity vectors of the flow could be calculated. The vorticity patterns of the wake flow can be calculated from the velocity field using a finite difference scheme. Streamlines and circulation can be obtained by post processing of the velocity data. The overall field of view was 80x25 mm^2 .Patterns of instantaneous particle images (total of 350 images for a continues series) were taken at a rate of 15 Hz, thereby spanning 13.4 s. Averaged patterns of the flow structure were calculated from these total number of instantaneous images. The time delay between pulses ranged from 1.5 to 2ms. A software developed in-house were then used to compete the velocity vector field, streamline topology and vorticity patterns. In terms of uncertainty of velocity measurement using the PIV technique, the digital PIV approach carried out during the experiments in similar to that employed by Westerweel (1993) who concluded that an uncertainly in velocity is less than 2%. A schematic of experimental set up is shown in Figure 3.2.

3.2. Measurement Techniques

3.2.1. Particle Image Velocimetry (PIV)

Particle image velocimetry (PIV) allows continuous measurement of instantaneous velocity vector fields over the area of interest. The PIV method has been proved to be a powerful tool for investigations of unsteady separated flows.

To measure the velocity in the flow of interest over a plane by DPIV, the flow region is illuminated with two short duration laser pulses and the fluid motion is made visible by adding tracer particles that diameter measured in microns. The particle images were recorded on the CCD array and captured directly on the computer through the frame grabber card. Each pair of single-exposed frames was then interrogated using a spatial cross-correlation technique to obtain an instantaneous velocity field, which, in turn, can be used to calculate instantaneous patterns of vorticity and corresponding streamline topology through numerical differentiation or integration.

PIV technology have some advantage and disadvantage then other velocimetry technique. These are respectively;

Advantages: Thousands of measurements per image, measurements are simultaneous, few fundamental limitations**,** non-intrusive.

Disadvantages: Very expensive, poor temporal resolution, elaborate set-up.

3.2.2. Principles of PIV

The basic relation of displacement divided by time to yield velocity is the fundamental principle of the PIV technique. Although PIV is a nonintrusive measurement technique, it requires tracer particles to be suspended in the flow under investigation. These tracer particles can be either naturally occurring or artificially added to the flow. Hence, PIV directly estimates the displacement information of these tracer.

The PIV apparatus consists of an illumination source, an image capture device, synchronization and data acquisition hardware, and software for user control and data analysis. This technology behind the PIV technique can be seen from Figure 3.3. Illumination of the tracer particles is done using a thin light sheet, which is pulsed to freeze the particle motion. The Mie scattering from the imaged tracer particles is recorded at two instances in time using a digital camera. The two sequential digital images are then sub-sampled at particular areas via a prescribed interrogation window, and a spatial cross-correlation is performed using fast Fourier transform (FFT) analysis, resulting in a surface function.

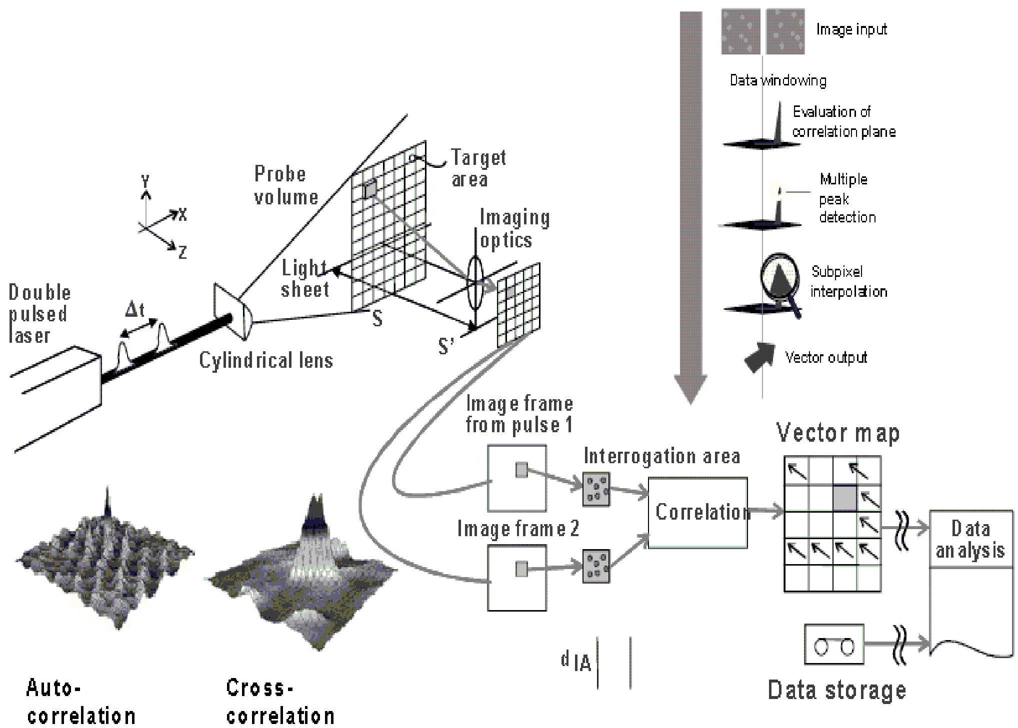

Figure 3.3. The PIV measurement principle.

3.2.3. Image Acquisition

Figure 3.4. shows a typical experimental arrangement for carrying out PIV measurements. Tracer particles added to the flow under investigation are illuminated by a laser sheet and images of the illuminated flow field are captured and stored for later analysis.

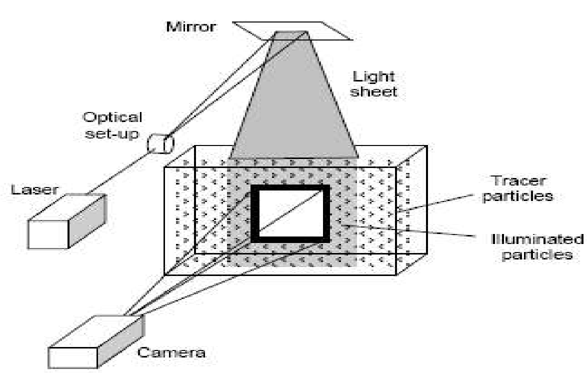

Figure 3.4. A typical PIV experimental set-up.

3.2.3.1. Seeding

The application of optical flow measurement techniques to gas and liquid flows usually requires artificial seeding of the flow. The seeding particles must faithfully follow the fluid flow. In the case of turbulent or high speed gas flows, seeding particle diameters of about 1 mm or smaller are necessary. As the contrast of the captured images is directly proportional to the scattered light power, the tracer particles must have strong scattering characteristics. In addition, the seeding material should not introduce any 2-phase effects into the flow.

3.2.3.2. Illumination

For the illumination, it is preferable to use a laser, since the laser beam is easy to form into a sheet by a cylindrical lens. A pulsed laser is to prefer, since one obtains a high light energy during a very short time interval (typically 5 ns for a YAG-laser), which means that the particle images will be practically frozen even for high velocities (> 100 m/s). The repetition rate of a YAG-laser is typically 10-30 Hz, which is too low except for very low velocities (< 1 cm/s). One therefore needs two lasers to get full freedom in terms of time separation between the pulses.

3.2.3.3. Image Capturing

Capturing images can be done photographically or digitally. With recent improvements in spatial resolution and the attraction of immediate image availability, the digital approach is becoming more and more favoured over photo-chemical processing. Indeed, Charge Couple Device (CCD) arrays are now widely used for PIV recordings. The arrays can be used alone or can be combined to increase the image capture rate.

3.2.4. Image Evaluation

Since the introduction of the first PIV image evaluation methods, alternative analysis algorithms have been developed as well as error correction and post-processing procedures designed to improve speed and accuracy of the PIV method. However, the classical PIV analysis method is still the most frequently used and forms the basis of many other algorithms. (Figure 3.5).

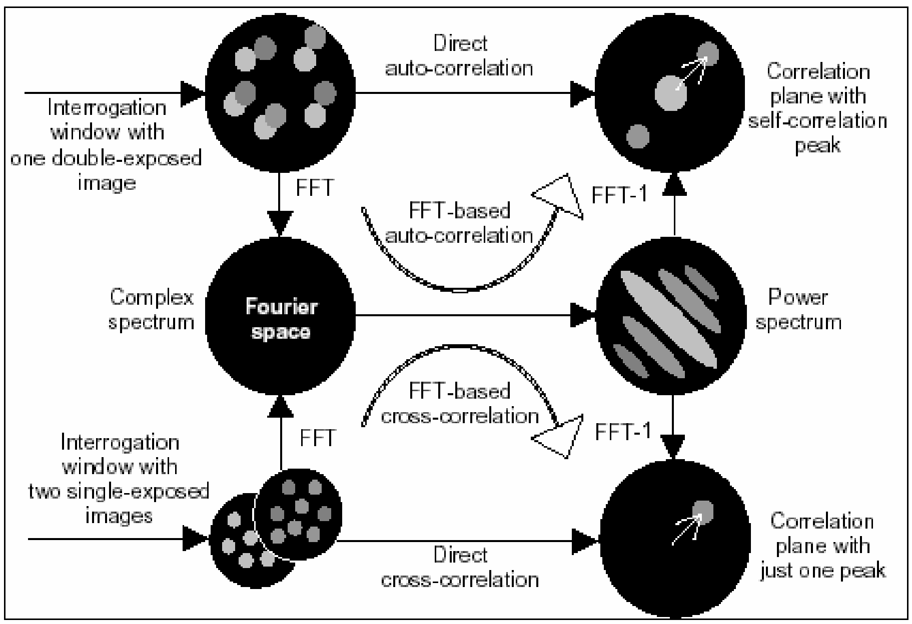

Figure 3.5. Basic PIV analysis process.

The heart of the PIV analysis is the correlation of regions of the input images (known as interrogation areas) with each other to determine the displacement vector of the flow in that part. Knowing the time interval between the image captures enables a velocity vector to be calculated from the displacement vector. The correlation technique can be used for a single frame multiply exposed (auto-correlation) or multiple frames singly exposed (cross-correlation). To speed up the convolution process, correlation of each pair of interrogation areas is carried out in Fourier space. After interrogating the images in this way and generating the vector map, post-processing is carried out to validate the data and to improve the vector map resolution and accuracy. Using this vector map, vorticity and Reynolds stress contours and streamline topology can be obtained.

3.3. Cross-Correlation Process

Cross correlation of corresponding areas of each image in the image pair is performed, generally using an FFT based algorithm, to find the relative displacement that provides the best fit between both particle image patterns. This displacement is taken as the estimation of the mean displacement in the considered area. At each selected location of the flow field a portion of each image in the image pair is isolated. These are called interrogation areas. The correlation function for integer pixel relative displacements is calculated by means of the FFT. That is, the 2D FFT of each interrogation area is performed, and the element by element conjugate product is taken in Fourier space. The result is transformed back using the FFT algorithm. The highest peak in the resulting correlation surface, indicates the relative displacement for which the best fit between image patterns was obtained, and is assumed to represent the real displacement.

Basically what happens is each image is broken up into many smaller parts, sub-windows or interrogation regions, of identical size and location. The software chooses one location on each image and shifts the second image though a complete array of possible displacements. It multiplies the intensities of each image at each displacement and sums over the entire sub-window. After each displacement is evaluated, the software looks at the new intensity distribution and chooses the highest peak. The highest peak should correspond to the displacement of the corresponding sub-window. The higher the peak, the higher the likelihood the computer found the actual displacement. It can be seen graphically from Figure 3.6.

Once a correlation peak has been computed sub-pixel accuracy is determined. There are several means of determining the peak location can be seen from Figure 3.7. The most accurate method is to fit a three point Gaussian curve to the peak intensity location.

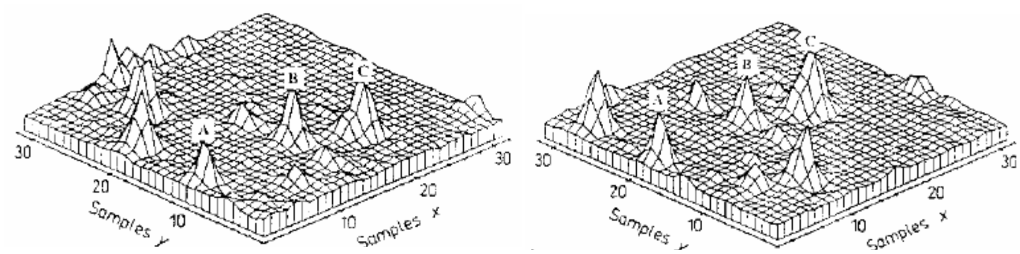

Figure 3.6. Intensity distribution of first and second image.

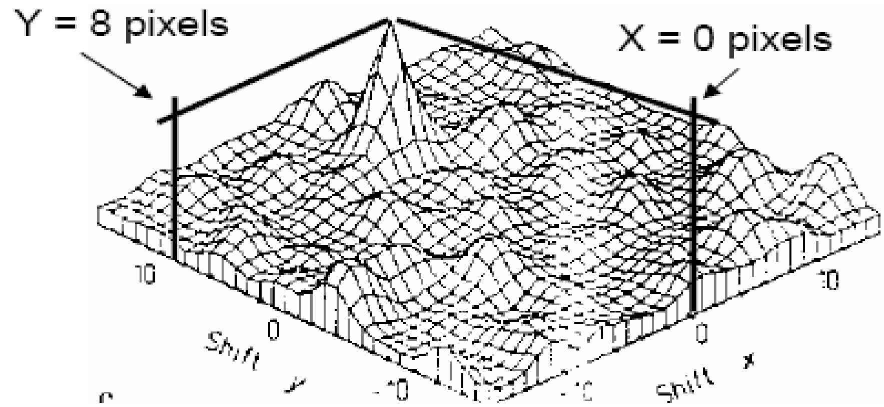

Figure 3.7. Correlation peak corresponding to 8 pixel y-displacement.

The maximum of the curve corresponds to that sub-window's displacement to sub-pixel accuracy. The software correlates and calculates the peak each sub-window creating the velocity field. Therefore, PIV doesn't compute velocities for each particle, rather it determines the velocity for a small group of particles. Technology keeps improving which allows smaller and smaller interrogation regions approaching individual particle tracking. With ideal conditions, correlation has been achieved by researchers down to 4 pixel square interrogation regions. Depending on the particle size this can be close to individual particles.

No matter how good the setup is, the software will always generate some erroneous vectors. These usually stand out from their neighbors as being much larger in magnitude or in the complete wrong direction as what was expected. Most software filters out these bad vectors based on range, comparison with neighbors, or other filtering criteria. This step is essential to good data as just a few bad vectors have a strong adverse effect on the field.

When the system is set up and image correlation is occurring data gathering can begin. Typically large number of image pairs are correlated and averaged to generate mean values of displacement and to lower precision error. Again, the data will need to be filtered before averaging of the vector fields occurs. Once good data has been gathered, calculations of strain, vorticity, or any variable involving velocity can be obtained from the data.

3.4. Image Post-Processing

The post-processing of the raw velocity field involves vector validation removal of spurious vectors, replacement of the removed vectors, and data smoothing and filtering. Once the vector fields are determined, time-averaging, phase-averaging and spectral analysis, can be employed. Spurious vectors are caused by improper correlation peak detection due to noise or artifacts e.g., non-uniform laser light illumination. They can be picked up either by close inspection of the raw flow field, or using special algorithms such as the global histogram operator.

Images were received from CCD camera that has resolution 1008 pixels × 1016 pixels at a rate of 15 frames per second. The time delay changes from 2 ms and 3 ms between frames. Digital image was analyzed using FLOWMAP software. The image was recorded on a CDD array. A Frame Grabber in the computer read the camera image from CCD camera and stored it as the digital image file format (TIFF) in the RAM. This digital image was processed and analyzed using the FLOWMAP software. During each continuous run, a total 350 images were taken. In order to determine the velocity field, a cross correlation technique, with 32×32 interrogation window, was employed, with an overlap of % 50. The magnification factor of lens was 1:19.022.

The resulting vector field obtained from FLOWMAP software and the corresponding boundaries of objects were then viewed using program V3 to determine incorrect vectors from interrogation. These type of vectors can result when an incorrect particle correlation is made near boundaries or within shadow regions, when the particle images are too widely spaced for interrogation window side specified, pr the power of laser sheet is poor (Kahraman, 2002).

Vector validation software called CLEANVEC was used to remove incorrect vectors. The software CLEANVEC contains four statistical filters designed for incorrect vectors removal:

- Absolute Range Filter
- RMS Tolerance Filter
- Magnitude Difference Filter
- Quality Filter

Three of these four filters were used for the purposes of eliminating incorrect vectors. Here the Quality Filter requires a correlated data, which are supposed to be done by interrogation and this data, was not provided by this software.

In the Absolute Range Filter, all u and v velocity components that lie outside of given range were removed. With this filtering method, one can identify a moving reference frame in order to save real vectors that are numerically specified and eliminated incorrect vectors on the main frame. Although very trivial, this filter might be very useful in removing the most tedious incorrect vectors, and hence improves the performance of the other filtering tools.

The RMS Tolerance Filter removes incorrect vectors those lay outside of given range. This filter must be applied to a velocity field in a reference frame moving with the mean velocity components in both directions, since it is involved with the fluctuating components only.

Finally, the Magnitude Difference tool removes unnecessary vectors based on the difference in magnitude between a vector and its neighborhood median. This is the local-median test defined by Westerweel (1994). This filter is the most effective among the available filters, as indicate by Westerweel (1994). However, it should be handled carefully, because it may lead to an excessive vector in a certain type of flows.

4. RESULTS AND DISCUSSION

4.1. General Information About the Performed Experiments

The objective of the present work is to conduct quantitative and qualitative studies in side-view laser planes for two cylinders in tandem arrangement for the purpose of revealing the structure of the details using flow data from PIV technique. All of the experiments were performed in the water of which height (h_w) is 25 mm. the diameter (D) of the cylinders are equal and 50 mm. Four types of experiments were performed at the case. The cylinders were placed onto a platform that gives the water height in the flow. For each experiments the distance (G) between the cylinders were changed in the interval of 0 mm and 225 mm. For each experiment, time-averaged velocity field $<V>$, streamline patterns $<\psi>$, and vorticity contours $<\omega>$ are inspected.

Side-view of the test section, direction of the laser and position of the cylinders are illustrated in Figure 4.1.

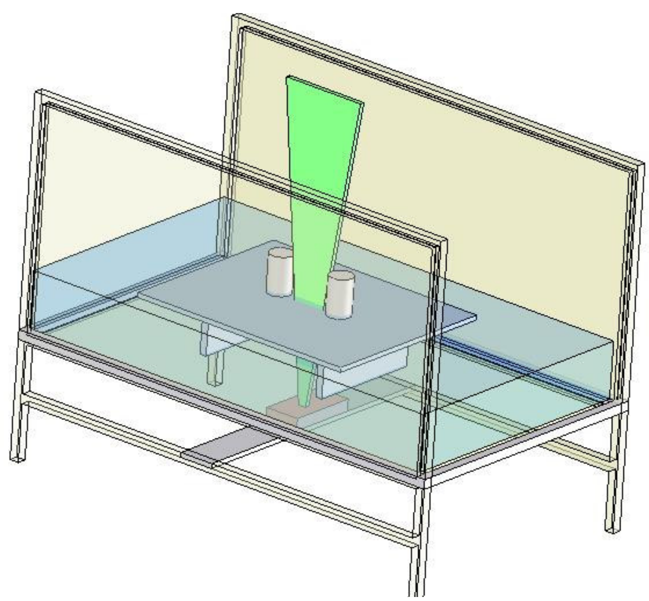

Figure 4.1. Visualization of the water channel with the side view of the test section.

During the all experiments, 80mmx25mm image area measuring section is used.

4.2. Free Stream Flow

Figure 4.2. shows the schematic view of test section. First of all, PIV experiments were carried out to obtain velocity profile for the case of no cylinders. Doing so, free-stream velocity profile was determined. Figure 4.3. shows the time-averaged velocity field, corresponding streamline patterns for free-stream flow of the shallow water obtained from PIV experiments. The time-averaged flow characteristics were obtained from 350 instantaneous images obtained from PIV technique. Velocity vector field and corresponding time-averaged streamline topology clearly shows that the magnitudes of spanwise extend of velocity are negligible. When it is checked the velocity profile at three different cross-sections, the same velocity profiles were obtained as can be seen in Figure 4.3.

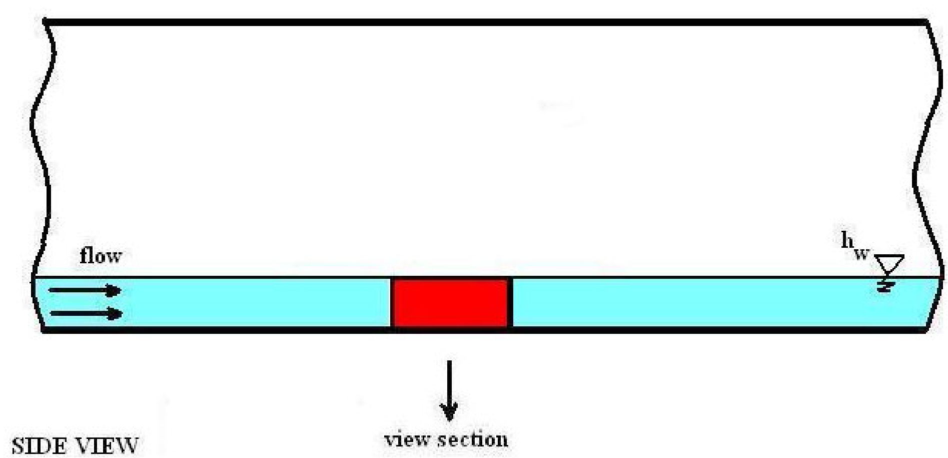

Figure 4.2. Schematic view of test section in free flow.

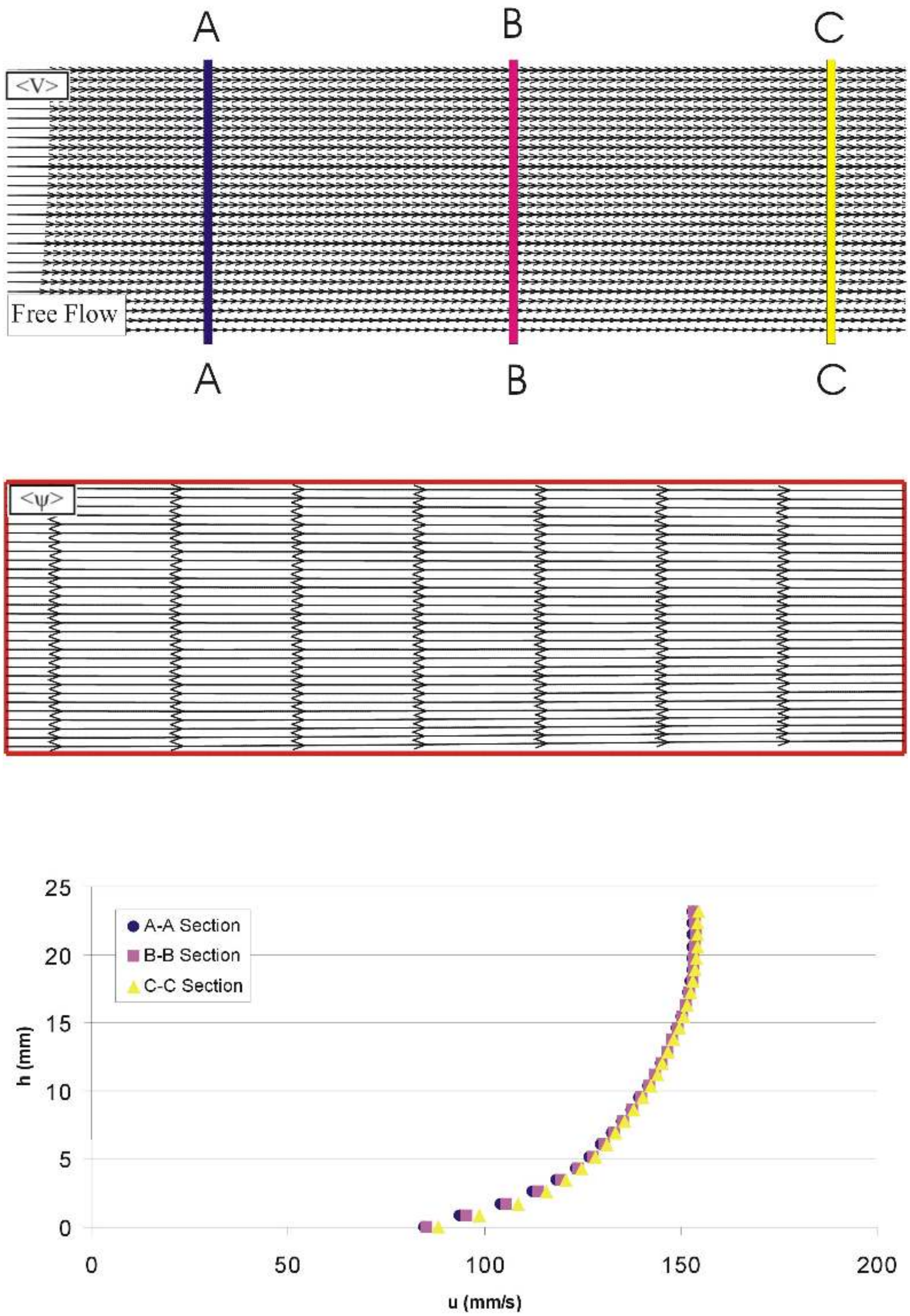

Figure 4.3. Time-averaged velocity field , <V> streamline patterns , <ψ> and velocity profile at different cross sections (A-A, B-B and C-C) in the view section of the free stream flow in side-view plane.

4.3. Flow Behind and Front of the Single Cylinder

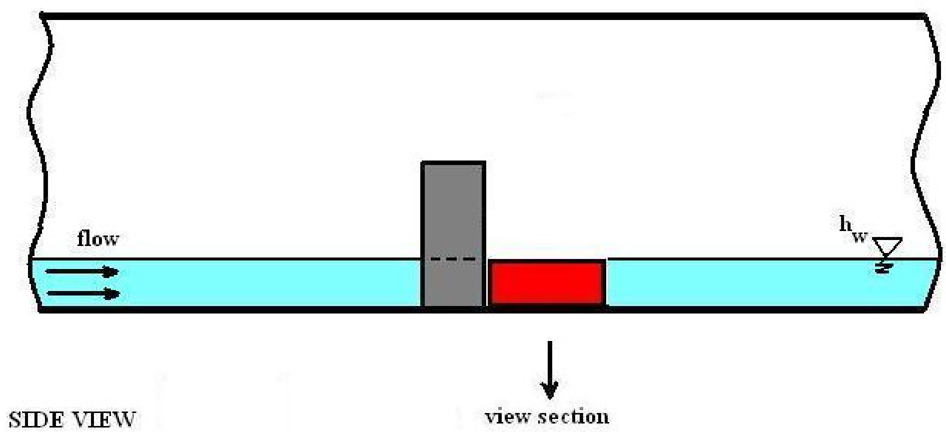

Figure 4.4. Schematic view of Flow Behind Single Cylinder.

Figure 4.4. shows the schematic view of test section in the view section of the flow behind single cylinder and the time-averaged velocity vector field <V>, corresponding streamline patterns <ψ>, and vorticity contours <ω> for the view section of the flow behind single cylinder obtained from PIV experiments shown in figure 4.5.

In the shallow water layer, the effect of the finite distance between the bed and the free surface is associated with a three-dimensional mechanism that gives rise to a horizontally oriented vortex, which is evident immediately beneath the free surface for a significant portion of the Karman vortex cycle. As can be seen the Figure 4.5. this flow shows flow separation after the cylinder walls for limited period and takes the uniform flow characteristics after the separation region. A focus observed just behind the base of the cylinder and a saddle point near the region of flow separation. Corresponding vorticty contours are concentrated in the same region. Black lines show positive vorticity, while red lines demonstrate negative vorticity values.

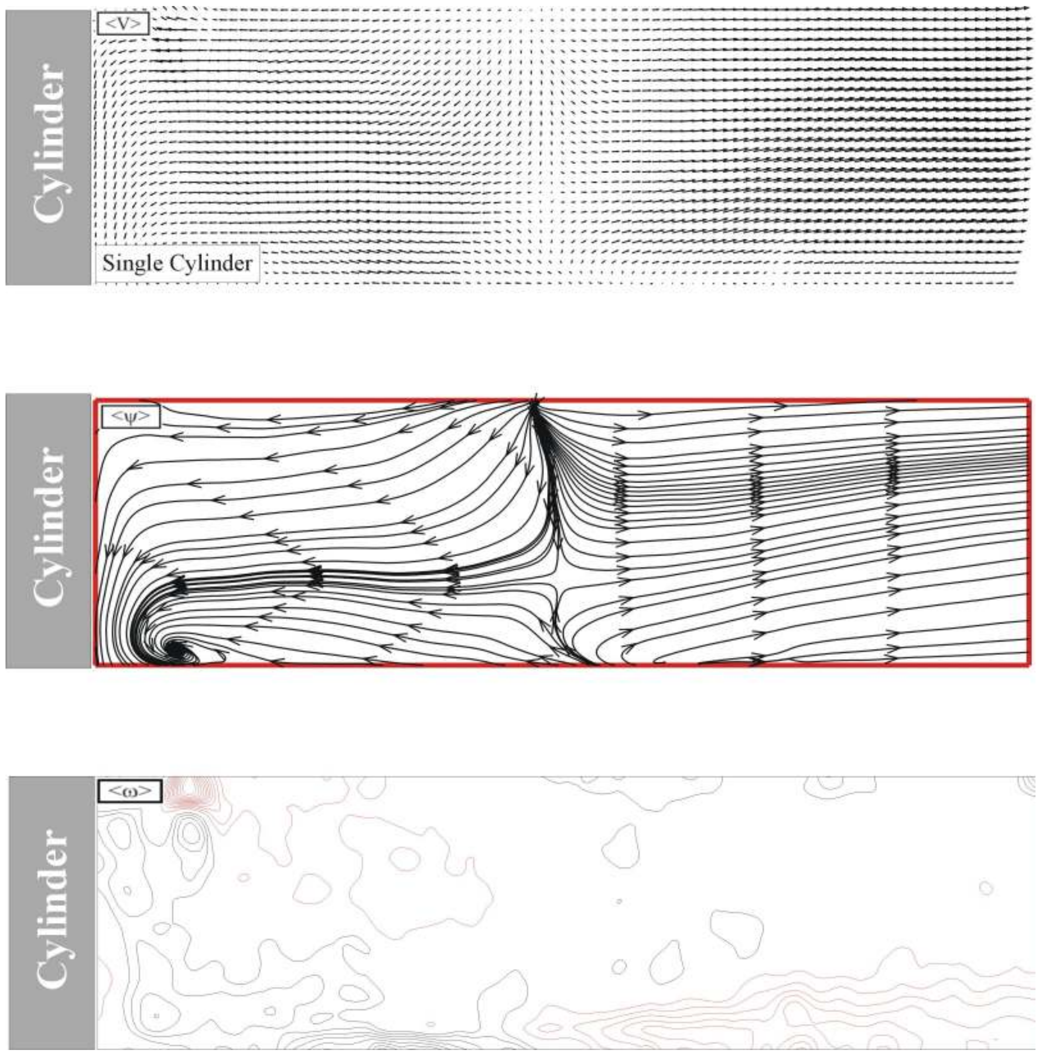

Figure 4.5. Time-averaged velocity field,<V> streamline patterns, <ψ> and vorticity contours, <ω> in the view section of the flow behind single cylinder in side-view plane. Minimum and incremental values of vorticity are $\omega_{min} = \pm 1 s^{-1}$ and $\Delta\omega = 1 s^{-1}$.

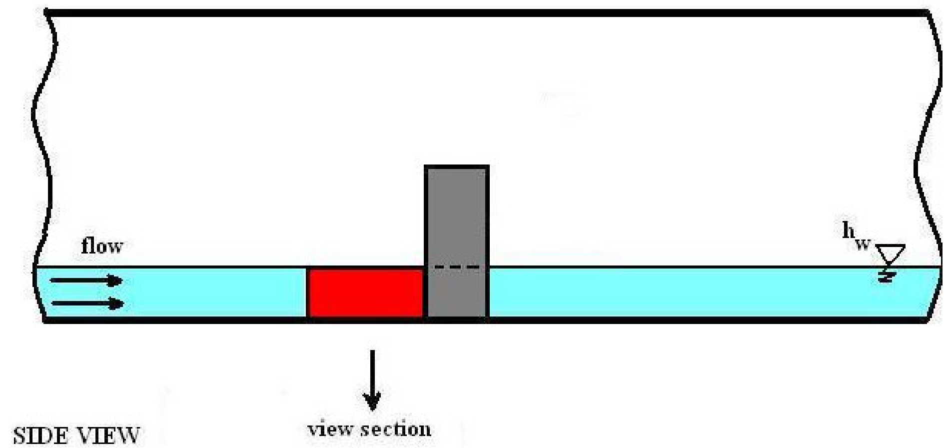

Figure 4.6. Schematic view of Flow in Front of Single Cylinder.

Figure 4.6. shows the schematic view of test section in the view section of the flow in front of single cylinder and the time-averaged velocity vector field <V>, corresponding streamline patterns <ψ>, and vorticity contours <ω> for the view section of the flow behind single cylinder obtained from PIV experiments shown in figure 4.7.

In this flow, uniform flow characteristics are observed except for the near cylinder region. When flow approaches cylinder wall, reverse flow occurs at approximately 10 mm front of the cylinder. This reverse flow leads horseshoe vortex system to occur in front of the cylinder. The magnitude of the vorticity contours increases at this reverse flow region. As it can be seen from streamline topology and corresponding vorticity contours negative vorticity and reverse flow observed easily. There are no foci and saddle points formed in this type of flow. Low level velocity vector field is obtained at the vicinity of the cylinder close to the free surface region due to the reflection of the laser sheet.

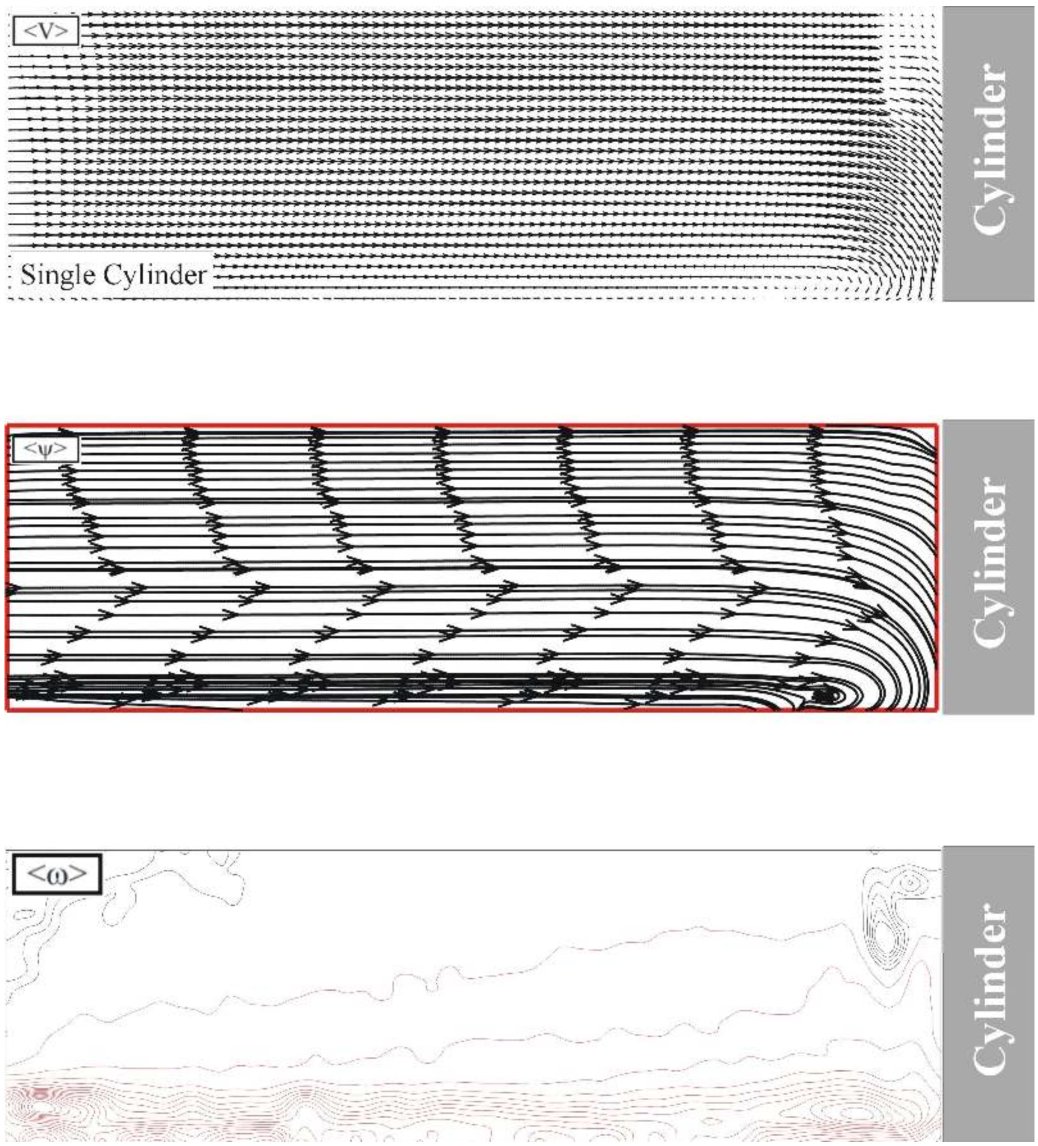

Figure 4.7. Time-averaged velocity field, $\langle V \rangle$ streamline patterns, $\langle \psi \rangle$ and vorticity contours, $\langle \omega \rangle$ in the view section of the flow front of single cylinder in side-view plane. Minimum and incremental values of vorticity are $\omega_{min} = \pm 1 s^{-1}$ and $\Delta\omega = 1 s^{-1}$.

4.4. Flow Structure Behind the First Cylinder

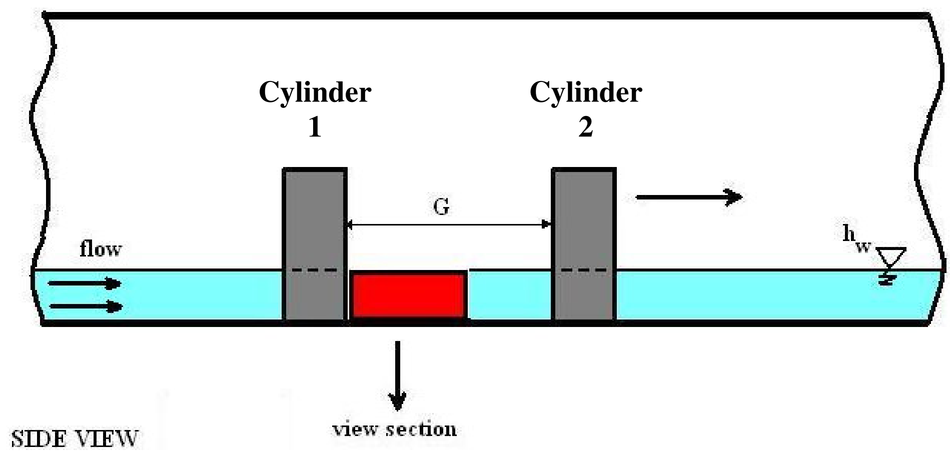

Figure 4.8. Schematic view of the flow behind cylinder 1 of two cylinders in tandem arrangement with G=25mm-225mm in side-view plane.

Figure 4.8. shows the schematic view of test section in the view section of the flow behind the first cylinder of two tandem arrangement cylinders. The time-averaged velocity vector field $\langle V \rangle$, corresponding streamline patterns $\langle \psi \rangle$, and vorticity contours $\langle \omega \rangle$ for the view section obtained from PIV experiments are shown in figures 4.9-4.17 for this flow field.

These experiments were carried out for two cylinders with tandem arrangement having different G/D ratios starting from 0.5 to 4.5. When the time-averaged velocity vector fields, corresponding streamline patterns and vorticity contours for these G/D ratios are investigated and different conclusions are obtained.

For the gap ratio of G/D=0.5, only reverse flow is observed due to the presence of the second cylinder. A focus is observed approximately 7 mm behind the first cylinder. Again in the same point positive vorticity clusters can be seen from vorticity contours. Second cylinder effect can also be seen easily from the time-averaged streamline topology as the aim of flow in vertical direction. Flow separation and saddle point were not observed in this flow configuration.

For the gap ratio of G/D=1 showed that the similar flow characteristics occurred compared to G/D=0.5. Here again a focus is observed at the same location with a larger diameter and positive vorticity clusters can be seen from vorticity contours. There are no flow separation and saddle point observed in this flow configuration. Different from the flow characteristics for the gap ratio of 0.5, the second cylinder effect starts getting decreasing. It can be understood from streamline topology that flow shows uniform aim after focus point up to the second cylinder.

For the gap ratio of G/D=1.5, similar flow behaviors can be seen similar the flow behavior for the gap ratio of 1. It is observed that focus occurred approximately at the same point, no flow separation and saddle point occurred, vorticity clusters and uniform type of flow are nearly same like the gap ratio of G/D=1.

From streamline topology for the gap ratio of G/D=2, focus is observed at same location easily but its diameter getting larger. Again no saddle point and flow separation are observed here. Base development of the flow from the previous ratio, vorticity condensation starts at the region of approximately 8 mm behind of the first cylinder.

In the ratio of G/D=2.5 it can be seen from streamline topology flow characteristics changes according to other ratios. Again the focus is observed at the same location and flow separation is occurred at the approximately 35 mm behind the first cylinder. After the separation region flow is aimed in uniform characteristics. There are no saddle point is observed in this ratio.

The flow separation and saddle point occupation can be seen exactly in the ratio of G/D=3. Saddle point is observed in the separation region at approximately 35 mm behind the first cylinder again. The focus is observed in the expected point like other ratios.

It can be said that second cylinder effect totally disappears at the gap ratio of G/D=3.5. Flow takes the character of single cylinder flow. This can be understood from streamline topology and vorticity contours because of they are nearly same. Focus is observed at same location. Flow separation and saddle point are observed at approximately 35 mm behind of the cylinder. After separation region flow is showed uniform flow characteristics up to the end of view section. Negative vorticity contours are observed in the region of uniform flow.

Conclusions of the gap ratios G/D=4 and G/D=4.5 can be investigated together. Foci occupation is observed at same location, flow separation and saddle point can be seen in the same region like the gap ratio of G/D=3.5. Negative vorticities are observed along the afterwards of the separation region in other words uniform flow characteristics region.

After from all notifications related with gap ratios it can be said that; first of all, each ratio shows its own characteristics. From gap ratio G/D=0.5 to G/D=2 nearly same characteristics are shown. All of these (0.5 -2) ratios it can be said that flow shows foci like the region of flow from single cylinder, there are no flow separation due to not enough distance and there are no saddle occurs. At gap ratios of 2.5-4.5 it can be seen that the effect of second cylinder disappeared. Flow shows the same characteristics as single cylinder that explained previous section. Finally it is concluded that from all gap ratios a critical ratio obtained from experiments. For these experiments it can be said that the ratio of G/D=2.5 is the critical ratio exactly.

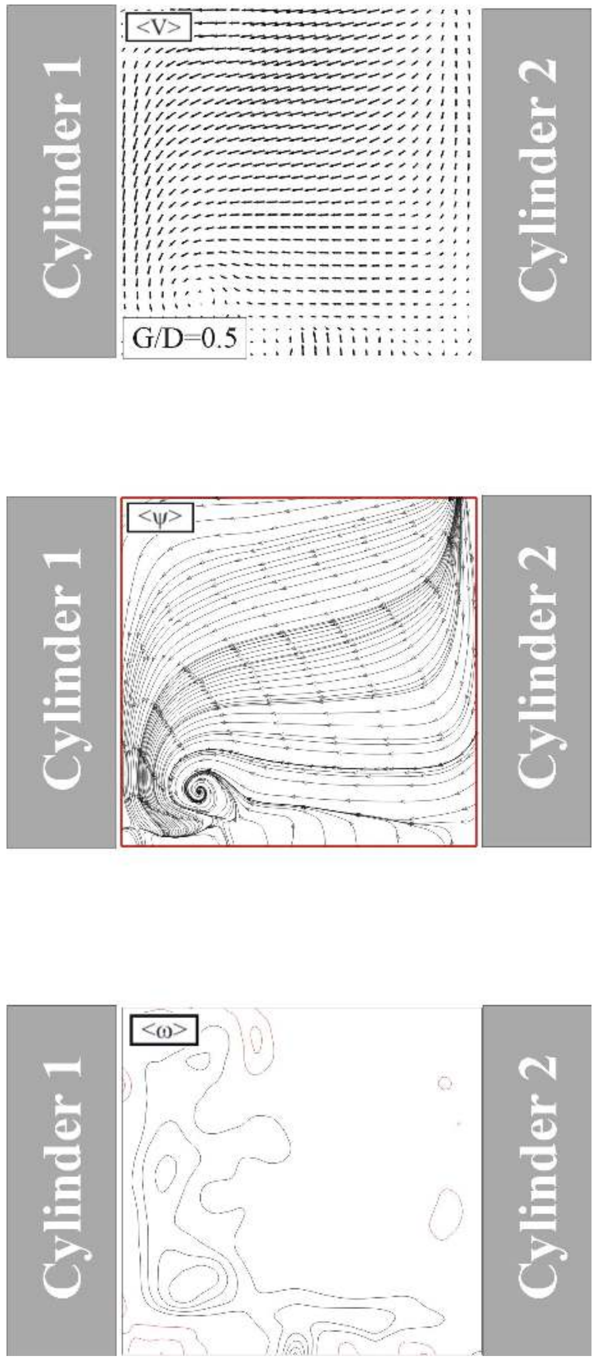

Figure 4.9. Time-averaged velocity field,$\langle V \rangle$ streamline patterns, $\langle \psi \rangle$ and vorticity contours, $\langle \omega \rangle$ in the view section of the flow between cylinders of two cylinders in tandem arrangement with G/D 0.5 in side-view plane. Minimum and incremental values of vorticity are $\omega_{min} = \pm 1 s^{-1}$ and $\Delta\omega = 1 s^{-1}$.

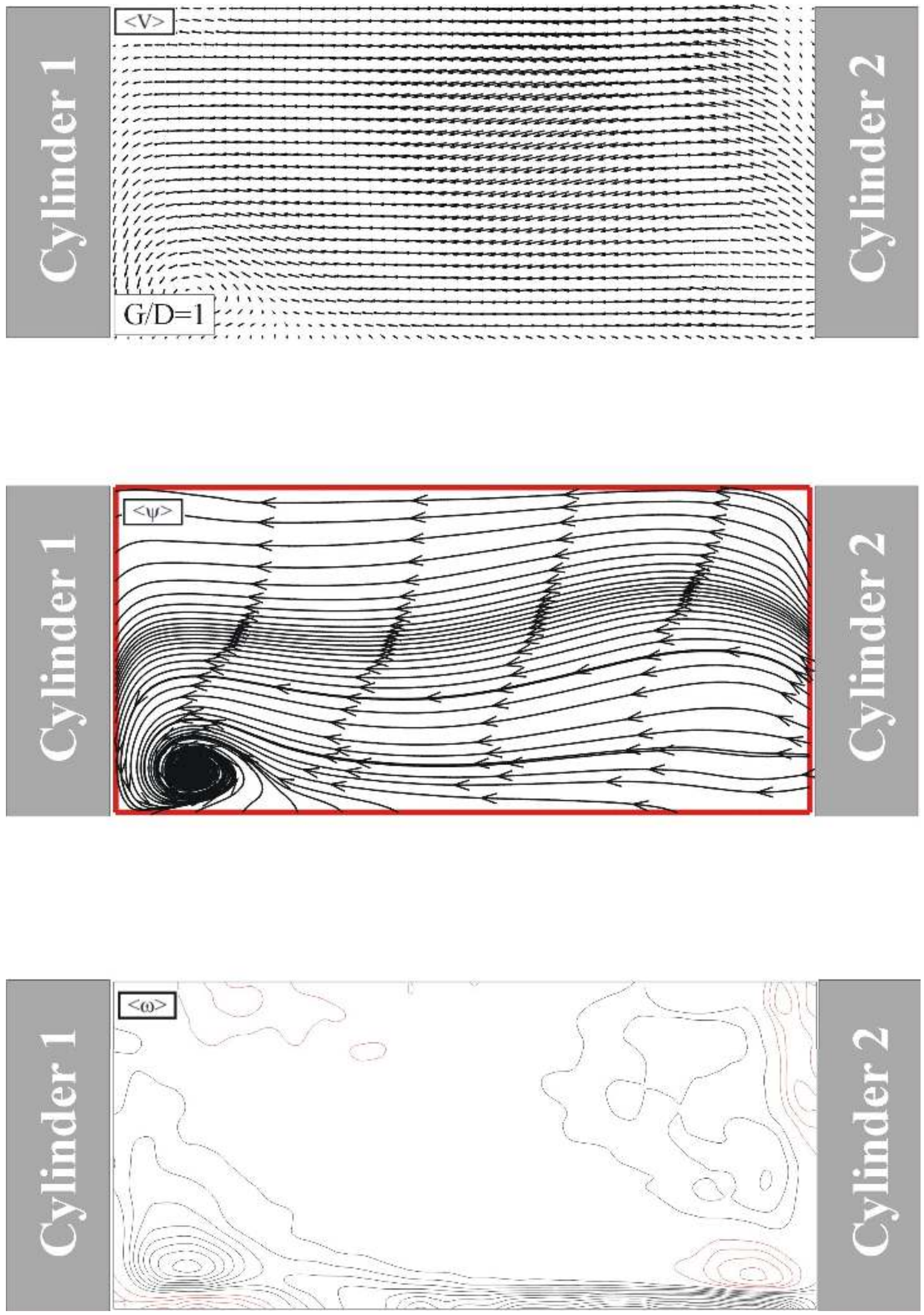

Figure 4.10. Time-averaged velocity field,<V> streamline patterns, <ψ> and vorticity contours, <ω> in the view section of the flow between cylinders of two cylinders in tandem arrangement with G/D 1 in side-view plane. Minimum and incremental values of vorticity are $\omega_{min} = \pm 1 s^{-1}$ and $\Delta\omega = 1 s^{-1}$.

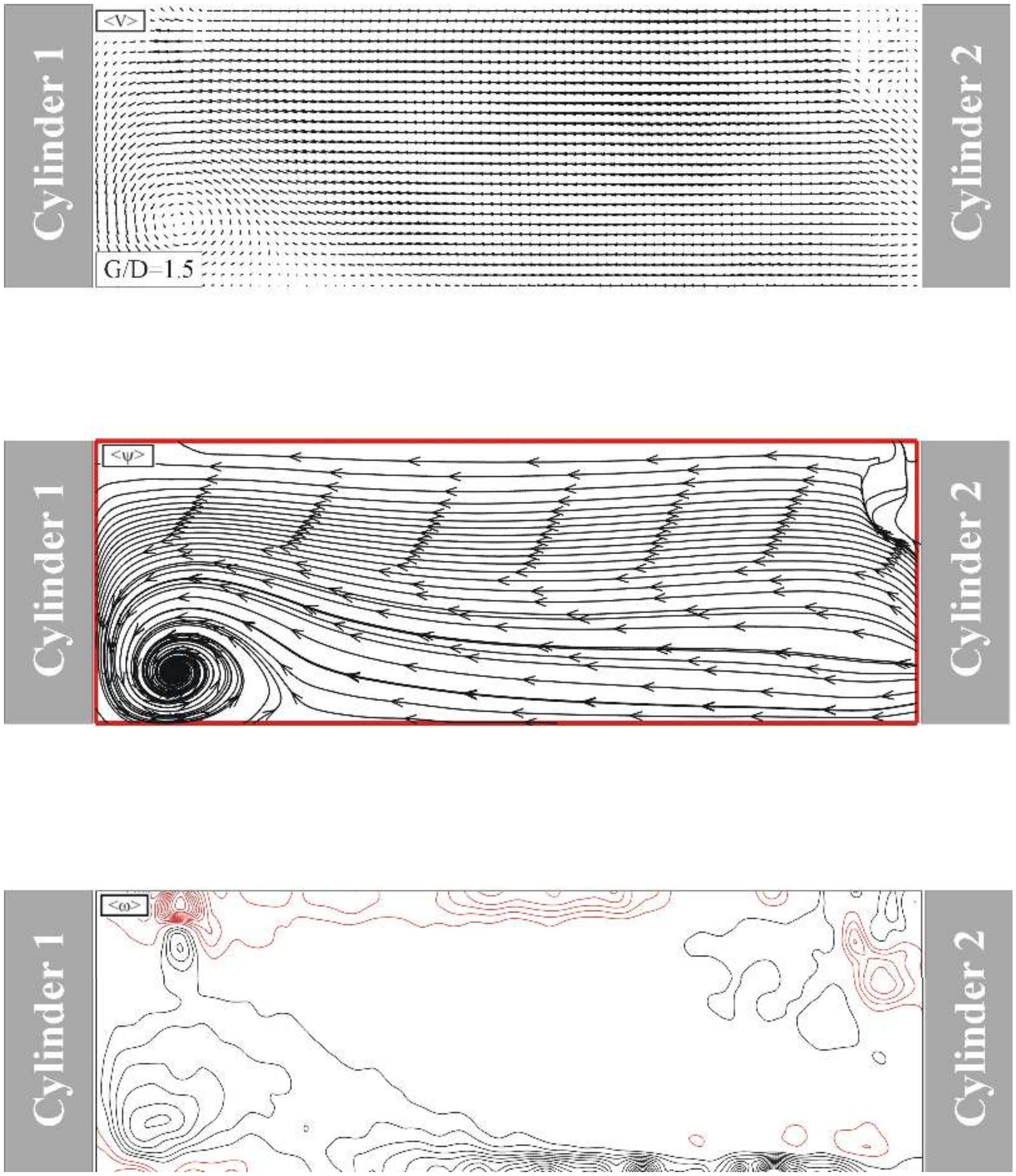

Figure 4.11. Time-averaged velocity field,<V> streamline patterns, <ψ> and vorticity contours, <ω> in the view section of the flow between cylinders of two cylinders in tandem arrangement with G/D 1.5 in side-view plane. Minimum and incremental values of vorticity are $\omega_{min} = \pm 1 s^{-1}$ and $\Delta\omega = 1 s^{-1}$.

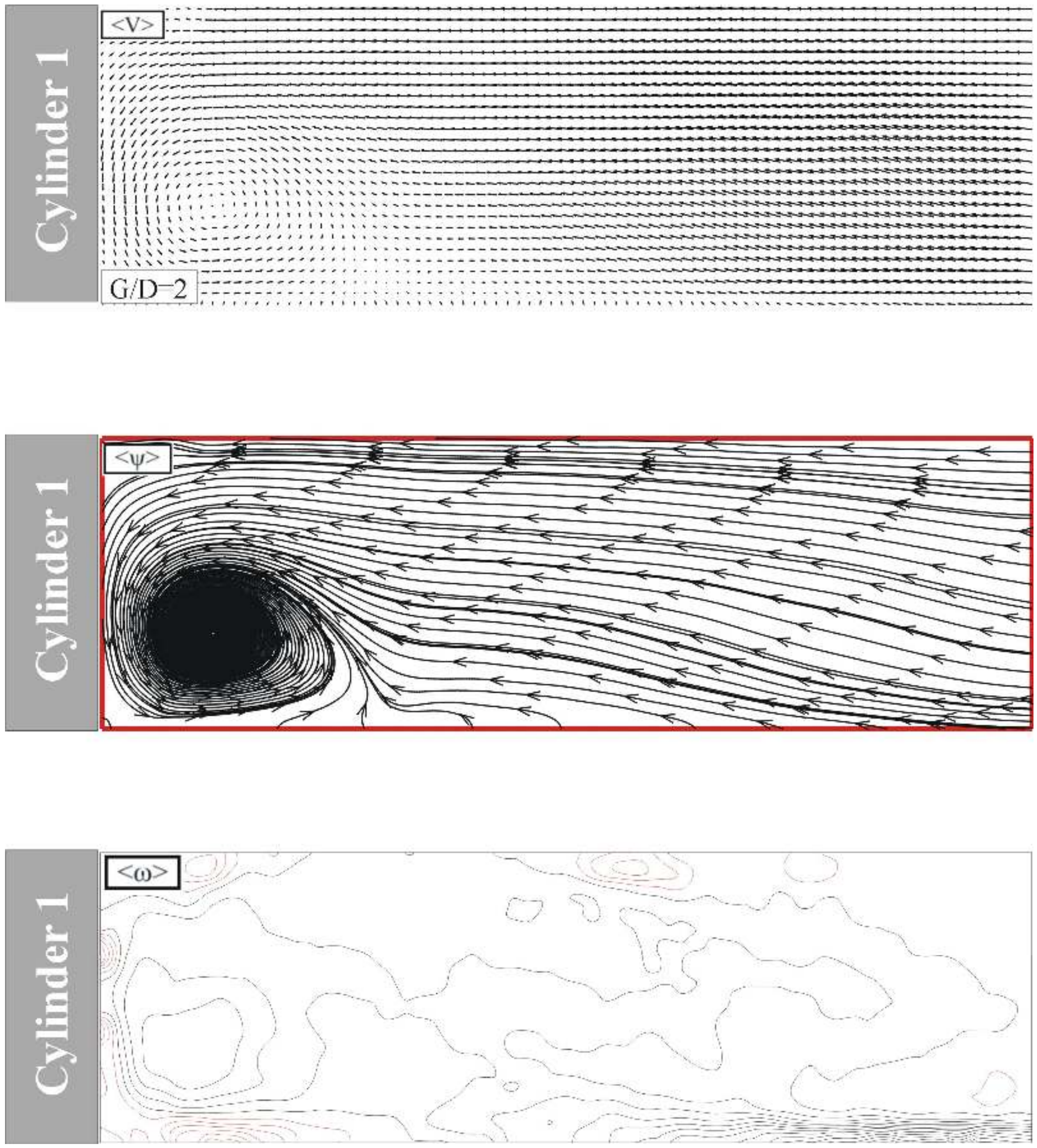

Figure 4.12. Time-averaged velocity field,<V> streamline patterns, <ψ> and vorticity contours, <ω> in the view section of the flow behind cylinder 1 of two cylinders in tandem arrangement with G/D 2 in side-view plane. Minimum and incremental values of vorticity are $\omega_{min} = \pm 1s^{-1}$ and $\Delta\omega = 1s^{-1}$.

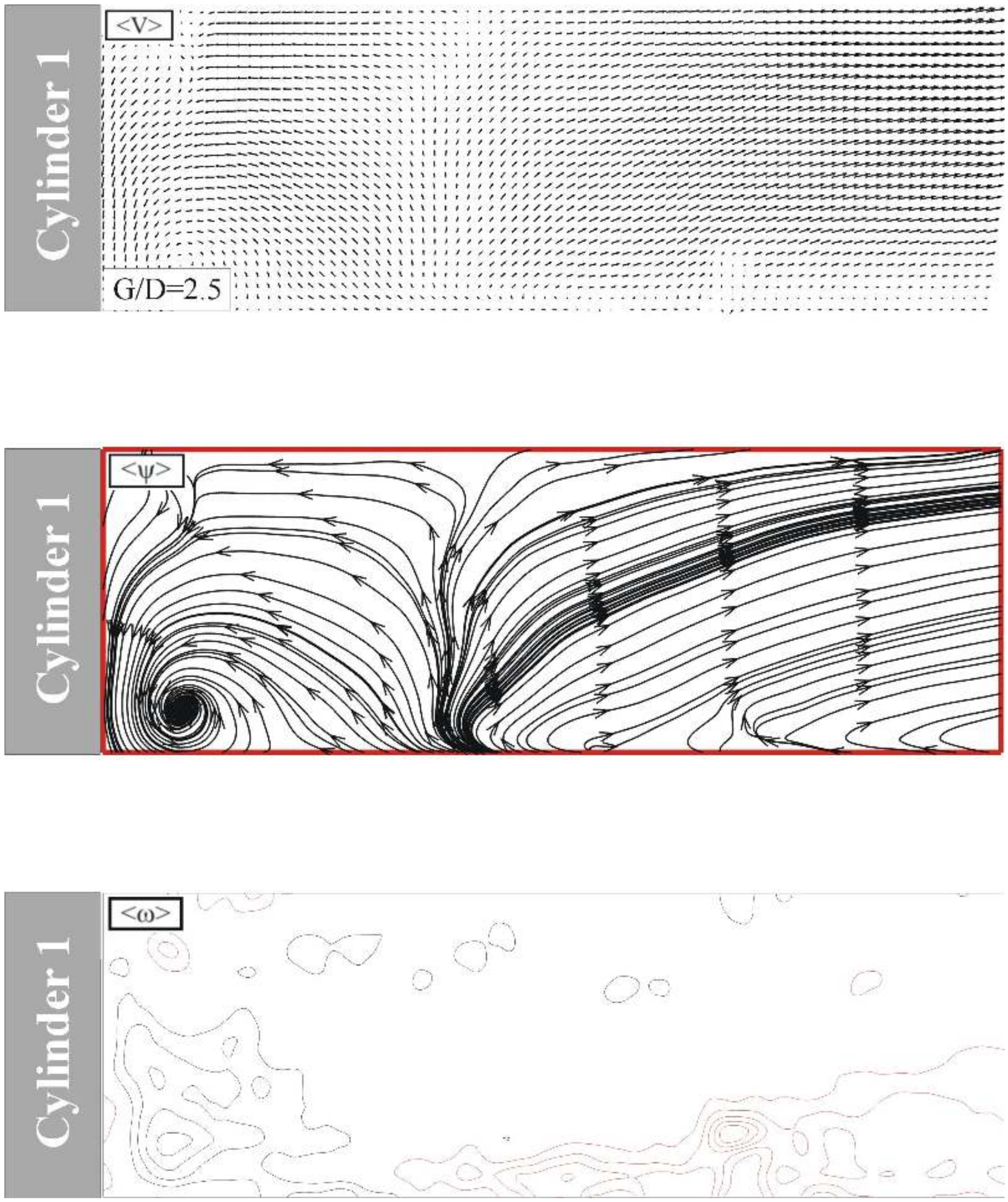

Figure 4.13. Time-averaged velocity field,<V> streamline patterns, <ψ> and vorticity contours, <ω> in the view section of the flow behind cylinder 1 of two cylinders in tandem arrangement with G/D 2.5 in side-view plane. Minimum and incremental values of vorticity are $\omega_{min} = \pm 1 s^{-1}$ and $\Delta\omega = 1 s^{-1}$.

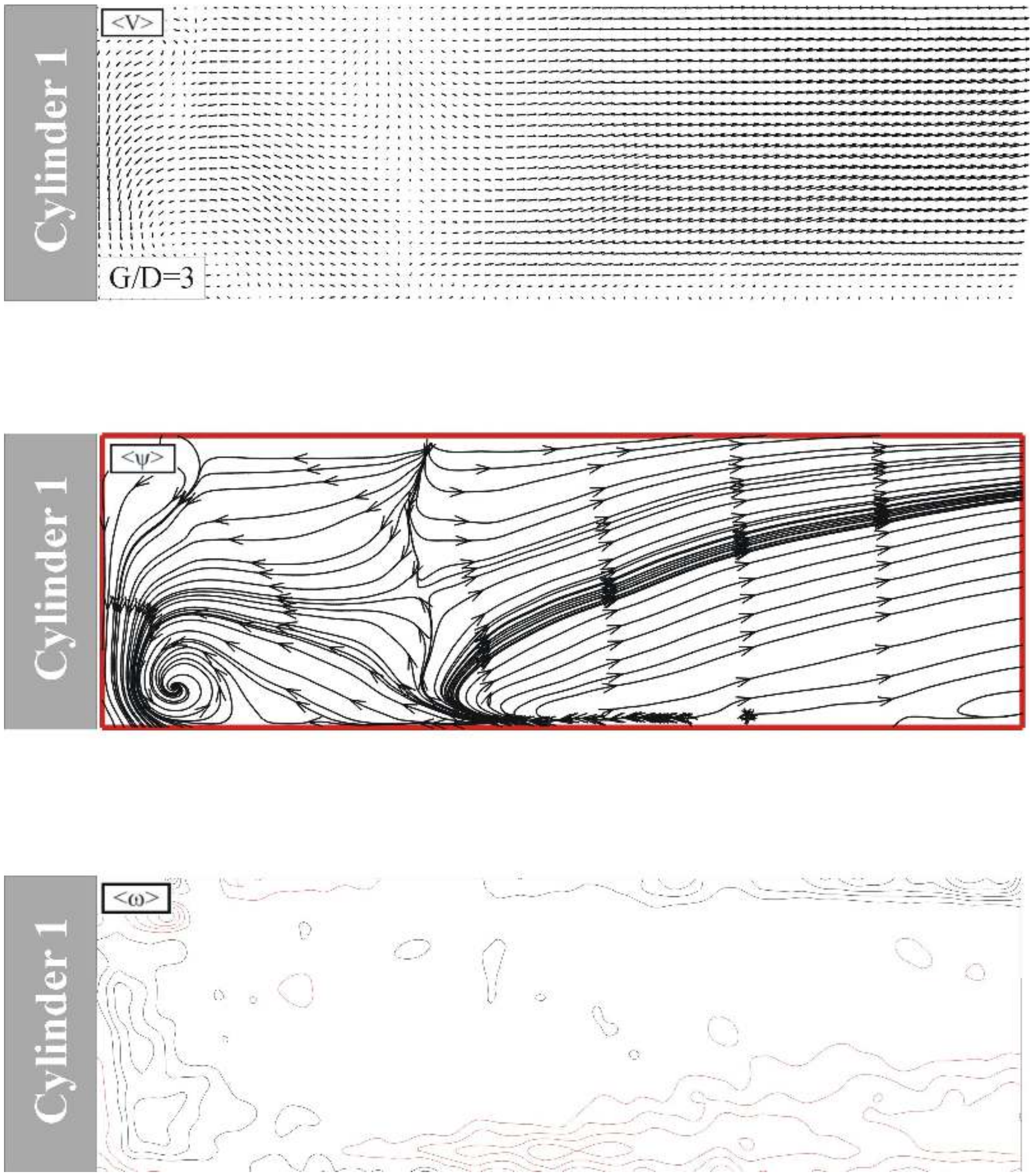

Figure 4.14. Time-averaged velocity field,<V> streamline patterns, <ψ> and vorticity contours, <ω> in the view section of the flow behind cylinder 1 of two cylinders in tandem arrangement with G/D 3 in side-view plane. Minimum and incremental values of vorticity are $\omega_{min} = \pm 1 s^{-1}$ and $\Delta\omega = 1 s^{-1}$.

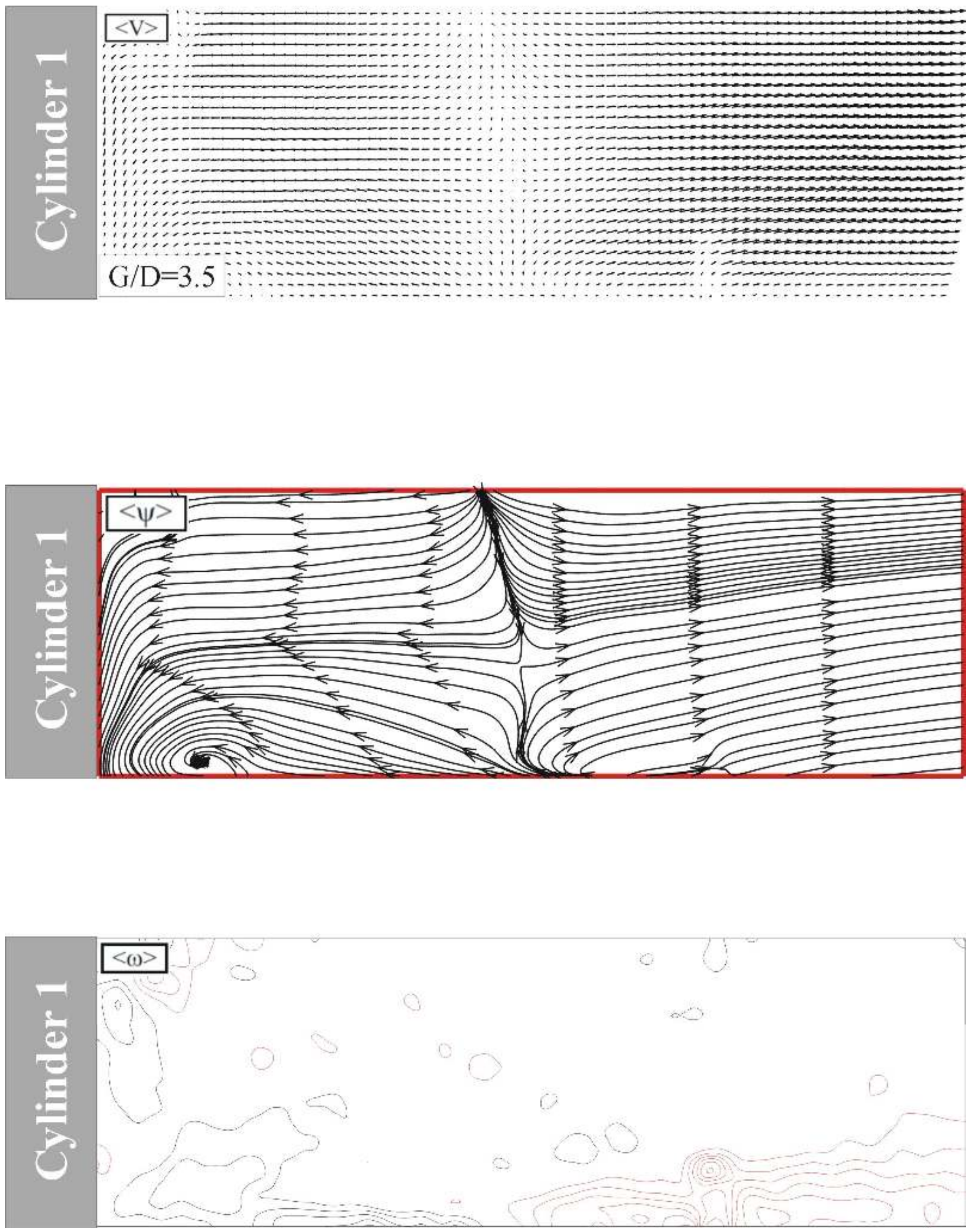

Figure 4.15. Time-averaged velocity field,<V> streamline patterns, <ψ> and vorticity contours, <ω> in the view section of the flow behind cylinder 1 of two cylinders in tandem arrangement with G/D 3.5 in side-view plane. Minimum and incremental values of vorticity are $\omega_{min} = \pm 1 s^{-1}$ and $\Delta\omega = 1 s^{-1}$.

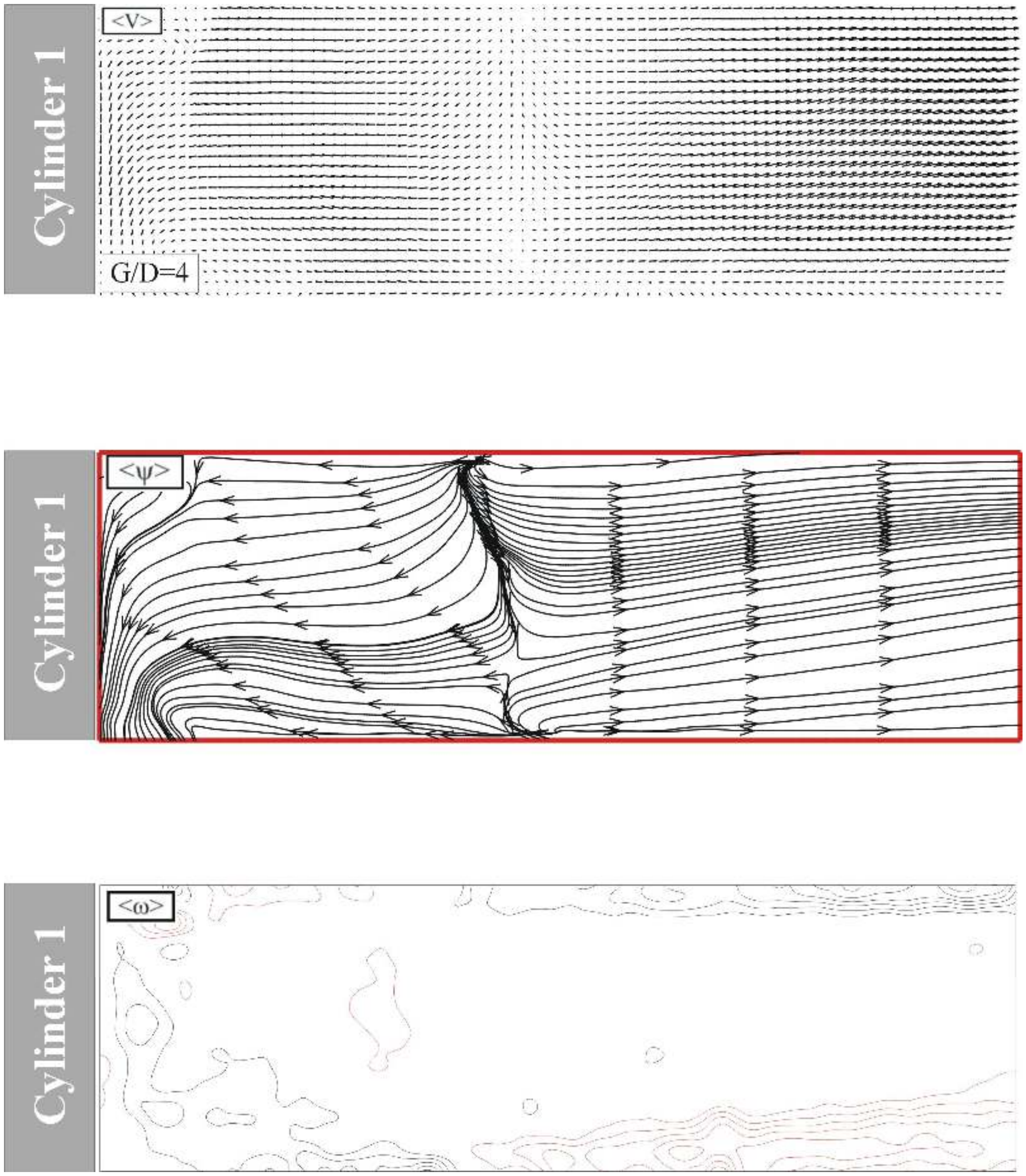

Figure 4.16. Time-averaged velocity field,<V> streamline patterns, <ψ> and vorticity contours, <ω> in the view section of the flow behind cylinder 1 of two cylinders in tandem arrangement with G/D 4 in side-view plane. Minimum and incremental values of vorticity are $\omega_{min} = \pm 1 s^{-1}$ and $\Delta\omega = 1 s^{-1}$.

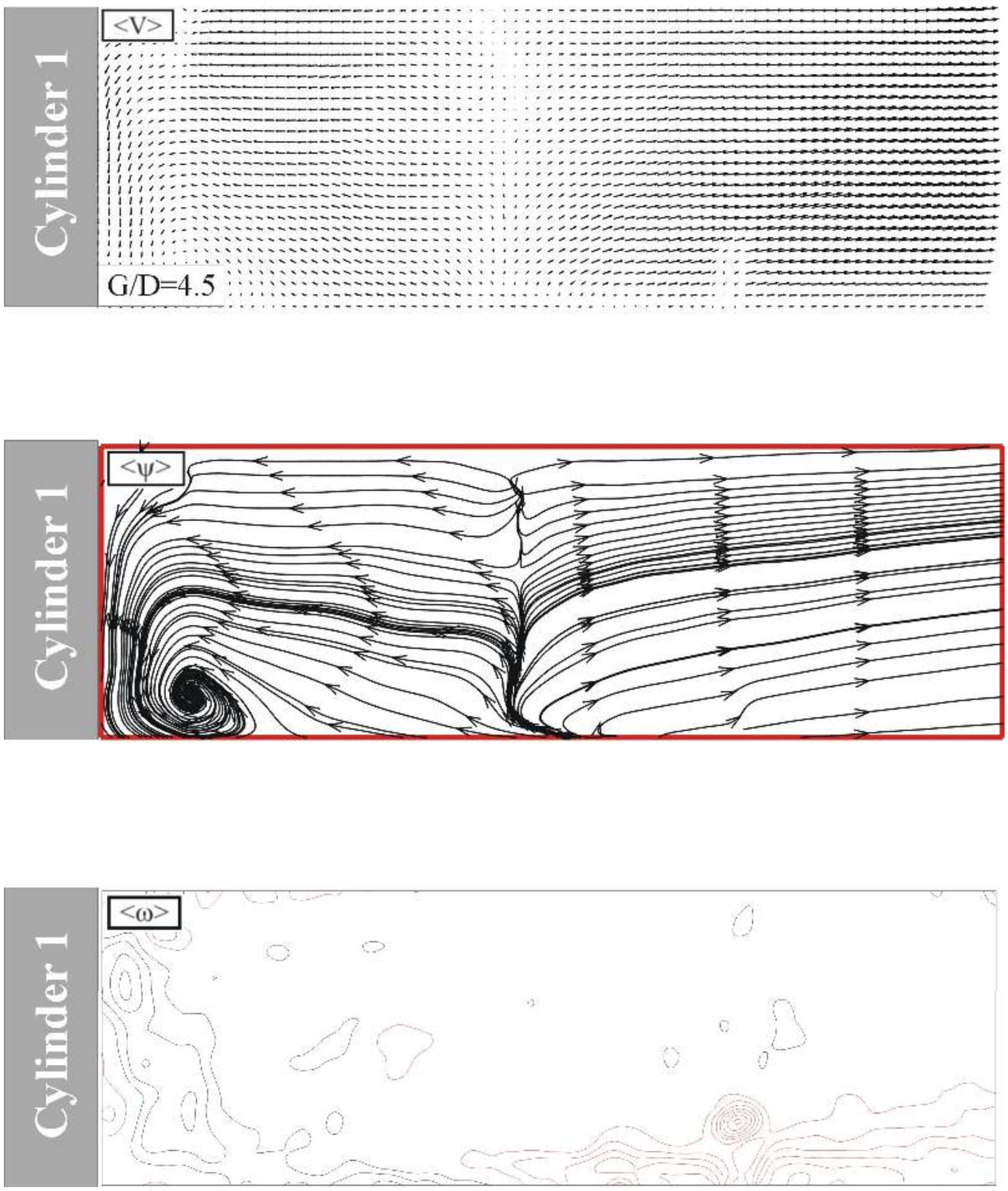

Figure 4.17. Time-averaged velocity field,<V> streamline patterns, <ψ> and vorticity contours, <ω> in the view section of the flow behind cylinder 1 of two cylinders in tandem arrangement with G/D 4.5 in side-view plane. Minimum and incremental values of vorticity are $\omega_{min} = \pm 1 s^{-1}$ and $\Delta\omega = 1 s^{-1}$.

4.5. Flow Structure in Front of the Second Cylinder

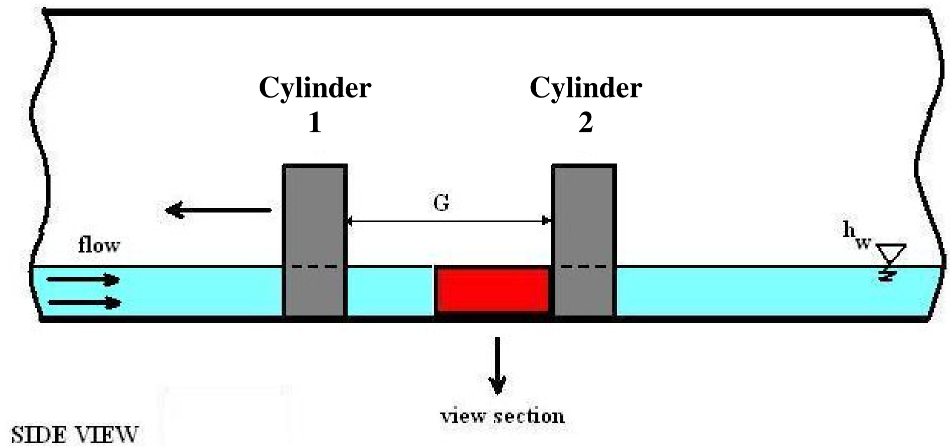

Figure 4.18. Schematic view of the flow in front of cylinder 2 of two cylinders in tandem arrangement with G=100mm-225mm in side-view plane.

Figure 4.18. shows the schematic view of test section in the view section of the flow in front of second cylinder of two tandem arrangement cylinders. The time-averaged velocity vector field $<V>$, corresponding streamline patterns $<\psi>$, and vorticity contours $<\omega>$ obtained from PIV experiments are shown in figures 4.19-4.24 for this flow field.

These experiments were carried out for two cylinders with tandem arrangement having different G/D ratios starting from 2 to 4.5. When the time-averaged velocity vector fields, corresponding streamline patterns and vorticity contours for these G/D ratios are inspected and different conclusions are obtained.

When the starting gap ratio of G/D=2 is investigated, a focus occupation is observed approximately 10 mm behind of the second cylinder. Another important character flow separation region is observed 50 mm behind of the second cylinder. Both of these there is no saddle point is observed. These foci and flow separation show the effect of first cylinder clearly.

From streamline topology for the gap ratio of G/D=2.5 it can be seen that the focus occupation at the same location but having a smaller diameter. Another important difference from previous gap ratio, flow separation can not be seen. It means that other cylinder effect getting decreases. No saddle point observed in this ratio. Vorticity clusters shown in the same location with focus.

In the gap ratio of G/D=3, the effect of other cylinder getting decreases more than the previous gap. The focus located at same point with smaller diameter. Flow shows the characteristic of uniform aim at the upper surface. Again here no saddle point and flow separation region observed.

It can be clearly observed that first cylinder effect disappeared from the gap ratio of G/D=3.5. The focus located at the same point and aim of uniform flow shown in upper surface larger than the other gap ratios. Exactly it can be said reverse flow shown in front of the cylinder like single cylinder. There are no saddle point and flow separation region observed.

For the gap ratio of G/D=4 and G/D=4.5 they must have inspected together because of their flow characteristic. In these ratios, uniform flow characteristics are observed except for the near cylinder region. When flow approaches cylinder wall, reverse flow occurs at approximately 10 mm front of the cylinder. The magnitude of the vorticity contours increases at this reverse flow region. As it can be seen from streamline topology and corresponding vorticity contours negative vorticity and reverse flow observed easily. There are no foci and saddle points formed in this type of flow.

For all results it can be said that; each ratio shows its own characteristics. From gap ratio G/D=2 to G/D=3.5 first cylinder effect observed in a decreasing way, but for the last two gap ratios this effect is disappeared and flow takes the character of single cylinder flow that explained in previous section. All of these (2-4.5) gap ratios it can be said that flow shows foci, except for the two ratios there are no flow separation and there are no saddle occurs. Totally it is concluded that from all ratios a critical ratio obtained from experiments. For these experiments it can be said that the gap ratio of G/D=3.5 is the critical ratio exactly because of first cylinder effect disappeared due to distance.

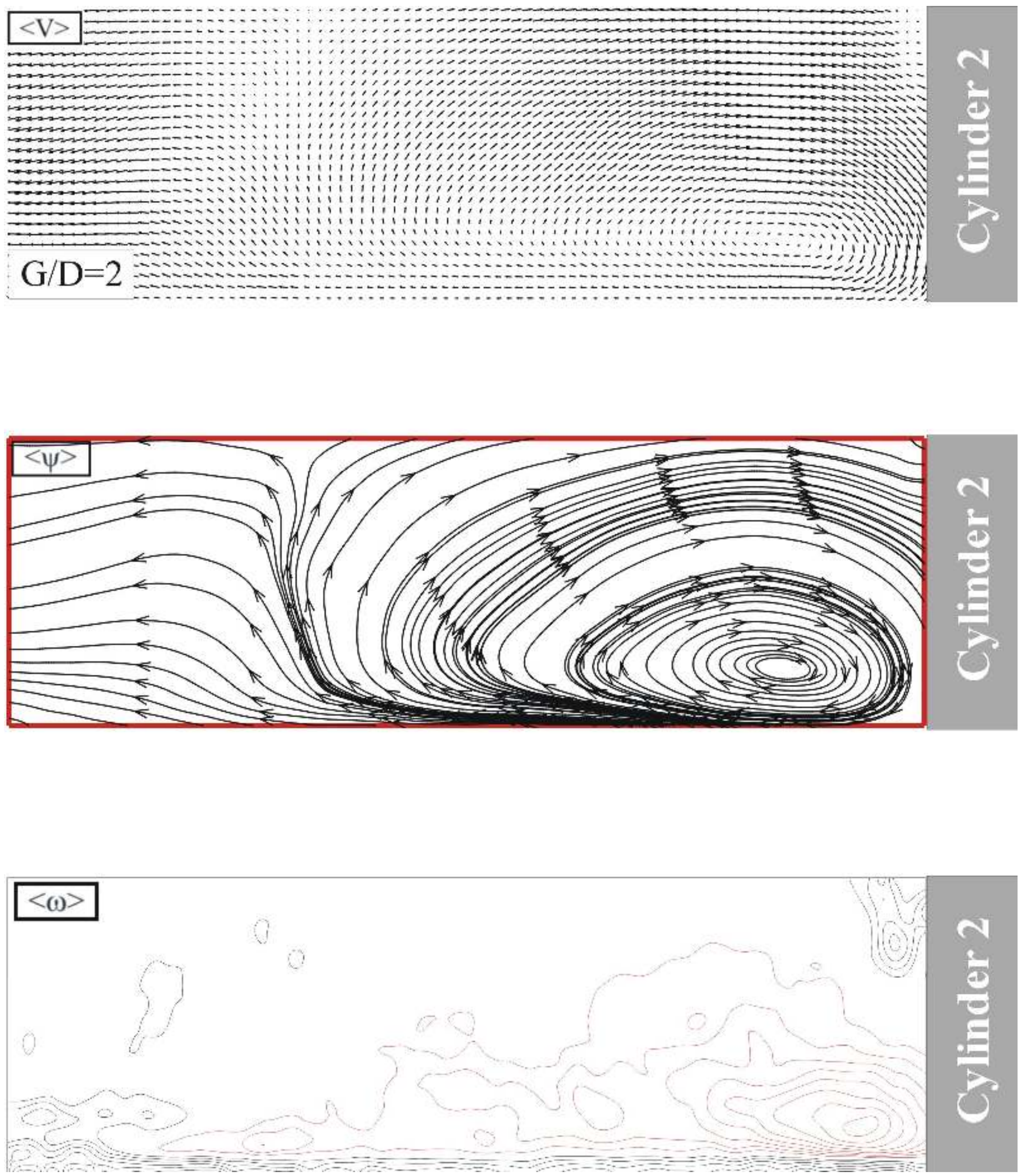

Figure 4.19. Time-averaged velocity field,<V> streamline patterns, $<\psi>$ and vorticity contours, $<\omega>$ in the view section of the flow front cylinder 2 of two cylinders in tandem arrangement with G/D 2 in side-view plane. Minimum and incremental values of vorticity are $\omega_{min} = \pm 1 s^{-1}$ and $\Delta\omega = 1 s^{-1}$.

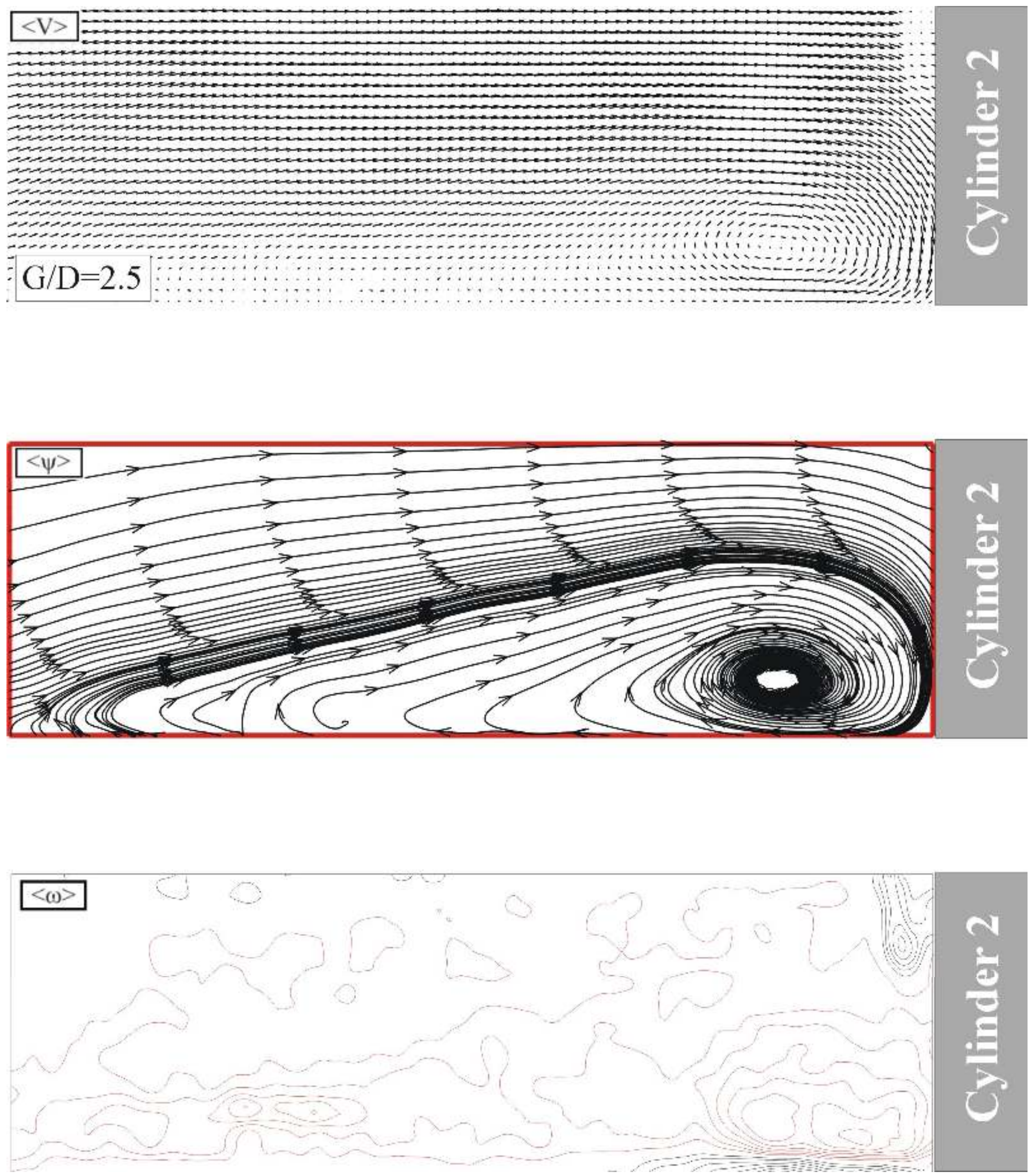

Figure 4.20. Time-averaged velocity field,<V> streamline patterns, <ψ> and vorticity contours, <ω> in the view section of the flow front cylinder 2 of two cylinders in tandem arrangement with G/D 2.5 in side-view plane. Minimum and incremental values of vorticity are $\omega_{min} = \pm 1 s^{-1}$ and $\Delta\omega = 1 s^{-1}$.

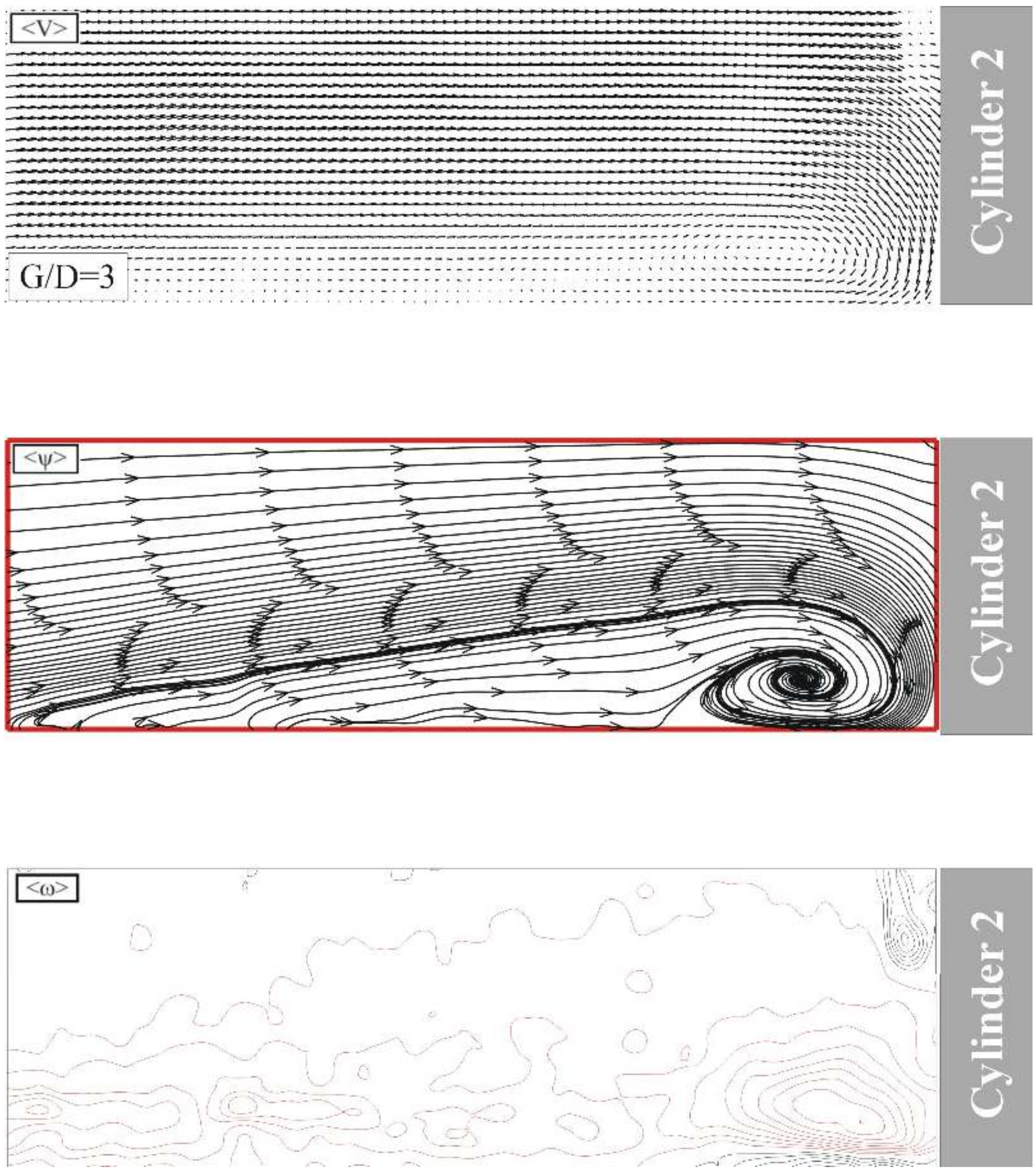

Figure 4.21. Time-averaged velocity field,<V> streamline patterns, <ψ> and vorticity contours, <ω> in the view section of the flow front cylinder 2 of two cylinders in tandem arrangement with G/D 3 in side-view plane. Minimum and incremental values of vorticity are $\omega_{min} = \pm 1 s^{-1}$ and $\Delta\omega = 1 s^{-1}$.

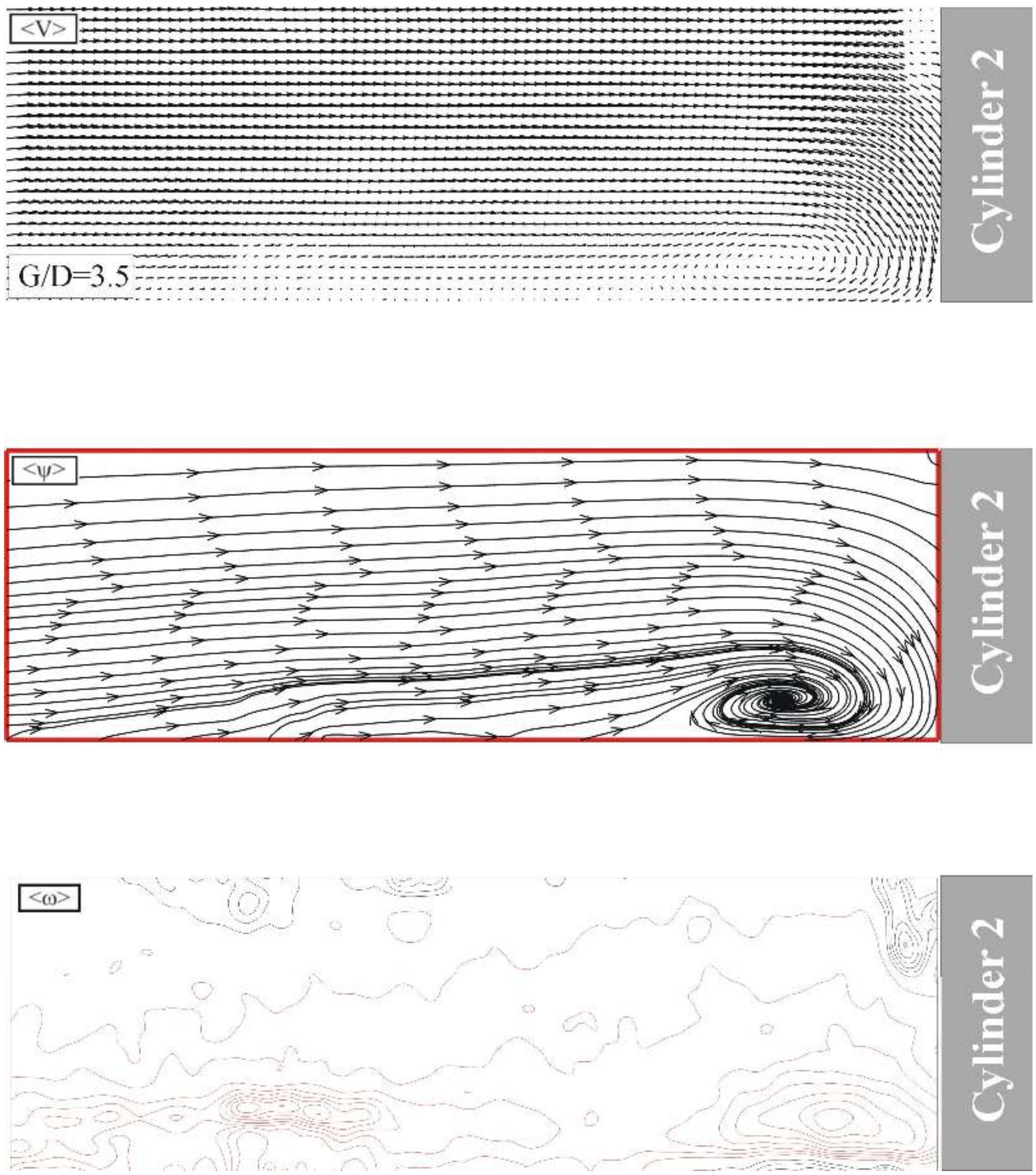

Figure 4.22. Time-averaged velocity field,$\langle V \rangle$ streamline patterns, $\langle \psi \rangle$ and vorticity contours, $\langle \omega \rangle$ in the view section of the flow front cylinder 2 of two cylinders in tandem arrangement with G/D 3.5 in side-view plane. Minimum and incremental values of vorticity are $\omega_{min} = \pm 1 s^{-1}$ and $\Delta\omega = 1 s^{-1}$.

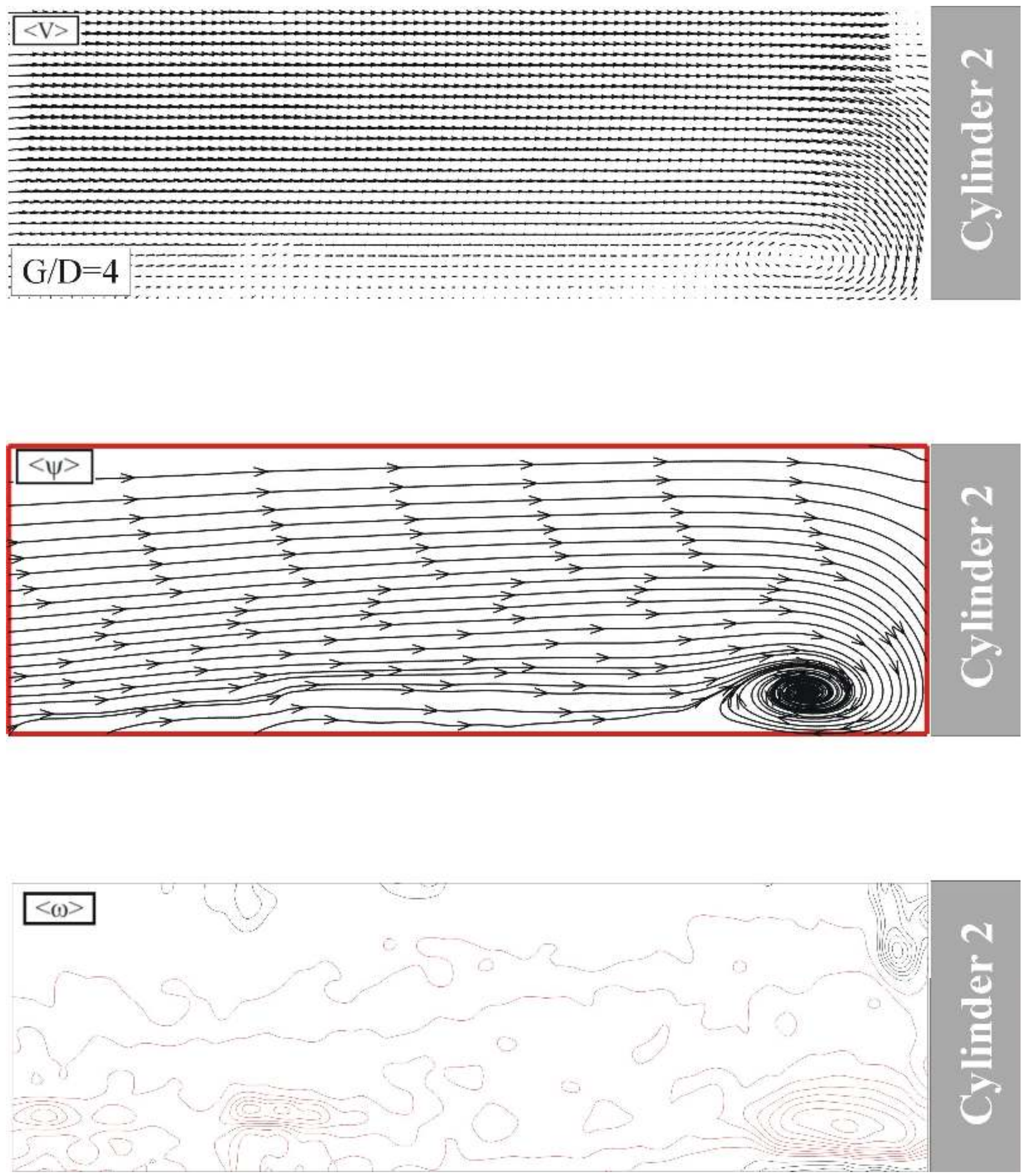

Figure 4.23. Time-averaged velocity field,<V> streamline patterns, <ψ> and vorticity contours, <ω> in the view section of the flow front cylinder 2 of two cylinders in tandem arrangement with G/D 4 in side-view plane. Minimum and incremental values of vorticity are $\omega_{min} = \pm 1 s^{-1}$ and $\Delta\omega = 1 s^{-1}$.

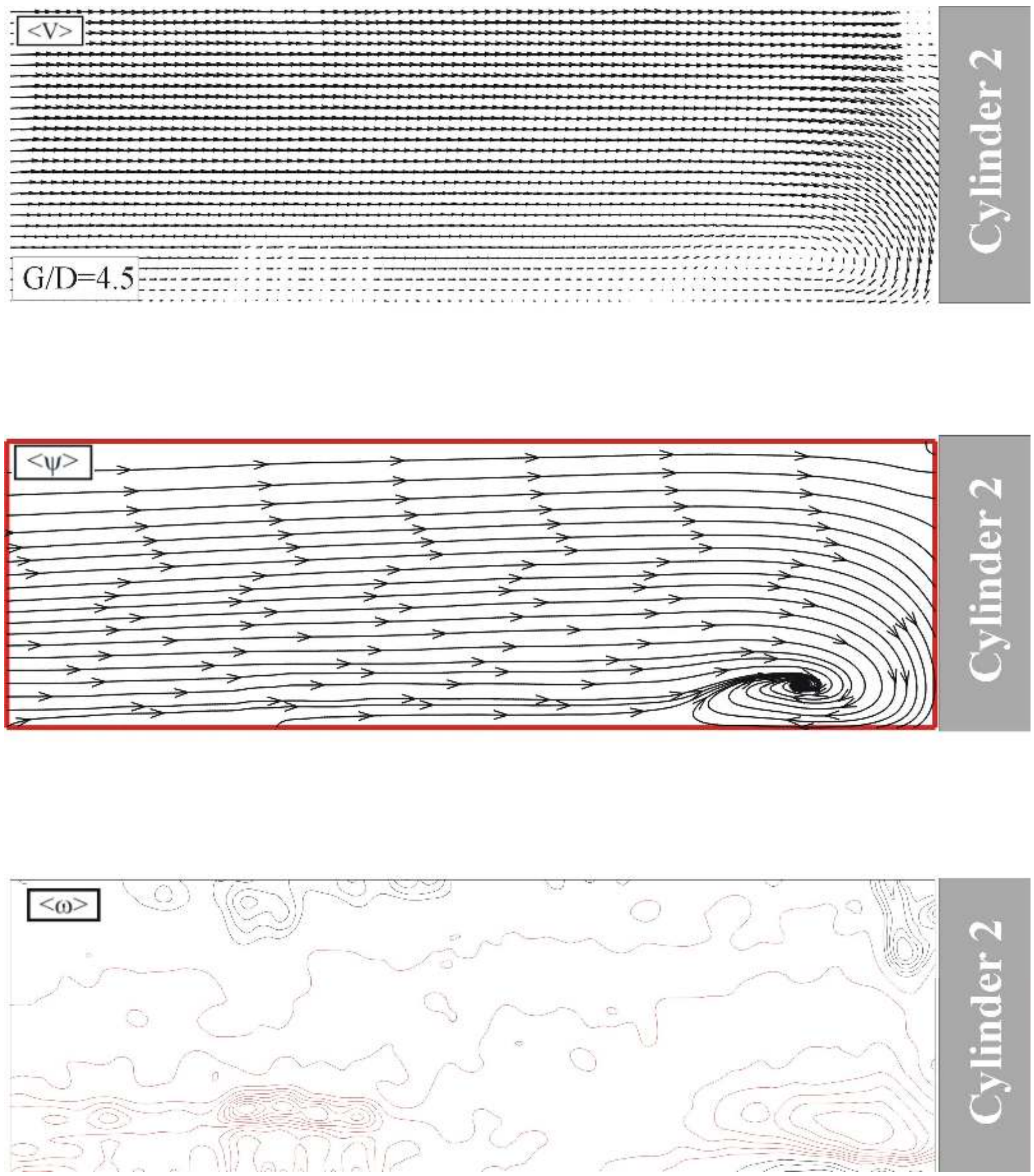

Figure 4.24. Time-averaged velocity field,<V> streamline patterns, <ψ> and vorticity contours, <ω> in the view section of the flow front cylinder 2 of two cylinders in tandem arrangement with G/D 4.5 in side-view plane. Minimum and incremental values of vorticity are $\omega_{min} = \pm 1 s^{-1}$ and $\Delta\omega = 1 s^{-1}$.

4.6. Flow Structure in Front of the First Cylinder

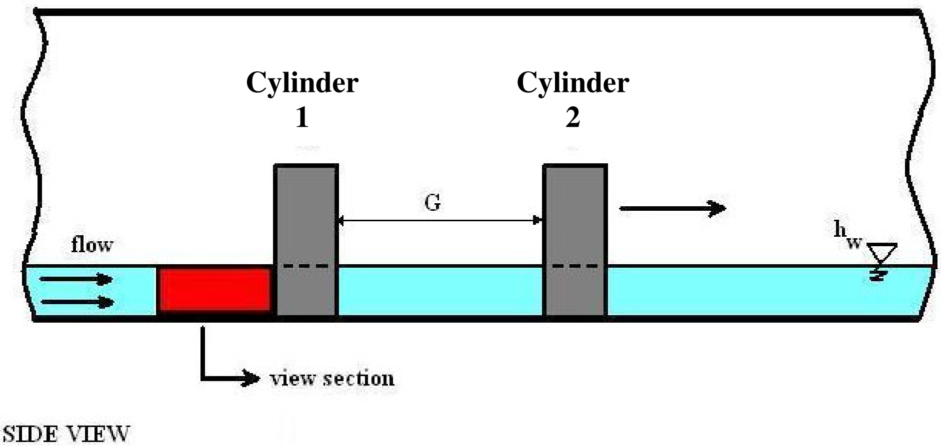

Figure 4.25. Schematic view of the flow in front of cylinder 1 of two cylinders in tandem arrangement with G=0mm-225mm in side-view plane.

Figure 4.25. shows the schematic view of test section in the view section of the flow front of first cylinder of two tandem arrangement cylinders. The time-averaged velocity vector field <V>, corresponding streamline patterns <ψ>, and vorticity contours <ω> obtained from PIV experiments are shown in figures 4.26-4.35 for this flow field.

These experiments were carried out for two cylinders with tandem arrangement having different G/D ratios starting from 0 to 4.5. When the time-averaged velocity vector fields, corresponding streamline patterns and vorticity contours for these G/D ratios are inspected and different conclusions are obtained.

Different from other experiments when the results are inspected for all gap ratios there is an obligation of evaluate all results together due to their similarity. For all of results a focus is observed approximately 10 mm behind the first cylinder. Again in the same point positive vorticity clusters can be seen from vorticity contours. It is observed that no saddle point and flow seperation occurred. In this flow, uniform flow characteristics are observed except for the near cylinder region. When flow approaches cylinder wall, reverse flow occurs at approximately 8 mm front of the cylinder. This reverse flow leads horseshoe vortex system to occur in front of the cylinder. As it can be seen from streamline topology and corresponding vorticity contours negative vorticity and reverse flow observed easily. It can be easily said that there is no critical gap ratio in this experiment because all of results nearly same. Another important conclusion for this experiment, when two tandem cylinders examine with a view section front of first cylinder, second cylinder movements shows no effect on to the inspection section.

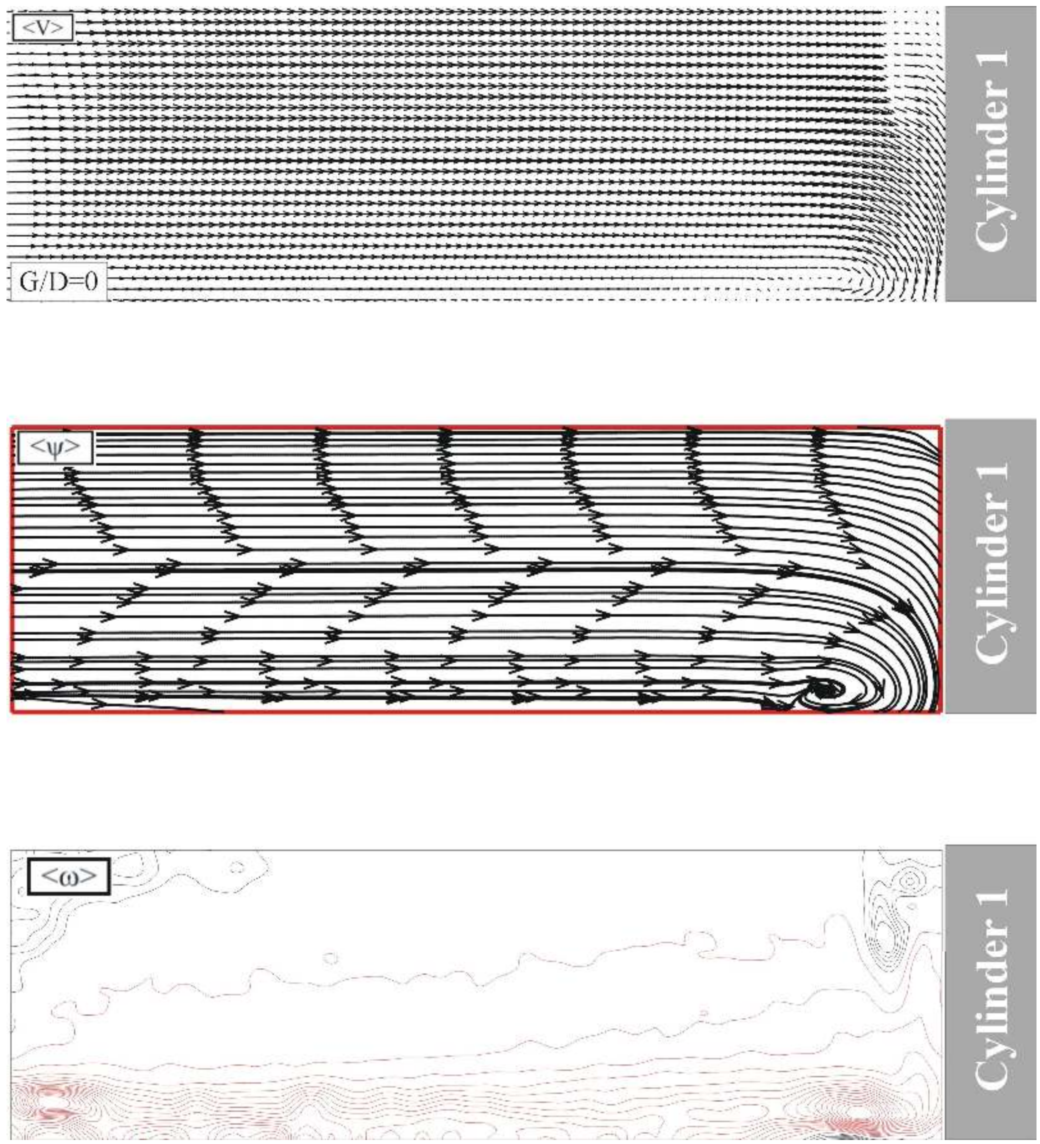

Figure 4.26. Time-averaged velocity field,<V> streamline patterns, <ψ> and vorticity contours, <ω> in the view section of the flow front cylinder 1 of two cylinders in tandem arrangement with G/D 0 in side-view plane. Minimum and incremental values of vorticity are $\omega_{min} = \pm 1 s^{-1}$ and $\Delta\omega = 1 s^{-1}$.

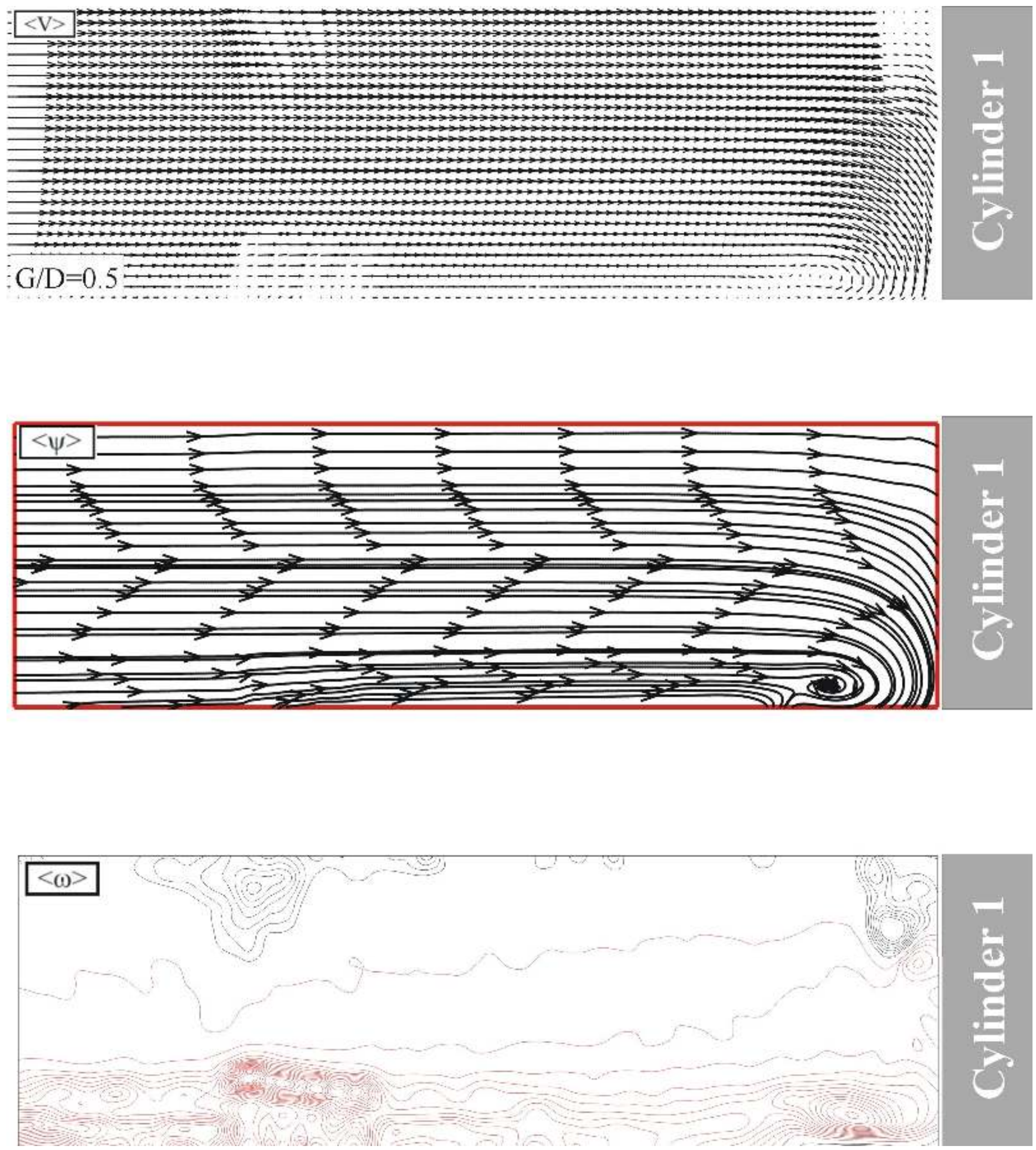

Figure 4.27. Time-averaged velocity field,<V> streamline patterns, <ψ> and vorticity contours, <ω> in the view section of the flow front cylinder 1 of two cylinders in tandem arrangement with G/D 0.5 in side-view plane. Minimum and incremental values of vorticity are $\omega_{min} = \pm 1 s^{-1}$ and $\Delta\omega = 1 s^{-1}$.

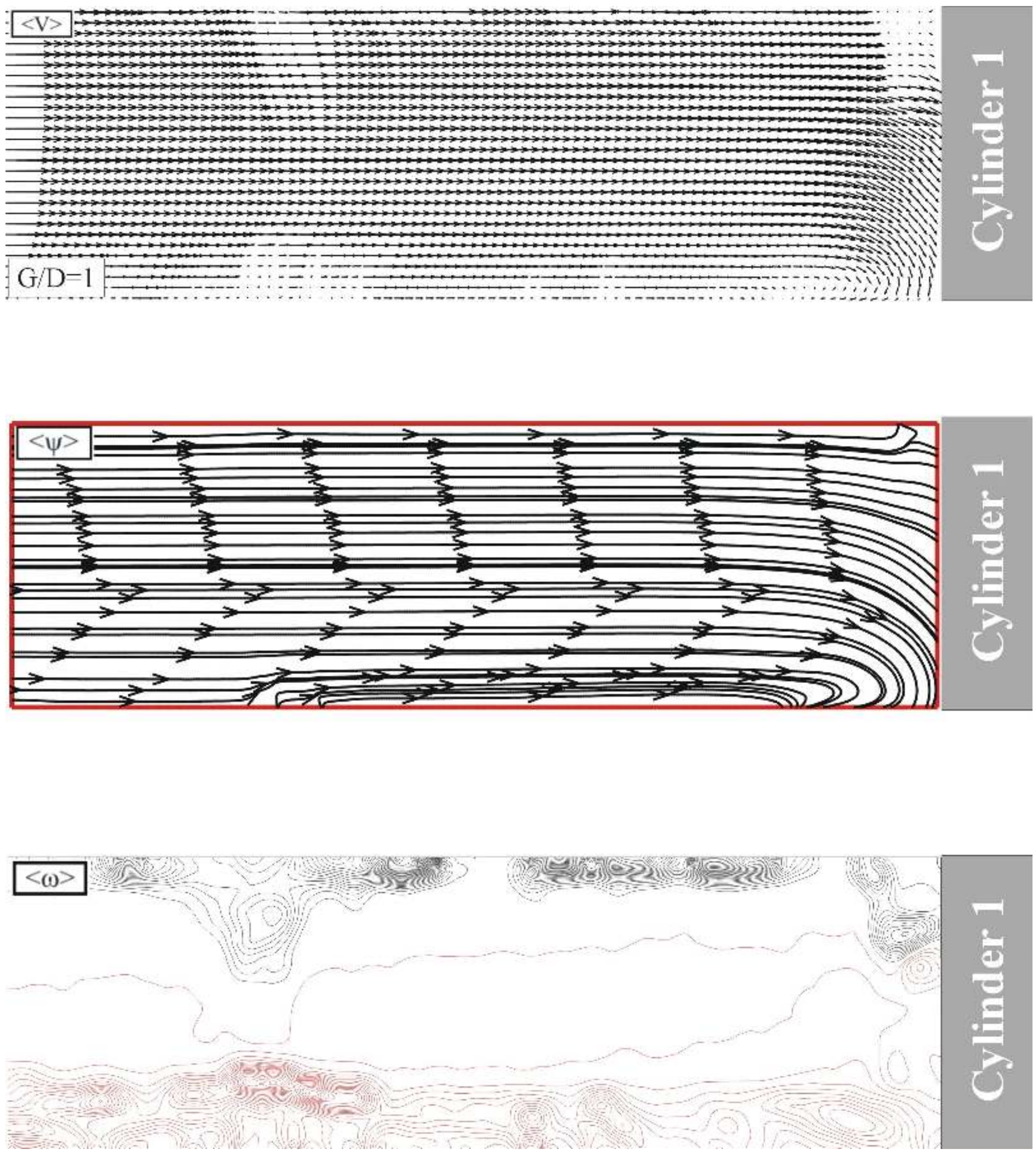

Figure 4.28. Time-averaged velocity field,<V> streamline patterns, <ψ> and vorticity contours, <ω> in the view section of the flow front cylinder 1 of two cylinders in tandem arrangement with G/D 1 in side-view plane. Minimum and incremental values of vorticity are $\omega_{min} = \pm 1 s^{-1}$ and $\Delta\omega = 1 s^{-1}$.

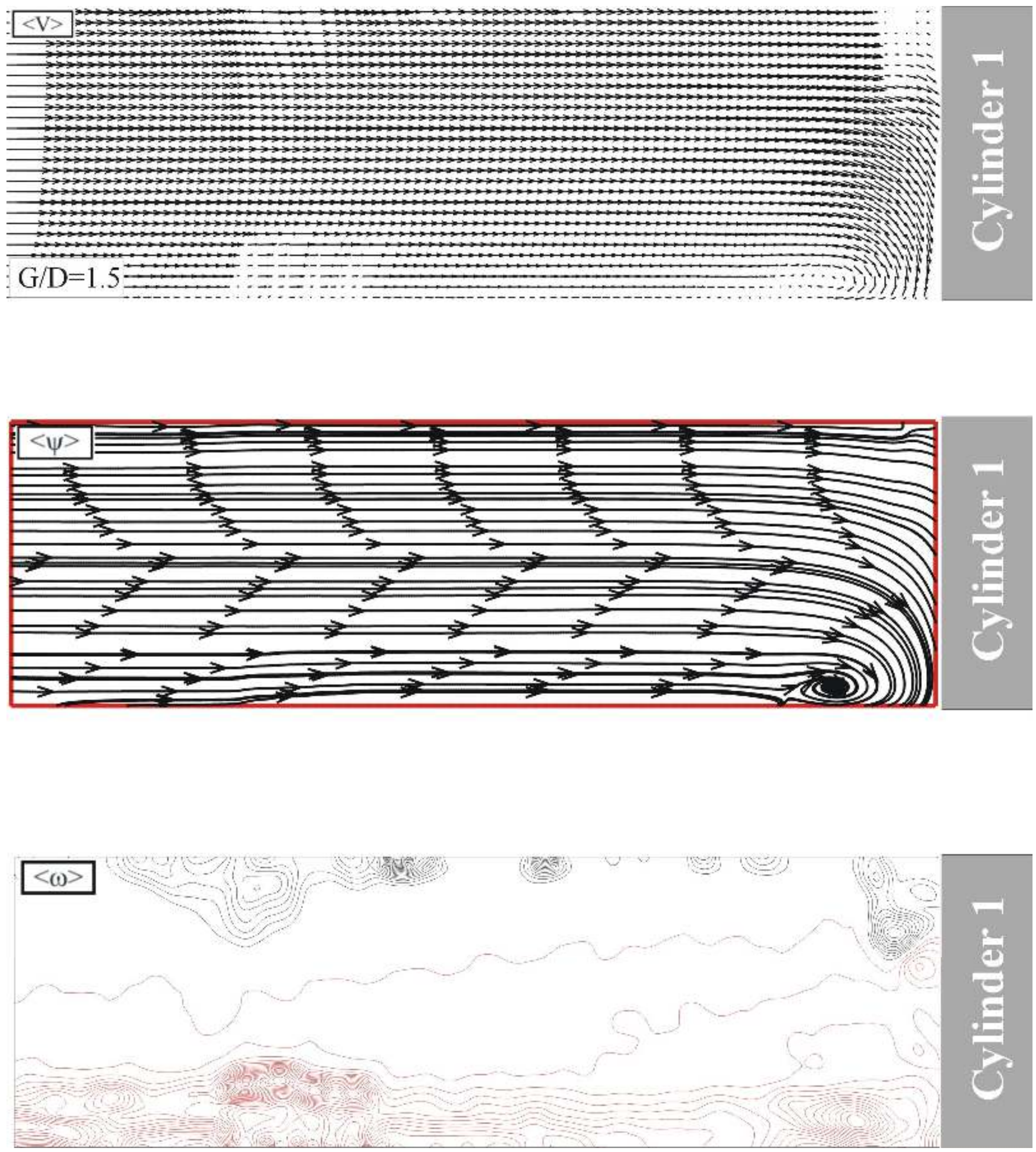

Figure 4.29. Time-averaged velocity field,<V> streamline patterns, <ψ> and vorticity contours, <ω> in the view section of the flow front cylinder 1 of two cylinders in tandem arrangement with G/D 1.5 in side-view plane. Minimum and incremental values of vorticity are $\omega_{min} = \pm 1s^{-1}$ and $\Delta\omega = 1s^{-1}$.

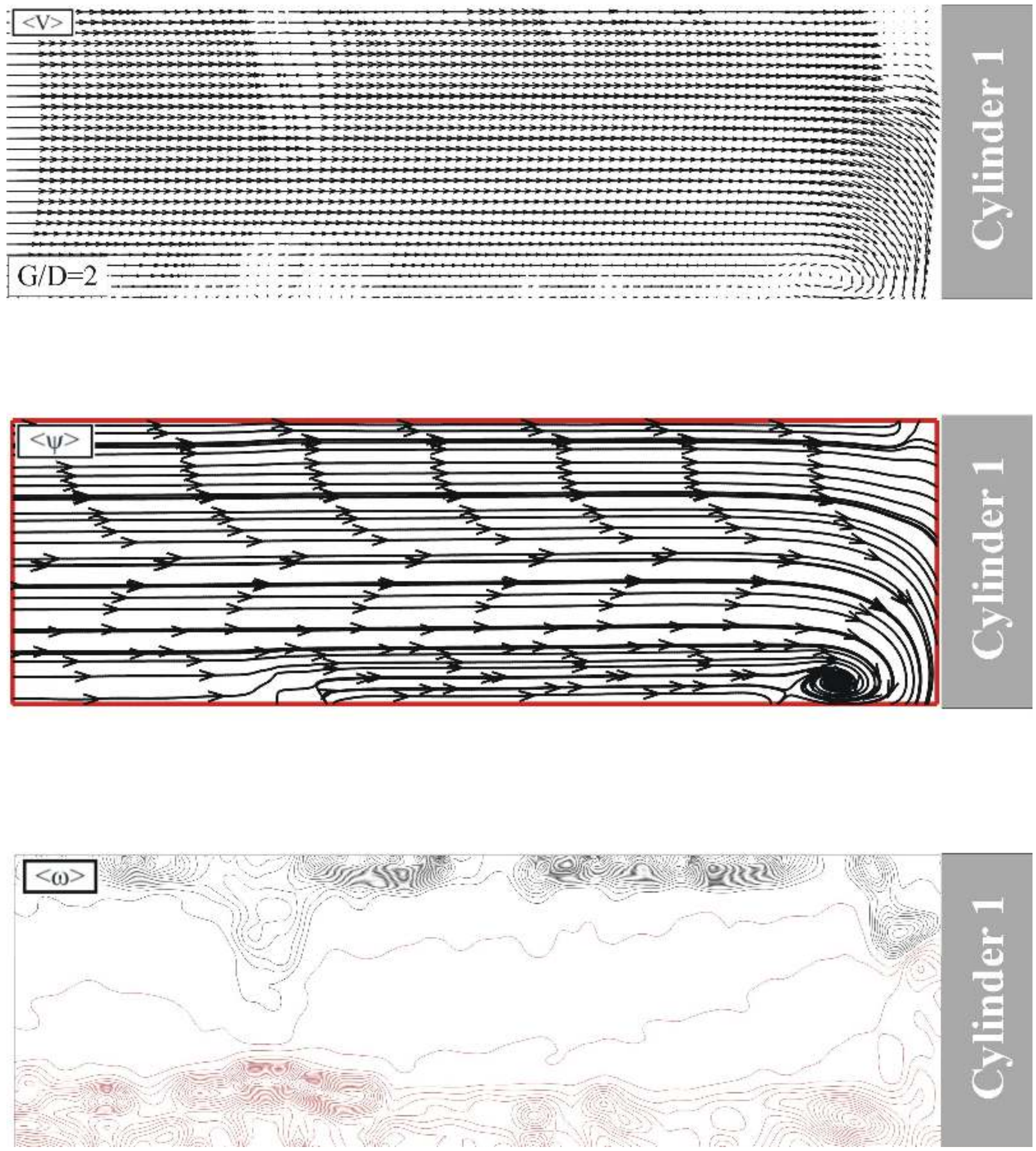

Figure 4.30. Time-averaged velocity field,<V> streamline patterns, <ψ> and vorticity contours, <ω> in the view section of the flow front cylinder 1 of two cylinders in tandem arrangement with G/D 2 in side-view plane. Minimum and incremental values of vorticity are $\omega_{min} = \pm 1 s^{-1}$ and $\Delta\omega = 1 s^{-1}$.

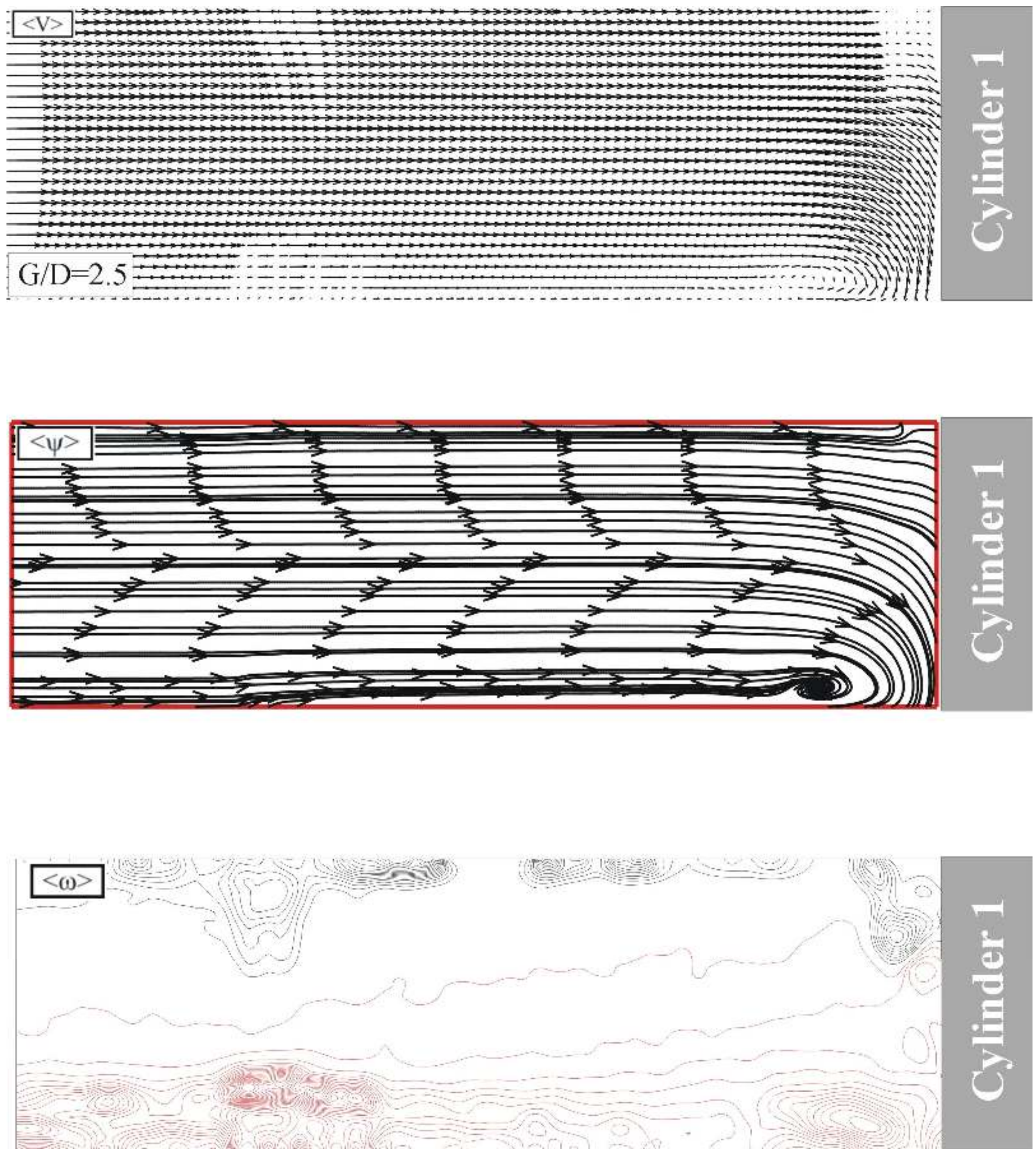

Figure 4.31. Time-averaged velocity field,<V> streamline patterns, <ψ> and vorticity contours, <ω> in the view section of the flow front cylinder 1 of two cylinders in tandem arrangement with G/D 2.5 in side-view plane. Minimum and incremental values of vorticity are $\omega_{min} = \pm 1 s^{-1}$ and $\Delta\omega = 1 s^{-1}$.

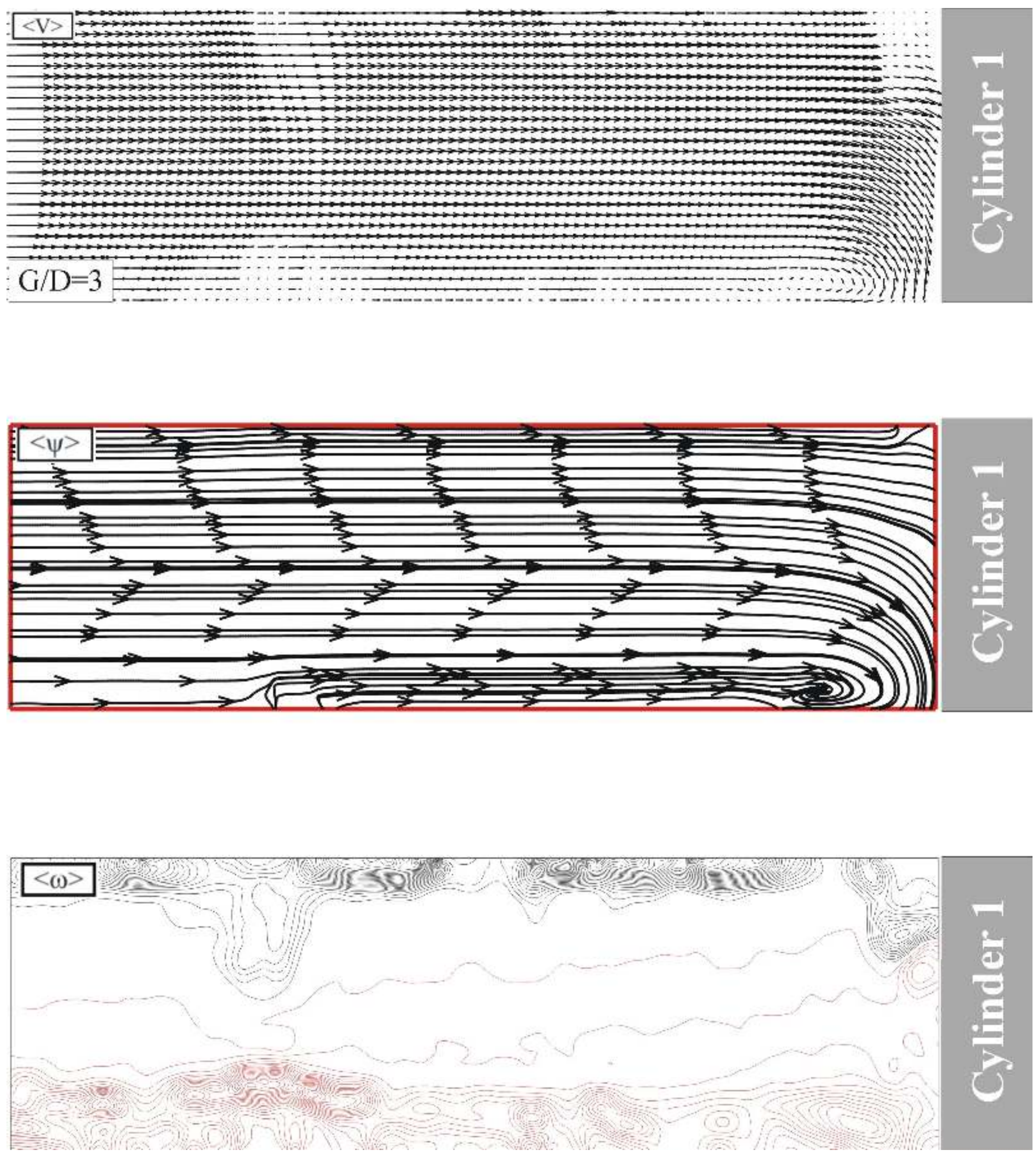

Figure 4.32. Time-averaged velocity field,$\langle V \rangle$ streamline patterns, $\langle \psi \rangle$ and vorticity contours, $\langle \omega \rangle$ in the view section of the flow front cylinder 1 of two cylinders in tandem arrangement with G/D 3 in side-view plane. Minimum and incremental values of vorticity are $\omega_{min} = \pm 1 s^{-1}$ and $\Delta\omega = 1 s^{-1}$.

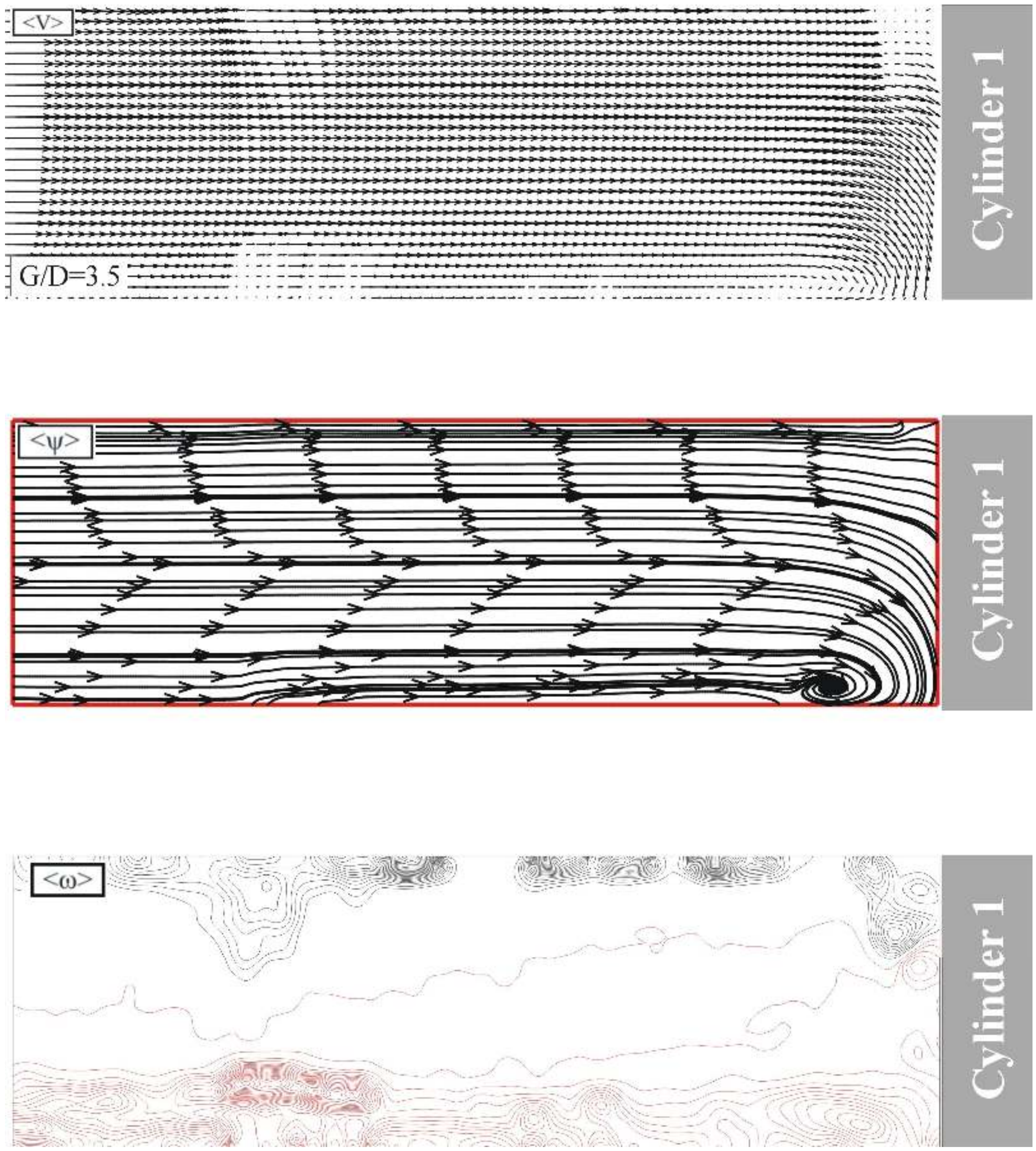

Figure 4.33. Time-averaged velocity field,$\langle V \rangle$ streamline patterns, $\langle \psi \rangle$ and vorticity contours, $\langle \omega \rangle$ in the view section of the flow front cylinder 1 of two cylinders in tandem arrangement with G/D 3.5 in side-view plane. Minimum and incremental values of vorticity are $\omega_{min} = \pm 1 s^{-1}$ and $\Delta\omega = 1 s^{-1}$.

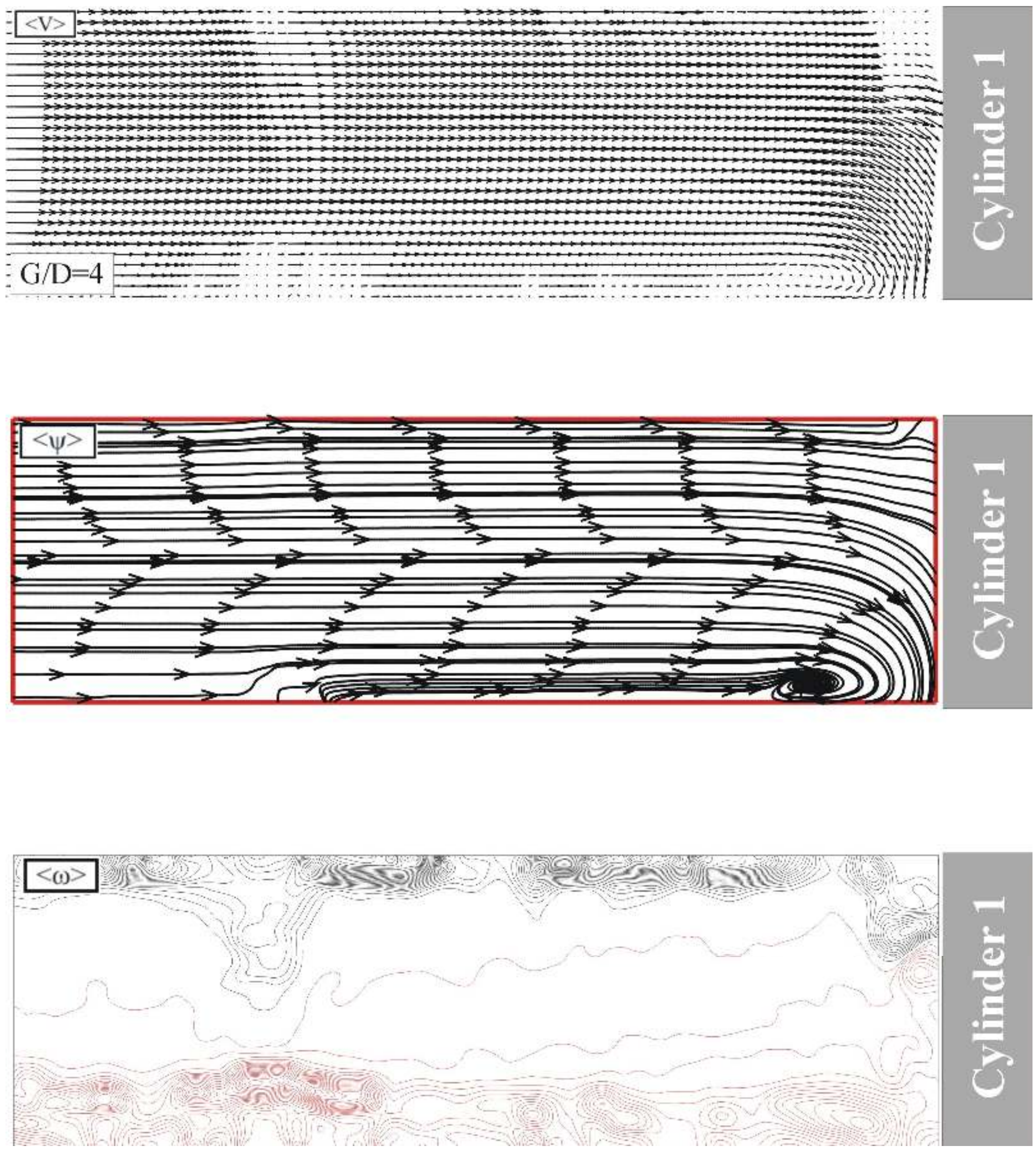

Figure 4.34. Time-averaged velocity field,<V> streamline patterns, <ψ> and vorticity contours, <ω> in the view section of the flow front cylinder 1 of two cylinders in tandem arrangement with G/D 4 in side-view plane. Minimum and incremental values of vorticity are $\omega_{min} = \pm 1s^{-1}$ and $\Delta\omega = 1s^{-1}$.

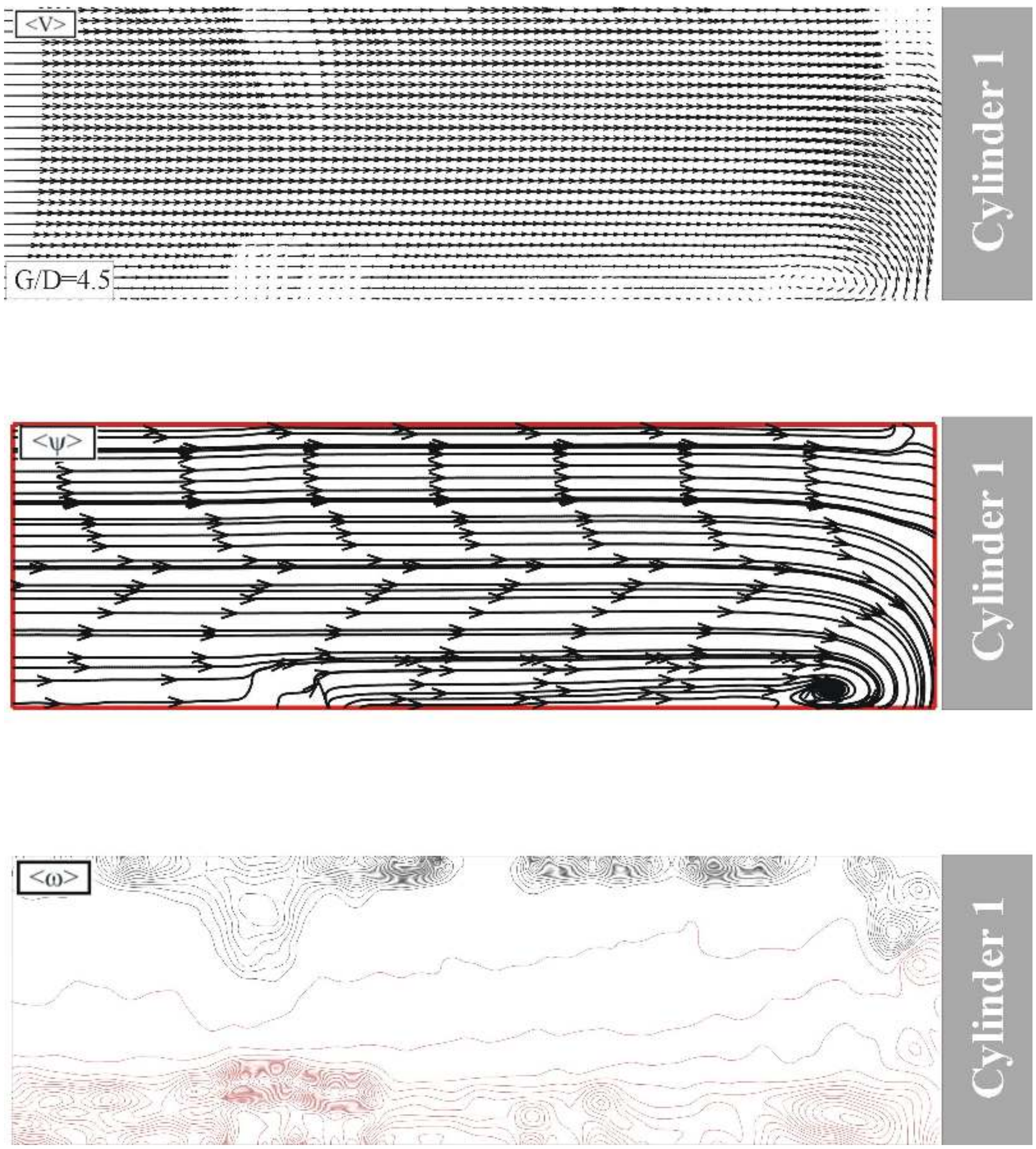

Figure 4.35. Time-averaged velocity field,<V> streamline patterns, <ψ> and vorticity contours, <ω> in the view section of the flow front cylinder 1 of two cylinders in tandem arrangement with G/D 4.5 in side-view plane. Minimum and incremental values of vorticity are $\omega_{min} = \pm 1 s^{-1}$ and $\Delta\omega = 1 s^{-1}$.

4.7. Flow Structure Behind the Second Cylinder

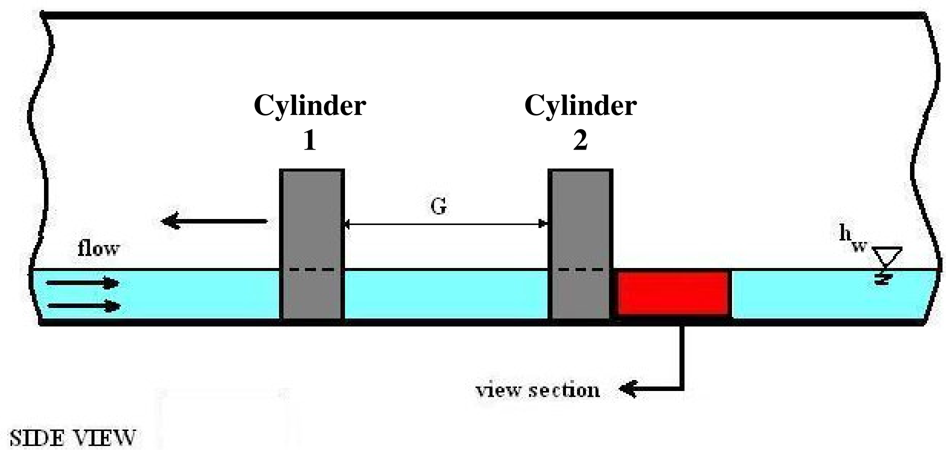

Figure 4.36. Schematic view of the flow behind cylinder 2 of two cylinders in tandem arrangement with G=0mm-225mm in side-view plane

Figure 4.36. shows the schematic view of test section in the view section of the flow behind of second cylinder of two tandem arrangement cylinders. The time-averaged velocity vector field <V>, corresponding streamline patterns <ψ>, and vorticity contours <ω> obtained from PIV experiments are shown in figures 4.37-4.46 for this flow field.

These experiments were carried out for two cylinders with tandem arrangement having different G/D ratios starting from 0 to 4.5. When the time-averaged velocity vector fields, corresponding streamline patterns and vorticity contours for these G/D ratios are inspected and different conclusions are obtained.

For the beginning gap ratio of G/D=0, the important conclusions are about flow separation and reverse flow presences. Here is approximately 55 mm behind the cylinder flow separation occurs. Due to this separation a reverse flow is shown between the separation region and cylinder wall. There is no focus is shown here but saddle point occurs in the separation region. After the separation region flow behaves in the aim of uniform flow. It can be easily said from the streamline topology that first cylinder effect shows itself clearly when the single cylinder experiment checked.

For the gap ratio of G/D=0.5 showed that the similar flow characteristics occurred compared to G/D=0. Again flow separation occurs at the same point behind the cylinder reverse flow is shown between the cylinder wall and separation region. There is no focus is observed but saddle point is shown on to the separation region. In this combination flow getting start uniform flow after the separation region.

In the gap ratio of G/D=1, different from previous ratios a focus is observed just 7 mm behind the cylinder and no saddle point occupation. The occupation of flow separation can be said at the point of 58 mm behind the cylinder. Reverse flow is shown between the cylinder wall and separation region as expected. The aim of the flow getting uniform after separation region and vertical direction on to here. As it can be seen from vorticity contours, vorticity clusters is shown just behind the cylinder.

From streamline topology for the gap ratio of G/D=1.5, no focus and saddle point is observed anywhere. Here this combination shows different characteristics. Flow separation starts approximately 35 mm behind the cylinder and reverse flow is shown up to the cylinder wall. Uniform flow type is shown after the separation region. Base development of the flow from the previous ratios, vorticity clusters starts at the region of approximately 40 mm behind of the cylinder.

In the ratio of G/D=2 it can be seen from streamline topology flow characteristics changes according to other ratios. A saddle point is observed approximately 8 mm behind the cylinder near to the upper surface. Two foci is shown approximately 35 mm and 40 mm behind the cylinder. Flow separation starts at nearly 10 mm behind the cylinder. Flow aims in vertical direction between the cylinder and separation region. It is observed that after the foci occupation region nearly 45 mm behind the cylinder flow takes the uniform character. Another important difference, as it can be seen from vorticity contours, condensation starts nearly 15 mm behind the cylinder goes up to the end of view section.

The flow separation and reverse flow occupation can be seen exactly in the gap ratio of G/D=2.5. A focus is observed in the region at approximately 35 mm behind the cylinder. 10 mm behind the cylinder flow separation is shown. And due to this reverse flow is observed between the region and the cylinder wall. Flow shows the characteristics of uniform flow nearly 40 mm behind the cylinder and the aim of vertical direction in the separation region. It is observed that vorticity clusters shown in focus occupation region.

In the gap ratio of G/D=3, basic flow characteristics are the observation of flow separation and focus. It is observed that flow separates at approximately 35 mm behind the cylinder. Reverse flow is shown here again. It can be seen from streamline topology a focus is shown nearly 43 mm behind the cylinder. And a saddle point is observed in the separation region near to the upper surface. Vorticity clusters is observed around the focus.

Conclusions of the gap ratios G/D=3.5, G/D=4 and G/D=4.5 can be investigated together. For these ratios it is not observed any focus presence. As it can be seen from streamline topology both ratios shows flow separation with a linear position change. Between cylinder and separation region reverse flow occurs. Negative vorticities are observed along the afterwards of the separation region in other words uniform flow characteristics region.

After from all notifications related with ratios it can be said that; first cylinder effect never disappears for these gap ratios. Because of wakes that affected on to second cylinder different flow characteristics are observed in different gap ratios except from last three ratios. It can be seen exactly from time averaged velocity field flow separation and reverse flow are inspected in both ratios. Only location differences appears but generally flow characteristics show similarity. For all applications it can be divided into three parts related with development of flow. For first four ratios only separation region is pronounced, after three ratios focus occupation pronounced and the last three ratios again separation and uniform flow stability after region are pronounced. Finally if a critical ratio is needed to notice, it must have been the ratio of G/D=3.5. Because it is expected that if experiments will go on with linear increasing of gap ratios, finally the result of single cylinder experiment with the view section of behind, can be obtained exactly.

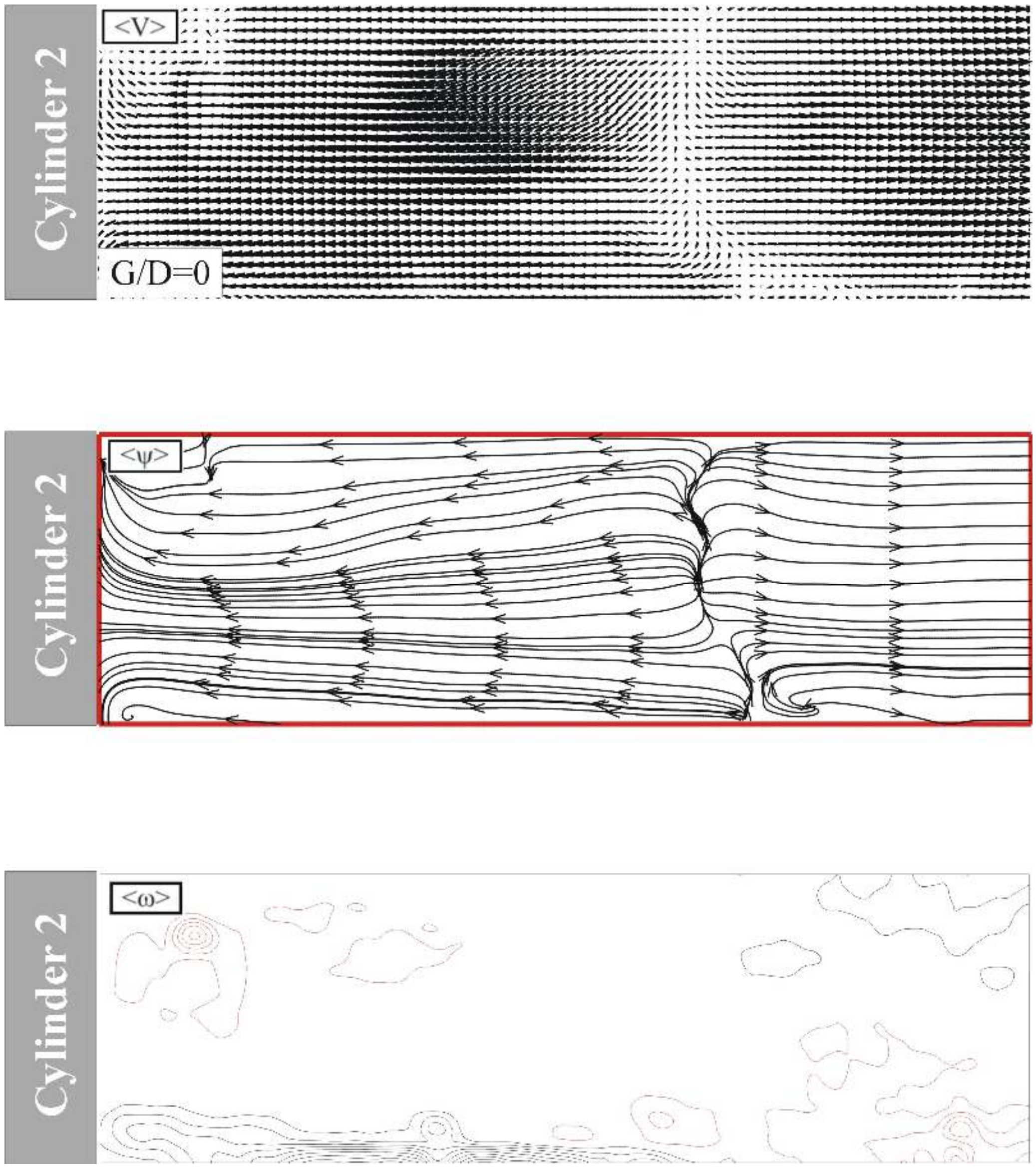

Figure 4.37. Time-averaged velocity field,<V> streamline patterns, <ψ> and vorticity contours, <ω> in the view section of the flow behind cylinder 2 of two cylinders in tandem arrangement with G/D 0 in side-view plane. Minimum and incremental values of vorticity are $\omega_{min} = \pm 1 s^{-1}$ and $\Delta\omega = 1 s^{-1}$.

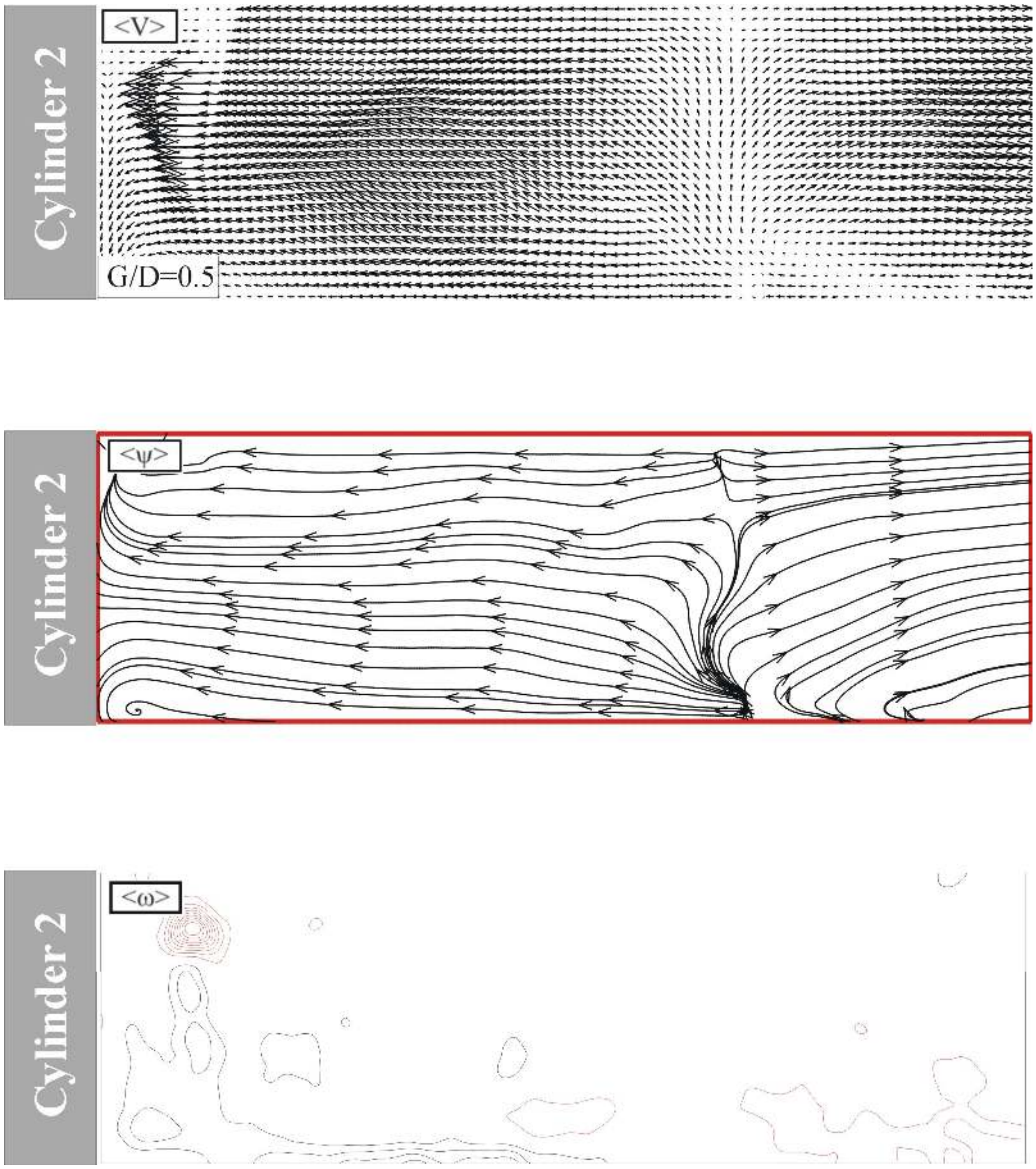

Figure 4.38. Time-averaged velocity field,<V> streamline patterns, <ψ> and vorticity contours, <ω> in the view section of the flow behind cylinder 2 of two cylinders in tandem arrangement with G/D 0.5 in side-view plane. Minimum and incremental values of vorticity are $\omega_{min} = \pm 1 s^{-1}$ and $\Delta\omega = 1 s^{-1}$.

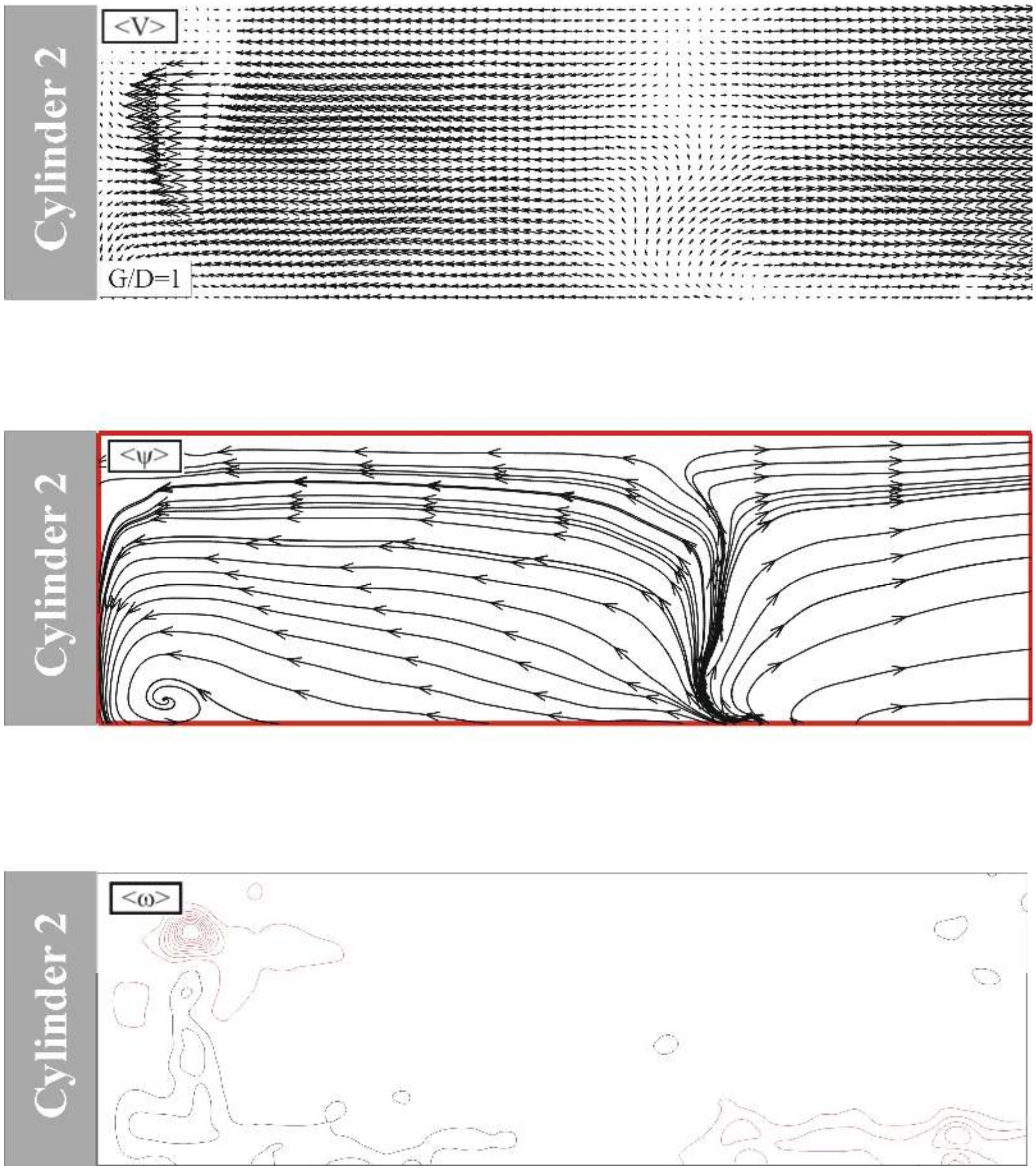

Figure 4.39. Time-averaged velocity field,<V> streamline patterns, <ψ> and vorticity contours, <ω> in the view section of the flow behind cylinder 2 of two cylinders in tandem arrangement with G/D 1 in side-view plane. Minimum and incremental values of vorticity are $\omega_{min} = \pm 1 s^{-1}$ and $\Delta\omega = 1 s^{-1}$.

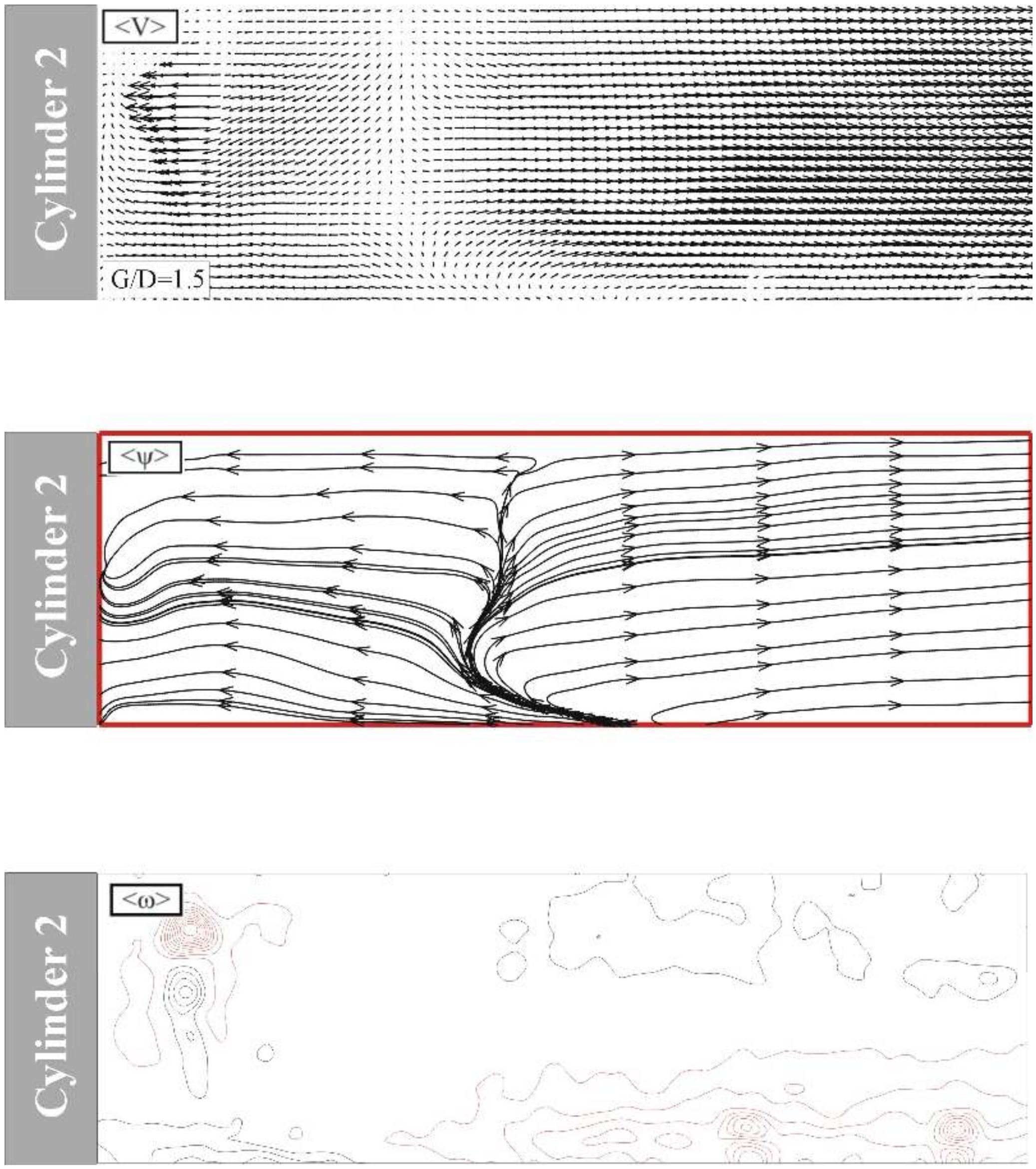

Figure 4.40. Time-averaged velocity field,<V> streamline patterns, <ψ> and vorticity contours, <ω> in the view section of the flow behind cylinder 2 of two cylinders in tandem arrangement with G/D 1.5 in side-view plane. Minimum and incremental values of vorticity are $\omega_{min} = \pm 1 s^{-1}$ and $\Delta\omega = 1 s^{-1}$.

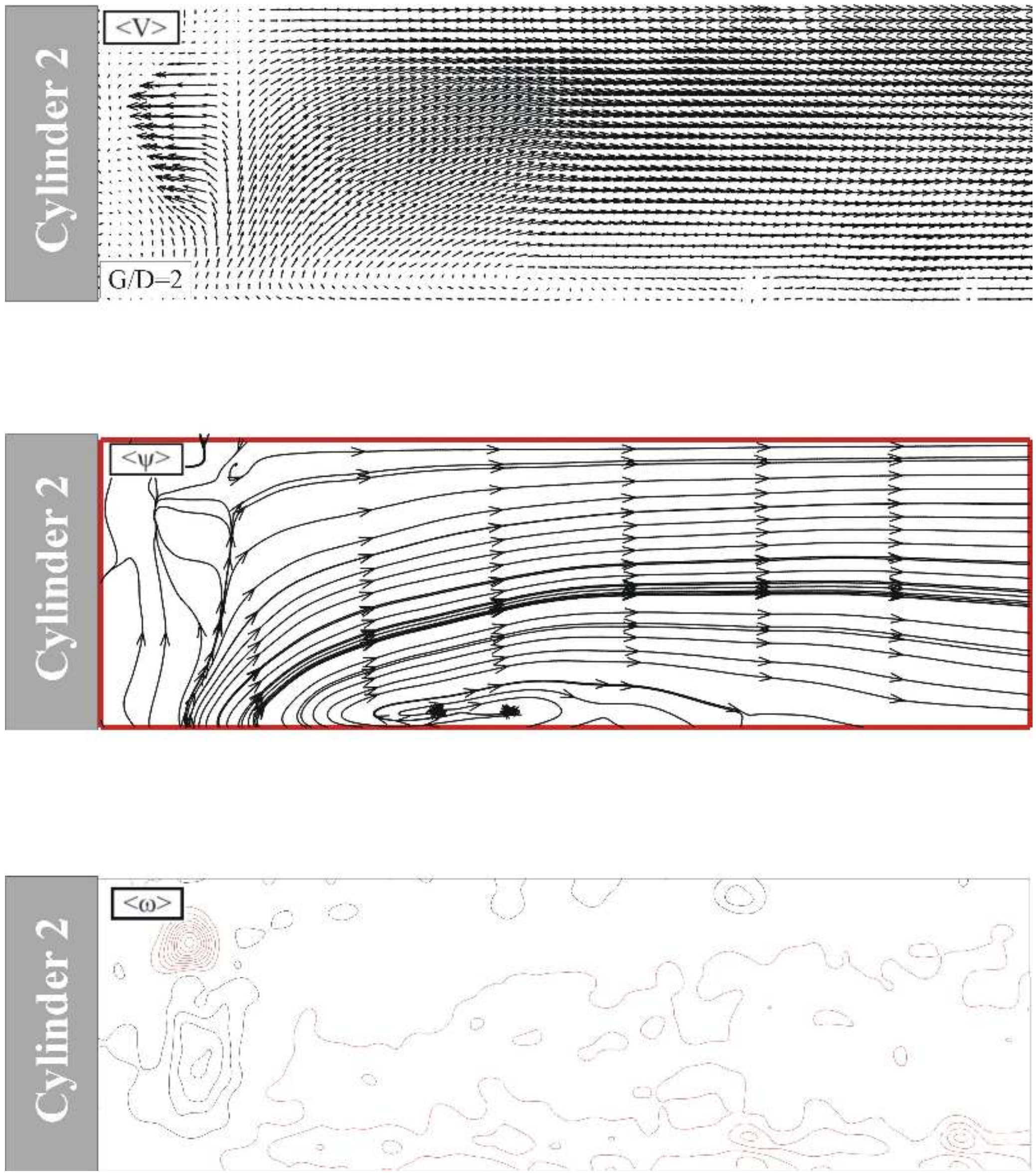

Figure 4.41. Time-averaged velocity field,<V> streamline patterns, <ψ> and vorticity contours, <ω> in the view section of the flow behind cylinder 2 of two cylinders in tandem arrangement with G/D 2 in side-view plane. Minimum and incremental values of vorticity are $\omega_{min} = \pm 1 s^{-1}$ and $\Delta\omega = 1 s^{-1}$.

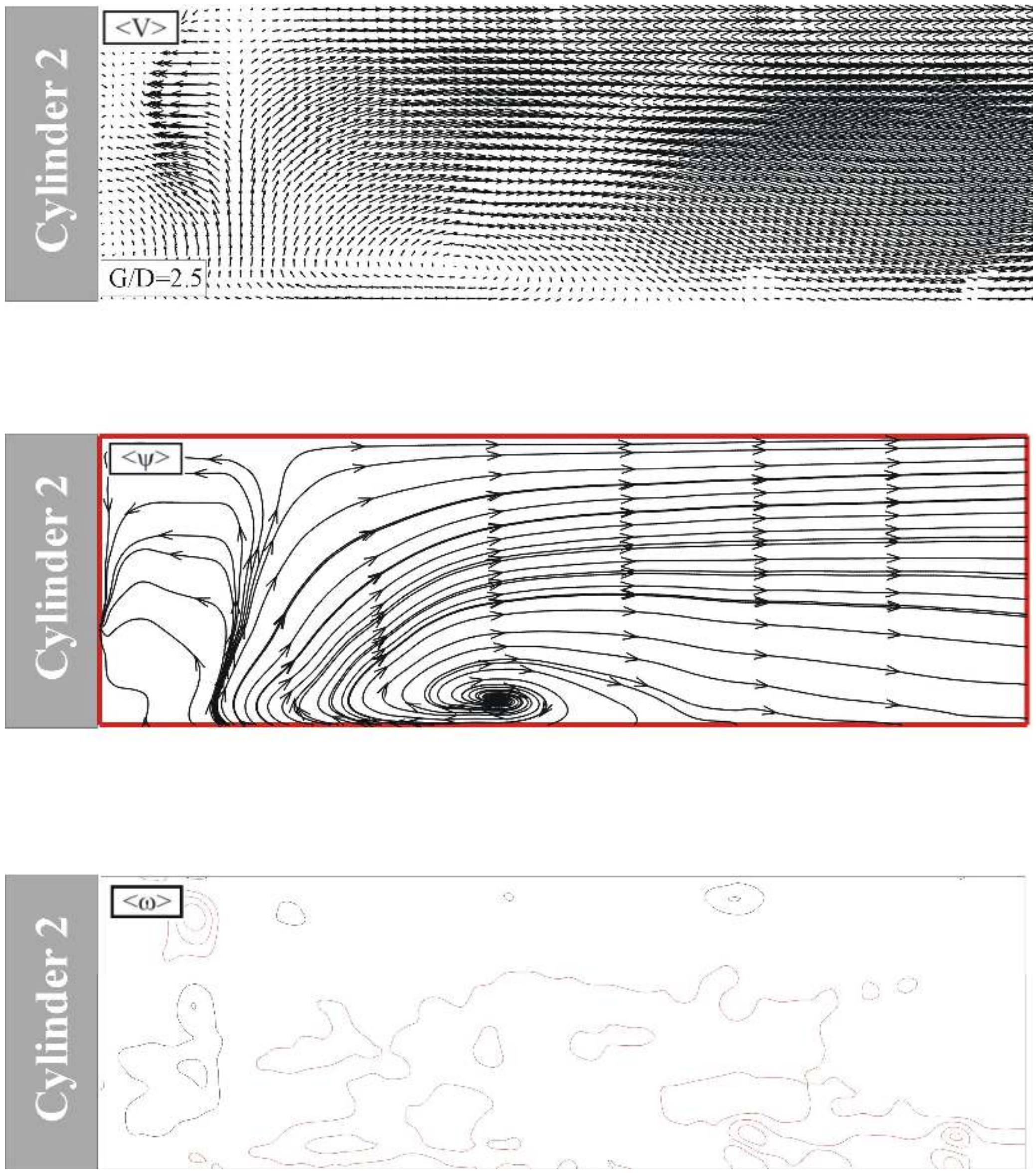

Figure 4.42. Time-averaged velocity field,<V> streamline patterns, <ψ> and vorticity contours, <ω> in the view section of the flow behind cylinder 2 of two cylinders in tandem arrangement with G/D 2.5 in side-view plane. Minimum and incremental values of vorticity are $\omega_{min} = \pm 1 s^{-1}$ and $\Delta\omega = 1 s^{-1}$.

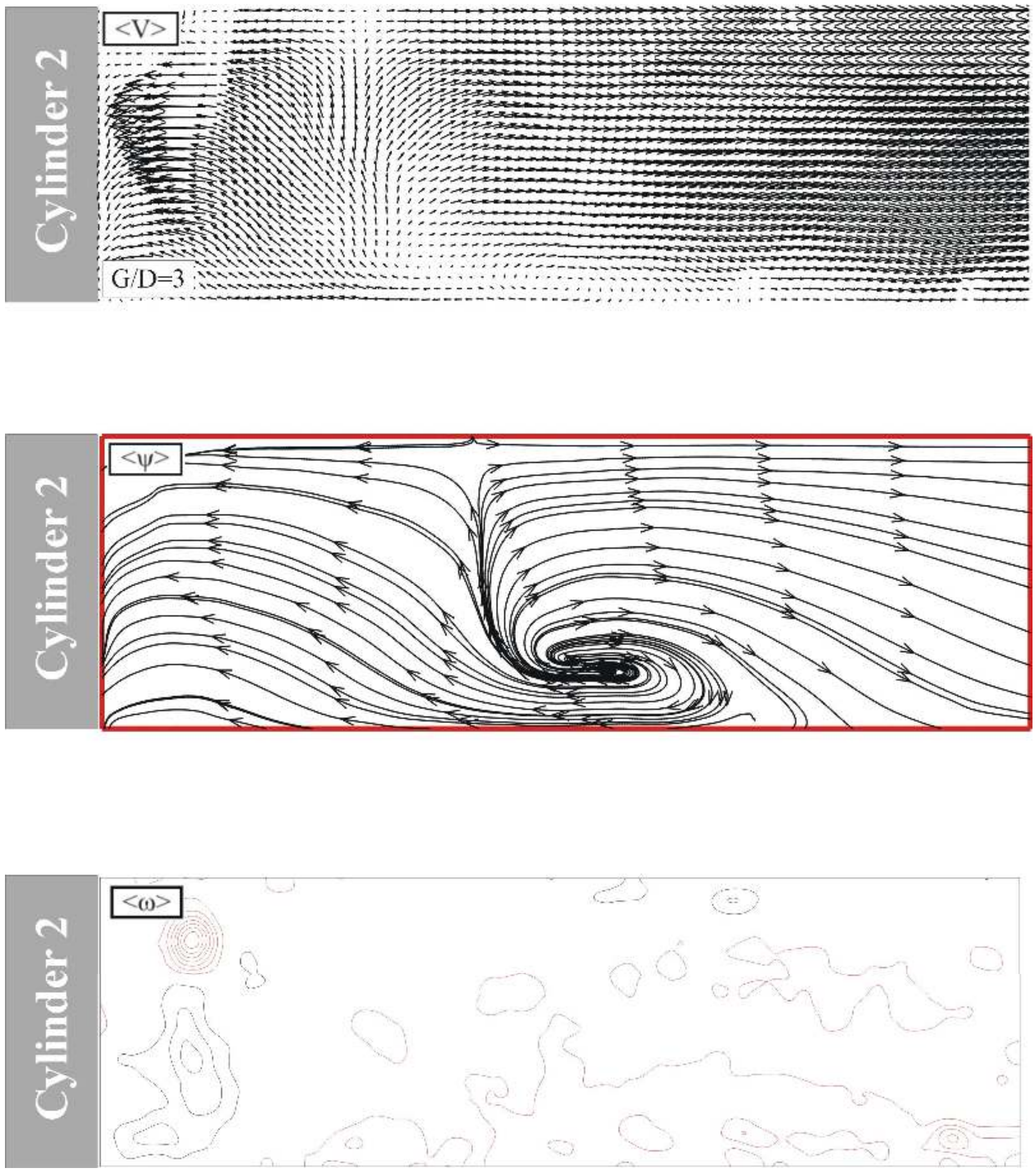

Figure 4.43. Time-averaged velocity field,$\langle V \rangle$ streamline patterns, $\langle \psi \rangle$ and vorticity contours, $\langle \omega \rangle$ in the view section of the flow behind cylinder 2 of two cylinders in tandem arrangement with G/D 3 in side-view plane. Minimum and incremental values of vorticity are $\omega_{min} = \pm 1 s^{-1}$ and $\Delta\omega = 1 s^{-1}$.

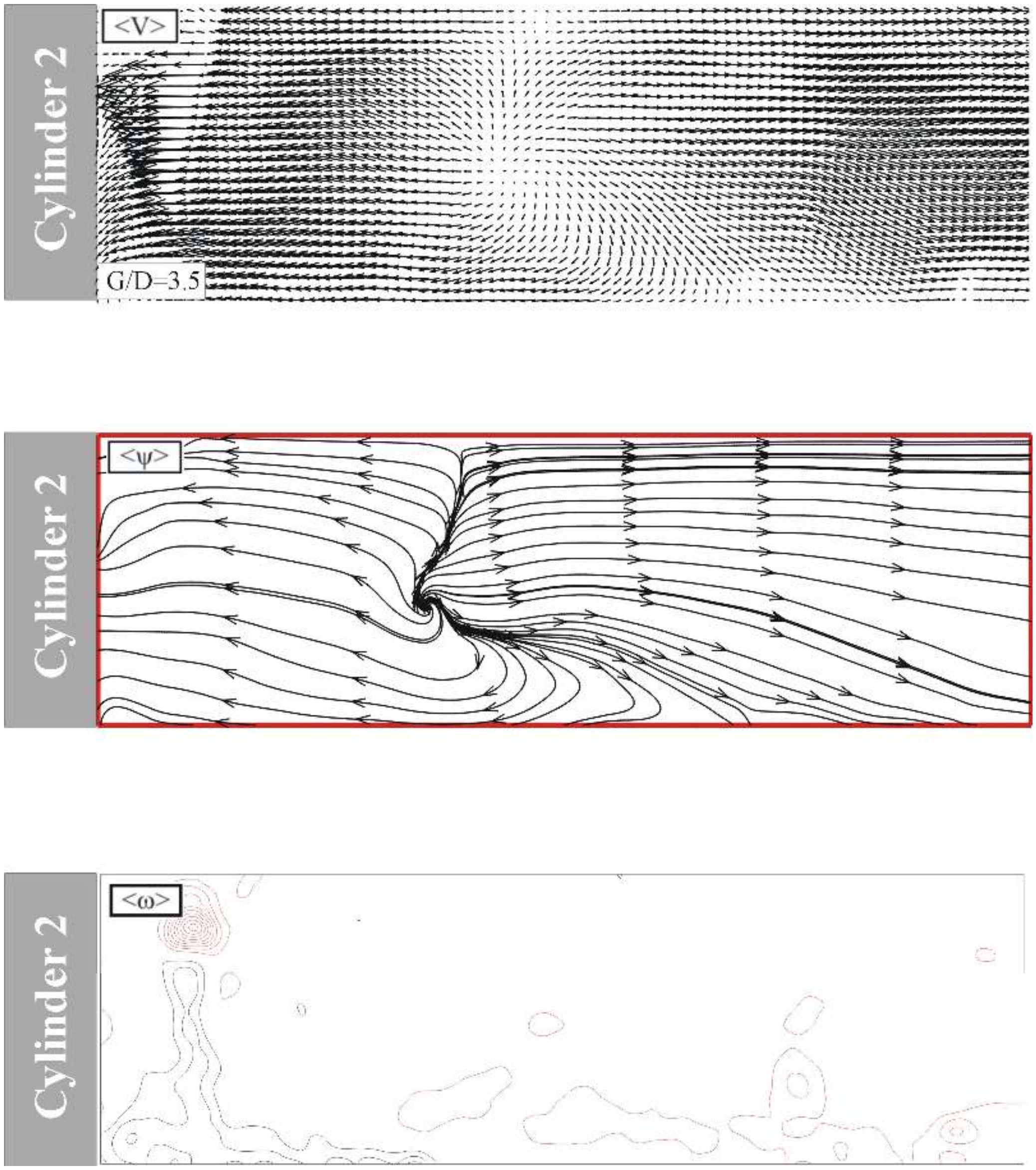

Figure 4.44. Time-averaged velocity field,<V> streamline patterns, <ψ> and vorticity contours, <ω> in the view section of the flow behind cylinder 2 of two cylinders in tandem arrangement with G/D 3.5 in side-view plane. Minimum and incremental values of vorticity are $\omega_{min} = \pm 1 s^{-1}$ and $\Delta\omega = 1 s^{-1}$.

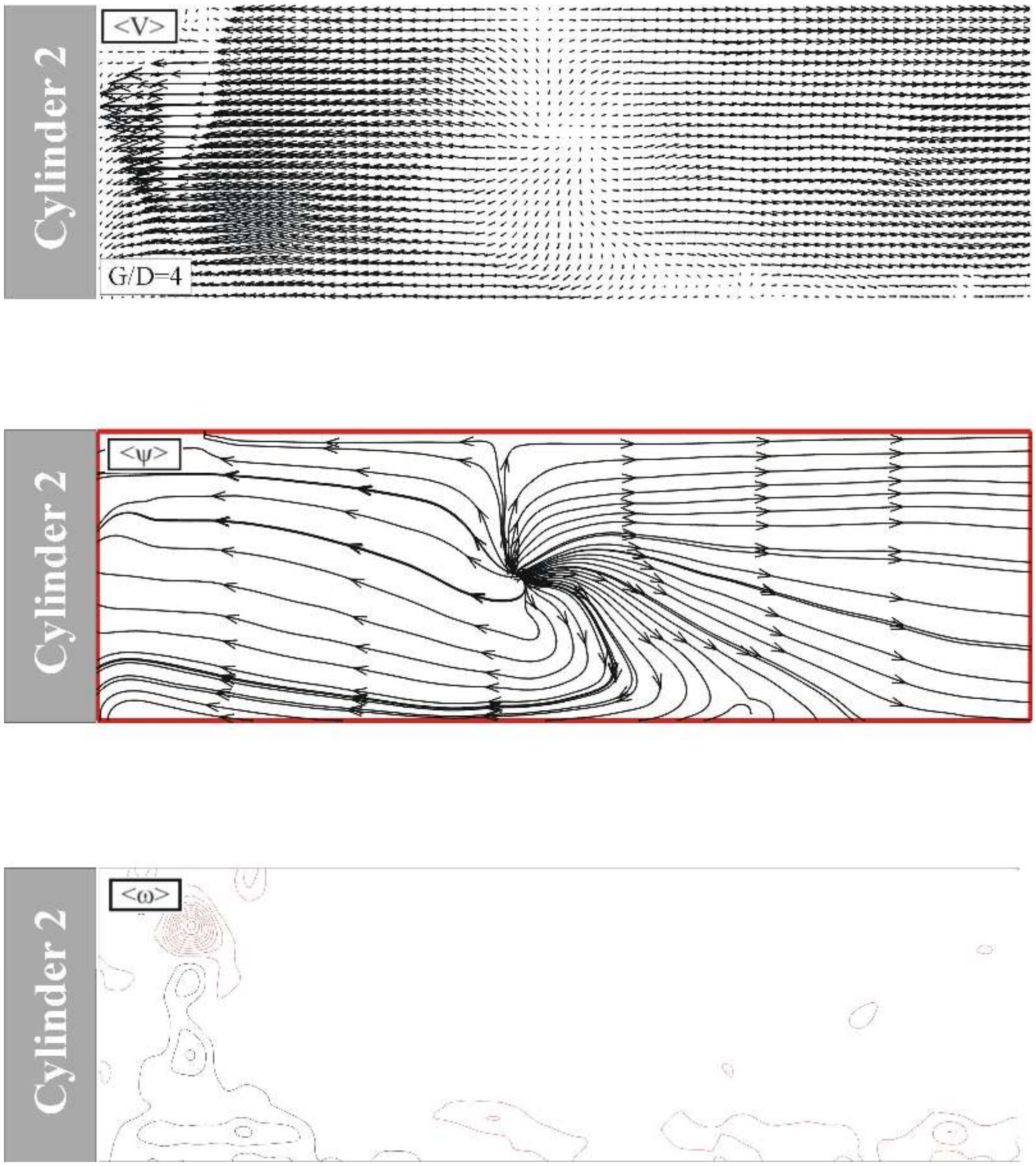

Figure 4.45. Time-averaged velocity field,<V> streamline patterns, <ψ> and vorticity contours, <ω> in the view section of the flow behind cylinder 2 of two cylinders in tandem arrangement with G/D 4 in side-view plane. Minimum and incremental values of vorticity are $\omega_{min} = \pm 1 s^{-1}$ and $\Delta\omega = 1 s^{-1}$.

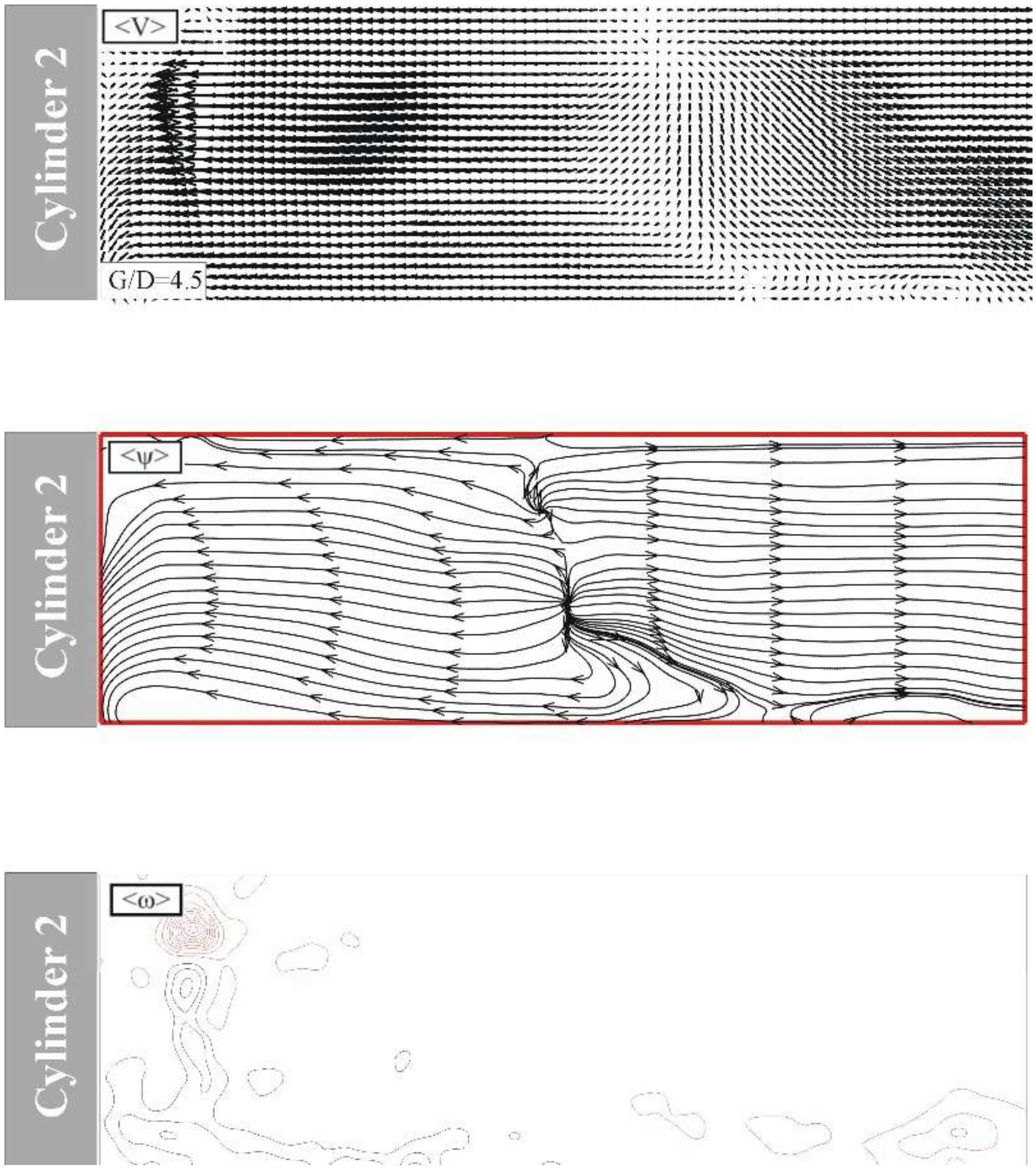

Figure 4.46. Time-averaged velocity field,<V> streamline patterns, <ψ> and vorticity contours, <ω> in the view section of the flow behind cylinder 2 of two cylinders in tandem arrangement with G/D 4.5 in side-view plane. Minimum and incremental values of vorticity are $\omega_{min} = \pm 1 s^{-1}$ and $\Delta\omega = 1 s^{-1}$.

5. CONCLUSION

This study represents a detailed investigation of the wake flows behind, between and front of two circular cylinders with the view section of 80 mm x 25 mm of equal diameter D=50 mm, arranged in tandem configurations and immersed in steady cross-flow in the shallow water using Particle Image Velocimetry (PIV) Technique. Totally, 342 sets of experiment were carried out.

Velocity vector field was obtained from PIV images and using this velocity vector field corresponding vorticity contours and streamline topology can be calculated. Time-averaged velocity vector field, vorticity contours, streamline topology were calculated using 350 instantaneous images.

During this experimental study, the effects the distance (G) between cylinders was investigated. In order to understand the effect of the distance between cylinders, four types of experiments were performed at the case. For each experiments the distance (G) between the cylinders were changed in the interval of 0 mm and 225 mm. First experiment was performed, cylinder 1 stationary and cylinder 2 mobile (cylinders are numbered from left to right in the direction of flow) and view section is behind (according to the flow direction) the cylinder 1 with G/D ratio of 0.5 to 4.5. Second experiment was performed, cylinder 1 mobile and cylinder 2 stationary and view section is front of the cylinder 2 with G/D ratio of 2 to 4.5. Third experiment was performed, cylinder 1 stationary and cylinder 2 mobile and view section is front of the cylinder 1 with G/D ratio of 0 to 4.5. Fourth experiment was performed, cylinder 1 mobile and cylinder 2 stationary and view section is behind the cylinder 2 with G/D ratio of 0 to 4.5.

As a result; each experiment has its own critical G/D ratio, flow develops its character after this critical gap ratio and other cylinder effects as appearing or disappearing directly related with the distance between cylinders.

REFERENCES

AKILLI, H., AND ROCKWELL, D., 2002. Vortex formation from a cylinder in shallow water. Physics of Fluids, 14 (9): 2957-2967.

ALAM M., MORIYA S., TAKAI AND SAKAMOTO H., 2002. Suppression of fluid forces acting on two square prisms in a tandem arrangement by passive control of flow. Journal of Fluids and Structures, 16(8): 1073–1092.

ALAM M., SAKAMOTO H. AND MORIYA M., 2003. Reduction of fluid forces acting on a single circular cylinder and two circular cylinders by using tripping rods. Journal of Fluids and Structures, 18:347–366.

ALAM M., SAKAMOTO H. AND ZHOU Y., 2006. Effect of a T-shaped plate on reduction in fluid forces on two tandem cylinders in a cross-flow. Journal of Wind Engineering and Industrial Aerodynamics, 94: 525–551.

BALACHANDAR, R., CHU, V.H., AND ZHANG, J., 1997. Experimental study of turbulent concentration flow field in the wake of a bluff body. Journal of Fluids Engineering, 199: 263-270.

BALACHANDAR, R., TACHIE, T.M., AND CHU, V.H., 1999. Concentration profiles in shallow turbulent wakes. Journal of Fluids Engineering, 121: 34-43.

BALACHANDAR, R., RAMACHANDRAN, S., AND TACHIE, M.F., 2000. Characteristic of shallow turbulent near wakes at low Reynolds number. Journal of Fluids Engineering, 122: 302-308.

BEARMAN, P.W., AND WADCOCK, A.J., 1973. The interaction between a pair of circular cylinders normal to a stream. Journal of Fluid Mechanics, 61: 499-511.

CARMO B.S. AND MENEGHINI J.R. 2005. Numerical investigation of the flow around two circular cylinders in tandem.

CHEN, D., AND JIRKA, H., 1995. Experimental study of plane turbulent wakes in a shallow water layer. Fluid Dynamics Research, 16: 11-41.

CHEN, D., AND JIRKA, H., 1997. Absolute and convective instabilities of plane turbulent wakes in a shallow water layer. Journal of Fluid Mechanics, 338: 157-172.

CHU, H.V., WU, J.H., KHAYAT, R.E., 1991. Stability of transverse shear flows in shallow open channels. Journal of Hydraulic Engineering, 117(10): 1370-1388.

DENG J., REN A., ZOU J. AND SHOU X. 2005. Three-dimensional flow around two circular cylinders in tandem arrangement . National Natural Science Foundation of China (Grant nos: 10272094, 10472104)

FITZPATRICK J.A., 2003. Flow/acoustic interactions of two cylinders in cross-flow. Journal of Fluids and Structures, 17: 97–113.

FU, H., ROCKWELL, D., 2005. Shallow flow past a cylinder: Transition phenomena at low Reynolds number. Journal of Fluid Mechanics, 540, 75-97.

GRUBISIC, V., SMITH R.B., AND SCHAR, C., 1995. The effect of friction on shallow-water flow past an isolated obstacle. Journal of the Atmospheric Sciences, 52: 1985-2005.

HALL J., ZİADA S. AND WEAVER D., 2003. Vortex-shedding from single and tandem cylinders in the presence of applied sound. Natural Sciences and Engineering Research Council of Canada (NSERC), L8S 4L7.

HO, C.M., AND HUERRE, P., 1984. Perturbed free shear layers. Annu. Rev. Fluid Mechanics, 16: 365-424.

IGARASHI, 1981. Characteristics of the flow around two circular cylinders arranged in tandem. Bulletin of JSME 24 (188), pp. 323–331

INGRAM, R.G., AND CHU, V.H., 1987. Flow around island in Rupert Bay: An Investigation of the bottom friction effect. Journal of Geophysical Research, 92 (C13): 14521-14533.

ISHIGAI, S., NISHIKAWA, E., NISHIMURA, K., AND CHO, K., 1972. Experimental study of structures of gas flow in tube banks with tube axes normal to flow (Part I, Karman vortex flow from two tubes at various spacing). Bulletin of the JSME, 15: 949-956.

ITOH Y. AND HIMENO R., 2002. Numerical simulation of three-dimensional flow around two circular cylinders in tandem arrangement. Focused on High Performance Computing in RIKEN, Review No. 48

JESTER W. AND KALLINDERIS Y., 2003. Numerical study of incompressible flow about fixed cylinder pairs Journal of Fluids and Structures, 17: 561–577.

KAHRAMAN, A., SAHIN, B., AND ROCKWELL, D., 2002. Control of vortex formation a vertical cylinder in shallow water: Effect of localized roughness elements. Experiments in Fluids, 33: 54-65.

LAMA K., LIB J.Y., CHANA K.T. AND SOA R.M.C., 2003. Flow pattern and velocity field distribution of cross-flow around four cylinders in a square configuration at a low Reynolds number. Journal of Fluids and Structures, 17: 665–679.

LANEVILLE A. AND BRIKA D., 1999. The fluid and mechanical coupling between two circular cylinders in tandem arrangement. Journal of Fluids and Structures, 13: 967-986.

LEGAL, P., CHAUVE, M.P., LIMA, R., AND REZENDE, J., 1990. Coupled waked behind two circular cylinder. Physical Review A, 41: 4566-4569.

LEGAL, P., PESCHARD, I., CHAUVE, M.P AND TAKEDA, Y. 1996. Collective behaviour of wakes downstream of a row of cylinders. Physics of Fluids, 8: 2097-2106.

LIN J.C., YANG Y. AND ROCKWELL D. 2002. Flow past two cylinders in tandem: instantaneous and averaged flow structure. Journal of Fluids and Structures, 16(8): 1059–1071.

LLOYD, P.M., AND STANSBY, P.K., 1997. Shallow-water flow around model conical island of small side slope. I: Surface piercing. Journal of Hydraulic Engineering, 123: 1057-1067.

MAHIR N. AND ROCKWELL D. 1996. Vortex formation from a forced system of two cylinders part 1 : tandem arrangement. Journal of Fluids and Structures, 10: 473 – 489

MENEGHINI J.R., SALTARA F., SIQUEIRA C. AND FERRARI J., 2001. Numerical simulation of flow interference between two circular cylinders in tandem and side-by-side arrangements. Journal of Fluids and Structures, 15: 327-350.

MITTAL S., KUMAR V. AND RAGHUVANSHI R., 1997. Unsteady incompressible flows past two cylinders in tandem and staggered arrangements. Int. J. Numer: Meth. Fluids, 25: 1315-1344 .

MITTAL S. AND KUMAR V., 2001. Flow-induced oscillations of two cylinders in tandem and staggered arrangements. Journal of Fluids and Structures, 15: 717-736.

PATNAİK B.S.V., NARAYANA P.A.A. AND SEETHARAMU K.N., 2000. Finite element simulation of transient laminar flow past a circular cylinder and two cylinders in tandem. International Journal of Numerical Methods for Heat & Fluid Flow, Vol. 10 No. 6, PP: 560-580.

SAKAMOTO H., 2002. Fluctuating fluid forces acting on two circular cylinders in a tandem arrangement at a subcritical Reynolds number. J. Wind Eng. Ind. Aerodyn. 26, PP: 85–103.

SCHAR, C., AND SMITH R.B., 1993. Shallow water flow past isolated topography. Part II: Transition to vortex shedding. Journal of the Atmospheric Sciences, 50: 1401-1412.

SUMNER D., PRICE J. AND PAIG DOUSSIS P., 1999. Tandem cylinders in impulsively started flow. Journal of Fluids and Structures, 13: 955-965.

SUMNER, D., PRICE, S. J., AND PAIDOUSSIS, M.P., 2000. Flow-pattern identification for two staggered circular cylinders in cross-flow. Journal of Fluid Mechanics, 411: 263-303.

SURMAS R., SANTOS L. AND PHILIPPI C., 2003. Lattice Boltzmann simulation of the flow interference in bluff body wakes. Elsevier B.V.: PACS: 47.27.Cn; 47.32.Cc; 02.70.Ns.

TACHIE, T.M., BALACHANDAR, R., 2001. Shallow wakes generated on smooth and rough surfaces. Experiments in Fluids, 30:467-474.

TOKAI N. AND OBİ S., 2005. Oscillatory turbulent flow around a pair of square cylinders in tandem. In: Proc. Int. Conf. Jets, Wakes and Separated Flows, Mie, 527–532.

ÜNAL, M.F., AND ROCKWELL, D., 1988. On vortex formation from a cylinder. Part I. The initial instability. Journal of Fluid Mechanics, 19: 491-512.

WOLANSKI, E., IMBERGER, J., AND HERON, M.L., 1984. Island wakes in shallow coastal water. Journal of Geophysical Research, 89: 10553-10569.

WOLFE D. AND ZIADA S., 2003. Feedback control of vortex sheddingfrom two tandem cylinders. Journal of Fluids and Structures, 17: 579–592.

XU G. AND ZHOU Y., 2004. Strouhal numbers in the wake of two inline cylinders. Experiments in Fluids, 37: 248–256.

ZDRAVKOVICH, M.M., 1968. Smoke observation of the wake of a group of three-cylinders at low Reynolds number. Journal of Fluid Mechanics, 32: 339-351.

ZHOU, Y., SO, R.M.C., LIU, M.H., AND ZHANG, H.J., 2000. Complex turbulent wakes generated by two and three side-by-side cylinders. International Journal of Heat and Fluid Flow 21: 125-123.

ZHOU, Y., WANG, Z.J., SO, R.M.C., XU, S.J., AND JIN, W., 2001. Free vibrations of two side-by-side cylinders in a cross-flow. Journal of Fluid Mechanics, 443; 197-229.

CIRRICULUM VITAE

Özgür ÇAKIR was born on November 14, 1978 in Aydın, Turkey. In 1996, he graduated from Söke Hilmi Fırat Anatolian High School, and enrolled in Mechanical Engineering Department of Çukurova University. In 2002, he graduated with a Bachelor of Science degree in mechanical engineering from the Department of Mechanical Engineering. He began his MSc education at the Department of Mechanical Engineering of Çukurova University. He worked in Sugözü Power Plant on 2002-2003. Then, he began to work in Turkish Army as Engineer Lieutenant on August, 2004. Now he still works in Turkish Army as Engineer First Lieutenant at Balıkesir.